ANALYSIS OF SINGLE PHASE CONVECTIVE HEAT TRANSFER IN MICROTUBES AND MICROCHANNELS

A THESIS SUBMITTED TO
THE GRADUATE SCHOOL OF NATURAL AND APPLIED SCIENCES
OF
MIDDLE EAST TECHNICAL UNIVERSITY

BY

BARBAROS ÇETİN

IN PARTIAL FULFILLMENT OF THE REQUIREMENTS
FOR
THE DEGREE OF MASTER OF SCIENCE
IN
MECHANICAL ENGINEERING

JANUARY 2005

Approval of the Graduate School of Natural and Applied Sciences

Prof. Dr. Canan Özgen
Director

I certify that this thesis satisfies all the requirements as a thesis for the degree of Master of Science.

Prof. Dr. Kemal İder
Head of Department

This is to certify that we have read this thesis and that in our opinion it is fully adequate, in scope and quality, as a thesis for the degree of Master of Science.

Prof. Dr. Sadık Kakaç
Co-Supervisor

Prof. Dr. Hafit Yüncü
Supervisor

Examining Committee Members

Prof. Dr. Ediz Paykoç (METU, ME) _____

Prof. Dr. Hafit Yüncü (METU, ME) _____

Prof. Dr. Sadık Kakaç (Unv. of Miami, ME) _____

Prof. Dr. Zafer Dursunkaya (METU, ME) _____

Assoc. Prof. Dr. Cemil Yamalı (METU, ME) _____

I hereby declare that all information in this document has been obtained and presented in accordance with academic rules and ethical conduct. I also declare that, as required by these rules and conduct, I have fully cited and referenced all material and results that are not original to this work.

Name, Last Name: Barbaros ÇETİN

Signature :

ABSTRACT

ANALYSIS OF SINGLE PHASE CONVECTIVE HEAT TRANSFER IN MICROTUBES AND MICROCHANNELS

Çetin, Barbaros
M.S., Department of Mechanical Engineering
Supervisor: Prof. Dr. Hafit Yüncü
Co-Supervisor: Prof. Dr. Sadık Kakaç

January 2005, 120 Pages

Heat transfer analysis of two-dimensional, incompressible, constant property, hydrodynamically developed, thermally developing, single phase laminar flow in microtubes and microchannels between parallel plates with negligible axial conduction is performed for constant wall temperature and constant wall heat flux thermal boundary conditions for slip flow regime. Fully developed velocity profile is determined analytically, and energy equation is solved by using finite difference method for both of the geometries. The rarefaction effect which is important for flow in low pressures or flow in microchannels is imposed to the boundary conditions of the momentum and energy equations. The viscous dissipation term which is important for high speed flows or flows in long pipelines is included in the energy equation. The effects of rarefaction and viscous heating on temperature profile and local Nusselt number are discussed. The results of the numerical method are verified with the well-known analytical results of the flow in macrochannels (i.e. Kn =0, Br =0) and with the available analytical results of flow in microchannels for simplified cases. The results show significant deviations from the flow in macrochannels.

Keywords: Microchannel Heat Transfer, Slip Flow, Heat Transfer in Ducts, Rarefaction Effect, Viscous Dissipation

ÖZ

MİKROTÜPLERDE VE MİKROKANALLARDA TEK FAZLI AKIŞKANLARDA KONVEKSİYONLA ISI TRANSFERİ

Çetin, Barbaros
Yüksek Lisans, Makine Mühendisliği Bölümü
Tez Yöneticisi: Prof. Dr. Hafit Yüncü
Ortak Tez Yöneticisi: Prof. Dr. Sdık Kakaç

Ocak 2005, 120 Sayfa

Mikrotüplerde ve mikrokanallardaki iki boyutlu, hidrodinamik olarak gelişmiş, ısıl olarak gelişmekte olan tek fazlı laminar akışın ısı transferi analizi sayısal olarak incelendi. Analiz kaygan akış rejiminde, sabit duvar sıcaklığı ve sabit duvar ısı akısı ısıl sınır koşulları için gerçekleştirildi. Akışkan sıkıştırılamaz, sabit termofiziksel özellikli kabul edildi. Eksen boyunca ısı iletimi ihmal edildi. Tam gelişmiş hız dağılımı analitik olarak belirlendi. Sıcaklık dağılımı her iki geometri için enerji denklemden, sonlu farklar yöntemi kullanılarak çözüldü. Basıncın düşük olduğu veya mikrokanallardaki akışlarda önemli olan seyrelme etkisi, momentum ve enerji denklemlerinde sınır koşulları olarak yüklendi. Hızın yüksek olduğu veya boyu uzun kanalardaki akışlarda önemli olan sürtünme kaybı terimi, enerji denklemine dahil edildi. Seyrelme ve sürtünme ısınmasının sıcaklık dağılımı ve yerel Nusselt sayısı üzerindeki etkisi incelendi. Elde edilen sayısal sonuçlar literatürdeki bilinen analitik ve sayısal sonuçlarla karşılaştırıldı. Mikrokanallardaki sonuçlar makrokanallardaki akıştan önemli sapmalar gösterdi.

Anahtar Kelimeler: Mikrokanallarda Isı Transferi, Kaygan Akış, Kanallarda Isı Transferi, Seyrelme Etkisi, Sürtünme Kaybı

for humanity…

insanlık için…

ACKNOWLEDGEMENTS

I would like to thank to my supervisor, Prof. Dr. Hafit Yüncü, and to my co-supervisor Prof. Dr. Sadık Kakaç to bring this important topic into my attention. I am deeply grateful to my supervisor and co-supervisor for their guidance, inspiration, invaluable help, and contributions to my scientific point of view throughout my graduate study.

I would like to thank to Prof. Dr. Zafer Dursunkaya for his contributions to the numerical work of this study and for the invaluable scientific discussions we have experienced.

I wish to express my sincere appreciation to my heat transfer colleagues; Başar Bulut, Özgür Bayer, Elif Dirgin, Yavuz Kayserioğlu, Cenk Evren Kükrer, Serkan Kasapoğlu and to our heat transfer laboratory technician Mr. Mustafa Yalçın for their support and motivation they provided me throughout my graduate study.

Finally, I express my deepest gratitude to my family, and to my friends Ece Er and Seda Kıyar for their continuous encouragement.

TABLE OF CONTENTS

LIST OF TABLES

LIST OF FIGURES

NOMENCLATURE

a_1, a_2	coefficients in Eq. (6.1)
b_1, b_2	coefficients in Eq. (6.2)
Br	Brinkman number
c_p	constant pressure specific heat, J/kgK
C_1, C_2, C_3, C_4	coefficients in the algebraic forms of the energy equation
D	tube diameter, m
F_M	tangential momentum accommodation coefficient
F_T	thermal accommodation coefficient
H	channel height, m
h	convective heat transfer coefficient, W/m^2K
k	thermal conductivity, W/mK
Kn	Knudsen number, λ / L
L	length, m
Nu	Nusselt number
p	pressure, kPa
Pr	Prandtl number, ν/α
$\Re$	gas constant, J/kgK
R	tube radius, m

r	radial coordinate
Re	Reynolds number, $U_m D/\nu$
T	fluid temperature, K
t	time, s
U_s	slip velocity, m/s
$\overline{u}$	dimensionless velocity
u	velocity in axial direction, m/s
v	velocity in radial (vertical) direction, m/s
x	axial coordinate
y	vertical coordinate

Greek Symbols

α	thermal diffusivity, m^2/s
β	coefficients in Eq. (5.9)
γ	specific heat ratio
λ	mean free path, m
μ	dynamic viscosity, kg/ms
ν	kinematic viscosity, m^2/s
ρ	density, kg/m^3
θ	dimensionless temperature
η	dimensionless radial (vertical) coordinate

ξ	dimensionless axial coordinate
τ	dimensionless time
κ	parameter defined in Eq. (3.23)

Subscripts

i	inlet values
i, j	radial (vertical) and axial location
m	mean values
s	fluid properties at the surface
w	wall values
x	local values

Superscript

k	location in time

CHAPTER 1

INTRODUCTION

The miniaturization trend of the electronic components since 1970' s and the development of the microfabrication and nanotechnology since 1980' s, led to the usage of the devices having the dimensions of microns in many fields such as biomedical applications, space industry and MicroElectroMechanicalSystems (MEMS), has significantly increased the problems associated with the overheating of these microcomponents and microdevices. The effective usage of these microcomponents and microdevices strongly depends on the removing of the heat dissipated by them, since their reliability is mainly influenced by their temperature. Because of their small dimensions, removing the heat dissipated by means of classical components, through natural and forced convection air cooling cannot solve the overheating problem, satisfactorily. Therefore, microchannel heat sinks have come into picture as the ultimate solution for removing the heat dissipated from a relatively small surface area, due to their large heat transfer area per unit volume.

For an effective and economical design of a microchannel heat sink, the key design parameters, such as;

- pressure required for pumping the cooling fluid,
- flow rate of the cooling fluid,
- hydraulic diameter of the channel,
- temperature of the fluid and the channel wall,
- number of channels,

have to be considered and optimized. In order to understand the importance of these parameters, the dynamic behavior of the fluid motion in such an extremely small channel should be understood.

Experimental studies in the literature have shown that many microchannel flow and heat transfer phenomena cannot be explained by conventional theories of transport phenomena, such as; the early transition from laminar flow to turbulent flow, and the several times higher friction factor of a liquid flowing through microchannel than that in conventional theories.

These special characteristics of flow and heat transfer are the results of the microscale channel size, surface roughness effect, the interfacial electrokinetic effects near the solid-fluid interface for liquid flow and rarefaction effect for gaseous flow.

Many analytical and experimental studies have been performed to have a better understanding of heat transfer at microscale, both for liquids and gases, as discussed in the next chapter. But, none of them has been able to come to a general conclusion up to now.

1.1. Fluid and Heat Transfer Modelling

In the literature, there are basically two ways of modeling for a flow field, as shown in Figure 1.1. Either the fluid is considered as a collection of molecules or is considered as a continuum where the matter is assumed to be continous and indefinitely divisible [1].

For macroscale, continuum model is being used. The velocity, density, pressure etc. are defined at every point in space and time. Conservation of mass, momentum and

energy lead to a set of nonlinear partial differential equations, which are the Navier-Stokes and energy equations. These equations are being solved for macro flow. But, Navier-Stokes and energy equations are inappropriate because of failure of the continuum assumption for micro flow.

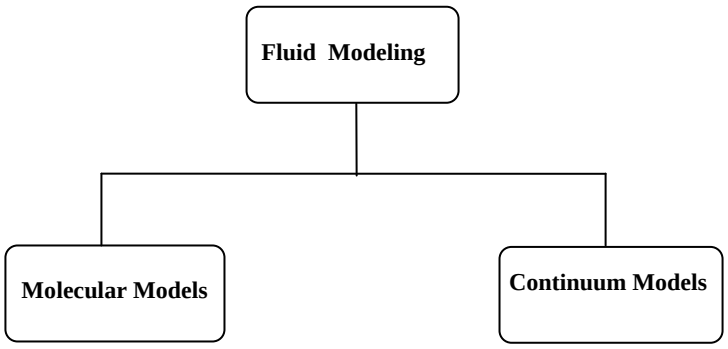

Figure 1.1. Flow Modeling Classification

The continuum assumption fails as the characteristic length of the flow (L) approaches to the average distance traveled by the molecules without colliding with each other, which is known as the mean free path (λ). The ratio of the mean free path to the characteristic length, a dimensionless quantity, is known as Knudsen number. As Knudsen number increases, fluid modeling is moving from continuum models to molecular models.

$$Kn = \frac{\lambda}{L} \qquad (1.1)$$

For small values of Kn (<0.01), the flow is considered as continuum flow and for large values of Kn (>10), the flow is considered as free-molecular flow. For values

0.01<Kn<0.1, the flow is in the slip-flow regime, and for values 0.1<Kn<10, the flow is in the transition flow regime. The flow regimes are tabulated in Table 1.1.

In continuum flow, the intermolecular collisions are dominant and the Navier-Stokes Equations are valid with the appropriate boundary conditions, which are; *(i)* the velocity of the fluid particle adjacent to the solid interface is equal to the zero relative to the surface (no-slip boundary condition), and *(ii)* the temperature of the fluid particle near the solid interface is equal to the temperature of the solid surface (no temperature-jump boundary condition).

Table 1.1. Flow Regimes for Different Kn Numbers

Knudsen number (Kn=λ/L)	Regime
Kn<0.01	"Continuum" Regime
0.01<Kn<0.1	"Slip-flow" Regime
0.1<Kn<3	"Transition" Regime
Kn>3	"Free-molecular" Regime

In free-molecular flow, the interaction of the molecules with the surface is of importance and the molecule to molecule collisions are neglected. The tool for dealing with this type of flow is the kinetic theory of gases [2].

In slip-flow regime, which is the main interest of this study, the Kn number is small, but not small enough to neglect the rarefaction effect. In this regime, the collision frequency of the fluid particles and the solid surface are not high enough to ensure the thermodynamic equilibrium between fluid particles and the solid surface.

Therefore, the fluid particles adjacent to the solid surface no longer attain the velocity and the temperature of the solid surface. The fluid particle has a tangential velocity at the surface (slip-velocity) and a finite temperature difference at the solid surface (temperature-jump). These slip velocity and temperature jump effects are related to the Knudsen number, some thermophysical properties of the fluid (specific heat ratio, Prandtl number), and the accommodation coefficients that are described by the molecule-surface interaction statistically[2]. By imposing these two effects into the boundary conditions, the Navier-Stokes Equations become applicable for this flow regime.

In transition flow regime, the flow field is neither dominated by the molecule to surface interaction, as in free-molecular flow nor by the intermolecular collisions, as in continuum flow. Therefore, it is difficult to solve the flow field in transition regime with theoretical consideration only.

For moderate pressures and dimensions, the flow is always in continuum regime. Only, flow in low density such as rarified gas dynamics applications and flow in small dimensions such as micro and nanoscales, the flow becomes slip-flow, transition flow or free-moleular flow. For gas flows in micro dimensions, generally, the regime is slip-flow regime; and for liquid flows, it is still in continuum regime. Therefore; in the solution of the gas flows in microchannels, the modification of the boundary conditions should be imposed into the equations to introduce the rarefaction effect. For liquid flow in micro dimensions, the interfacial electrokinetic effects near the solid-liquid interface should be imposed to the equation.

1.1.1. Slip Velocity Boundary Condition

By using the kinetic theory of gases and neglecting the intermolecular collisions within the immediate vicinity of the surface, the slip velocity can be obtained,

$$U_s = -\frac{2-F_M}{F_M}\lambda\left(\frac{du}{dy}\right)_{y=0} + 3\sqrt{\frac{\Re T}{8\pi}}\frac{\lambda}{T}\left(\frac{\partial T}{\partial x}\right)_{y=0} \quad (1.2)$$

for the Cartesian coordinate system[2], and

$$U_s = -\frac{2-F_M}{F_M}\lambda\left(\frac{du}{dr}\right)_{r=R} + 3\sqrt{\frac{\Re T}{8\pi}}\frac{\lambda}{T}\left(\frac{\partial T}{\partial x}\right)_{r=R} \quad (1.3)$$

for the cylindrical coordinate system[3], where λ is the mean free path, $\Re$ is the gas constant and F_M is the momentum accommodation factor which represents the fraction of the molecules undergoing diffuse reflection. For idealized smooth surface, F_M is equal to zero, which means specular reflection. For diffuse reflection, F_M is equal to one, which means the tangential momentum lost at the wall. Its value depends on the gas, solid, surface finish and surface contamination and has been determined experimentally and varies between 0.5 and 1.0. For most of the gas solid couples used in engineering applications, this parameter is close to the unity[2]. Therefore; for this study, F_M in this Eqs. (1.2) and (1.3), is also taken as unity.

The second term on the right hand sides of Eqs (1.2) and (1.3) is known as thermal creep, which accounts for the fluid flow induced by the temperature gradient. By using the kinetic theory of gases and some mathematical manipulations, it can be shown that this term is second order in Knudsen number[3]. Therefore; for moderate temperature gradients, the second term is negligible compared with the first term for low Knudsen numbers, which is the case in slip-flow regime.

1.1.2. Temperature Jump Boundary Condition

With the similar considerations in slip velocity, temperature jump at the wall can be obtained as [1],

$$T_s - T_w = -\frac{2-F_T}{F_T}\frac{2\gamma}{\gamma+1}\frac{\lambda}{\Pr}\left(\frac{\partial T}{\partial y}\right)_{y=0} \qquad (1.4)$$

for the Cartesian coordinate [2], and

$$T_s - T_w = -\frac{2-F_T}{F_T}\frac{2\gamma}{\gamma+1}\frac{\lambda}{\Pr}\left(\frac{\partial T}{\partial r}\right)_{r=R} \qquad (1.5)$$

for the cylindrical coordinate [3], where γ is the specific heat ratio, λ is the mean free path, Pr is the Prandtl number of the fluid and F_T is the thermal accommodation factor which represents the fraction of the molecules reflected diffusively by the wall and accommodated their energy to the wall temperature. Its value depends on the type of gas, type of solid, surface roughness, gas temperature, gas pressure and the temperature difference between solid surface and the gas and has also been determined experimentally. F_T varies between 0 and 1.0, and it can take any arbitrary value, unlike momentum accomodation factor [2].

This study considers the two-dimensional, incompressible, constant property, hydrodynamically developed, thermally developing, single phase laminar flow in microtubes and microchannels between parallel plates with negligible axial conduction for both uniform wall temperature and uniform wall heat flux thermal boundary conditions by imposing the rarefaction effects into the boundary conditions, including the viscous dissipation term. The fully developed velocity profiles for both of the geometries are determined by solving momentum equations, analytically. By substituting the fully developed velocity profile, the energy equation is solved by using numerical methods to determine the temperature distribution within the solution domain and obtain the Nusselt number. The numerical method is verified by comparing the present numerical results with the analytical results that are available for simplified cases in literature. The numerical code is written using Pascal computer programming language.

CHAPTER 2

LITERATURE SURVEY

For the last two decades, there has been an increasing interest in the area of microchannel flow and heat transfer. In the literature, there are numbers of publications on single-phase and two-phase flows in microchannels. In this chapter, only the works on single-phase microchannel flow including the experimental, analytical and numerical studies, are reviewed.

Tuckerman and Pease [4] demonstrated that electronic chips can effectively be cooled by means of water flow through microchannel heat sinks without a phase change. They reported that convective heat transfer coefficient for laminar flow through microchannels might be higher than that of for turbulent flow through conventionally sized channels. This conclusion accelerated the research on the topic of convection through microchannels.

Peng and Peterson [5] examined the single-phase convective heat transfer by conducting a series of experiments with several different microchannels to determine the influence of the liquid flow, thermal conditions and microchannel size using water as the working fluid. They indicated that laminar flow exists for Reynolds number less than 400, a transition regime in the regime where Reynolds number is between 400 and1000, and a fully developed turbulent regime in the region where Reynolds number is larger than 1000. They also indicated that the range of the transition zone and the heat transfer characteristics of both the transition and laminar flow regimes are strongly affected by the liquid temperature, liquid velocity and

microchannel size; and hence, are not only determined by Reynolds number. In addition, they showed that there is an optimum channel size in terms of the forced convective flow heat transfer for a single-phase liquid flowing in a rectangular microchannel.

Peng and Peterson [6] experimentally investigated the forced convective heat transfer and flow characteristics of water flowing through microchannel plates with extremely small rectangular channels having hydraulic diameters of 0.133-0.367 mm. and different geometric configurations to determine the effect of the geometric configuration on the flow and heat transfer, and they proposed heat transfer and flow friction correlations, which would be readily applicable to engineering design and practical applications.

Mala and Li [7] studied flow characteristics of water flowing through cylindrical microtubes of stainless steel and fused silica with the diameters range from 50 to 254 μm. They observed that for a fixed volumetric flow rate, the pressure gradient required to force the liquid through microtube was in a rough agreement with the conventional theory for small flow rates, i.e. small Reynolds number. However, as the Reynolds number increased, they observed a significant deviation from the conventional theory, and the deviation increased as the diameter of the microtubes decreased. They concluded that there might be an early transition from laminar to turbulent flow mode at Re>300-900, and the flow changes to fully developed turbulent flow at Re>1000-1500. In addition, they observed that the flow behavior also depend on the material of the microtubes. They discussed two possible reasons for higher flow resistance one of which is the early transition from laminar to turbulent, and the other is the effect of the surface roughness. To include the effect of the surface roughness, they proposed the use of the roughness-viscosity model (RVM) by introducing a roughness viscosity function.

Rahman [8] investigated the integrated microchannel heat sinks for the cooling of high power and high reliability electronic devices experimentally using water as the working fluid. Tests were performed with devices fabricated using standard Silicon 100 wafers. Two different channel patterns; parallel and series pattern, were designed to see the effects of flow branching, channel length and fluid velocity. He studied channels of different aspect ratios. He measured the fluid flow rate as well as the pressure and temperature of the fluid at the inlet and outlet of the device, and temperature at several locations to calculate local and average heat transfer coefficients, and pressure drop in the device for different flow rate, channel size and channel configuration. His results showed that the measured values of average Nusselt number were usually larger than those predicted by correlations for larger size channels. He concluded that the larger heat transfer was caused by the breakage of velocity boundary layer by surface roughness associated with etched channel structure, and the transition from laminar to turbulent was somewhat gradual because of small channel dimension.

Harms et al. [9] investigated the hydrodynamic and thermal performance of two deep microchannel configurations; a single channel system and a multiple channel system, both theoretically and experimentally using the deionized water as the working fluid. They observed that for fully developed laminar flow, the thermal resistance was independent of the pressure drop; however an inverse relationship between pressure drop and thermal resistance was observed for the developing laminar flow. The analysis showed that decreasing the channel width and increasing the channel depth provided better flow and heat transfer performance. For multiple channel design, the experimental friction factor agreed with the theoretical values reasonably well in both laminar and turbulent regime, and a critical Reynolds number of 1500 was indicated in the plot of the experimental friction factor. For the single channel design, the experimental Nusselt number was higher than predicted at all flow rates, which was addressed to the effect of the inlet bent. For multiple channel design,

experimental Nusselt number results agreed with the theory reasonably well at high flow rates, but deviated significantly from theory at low flow rates. They noted that the thermal resistance of the multiple channels was always lower than that of the single channel design for a given level of pressure drop, and they concluded that for their systems developing laminar flow provided better overall performance than turbulent flow.

Wu and Cheng [10] investigated the effect of geometric parameters, the surface roughness and surface interfacial properties on pressure drop and heat transfer in 13 different trapezoidal silicon microchannels, using the deionized water as the working fluid. They fabricated the silicon microchannels by etching. They obtained different geometries depending on the etching method and etching time, various surface roughness depending on the concentration and temperature of the etching solutions, and different surface interfacial properties depending on the thickness of the oxide layer on a silicon layer. They founded that the values of Nusselt number and apparent friction factor depend greatly on different geometric parameters, and laminar Nusselt number and the apparent friction factor increase with the increase of surface roughness and surface interfacial property.

Tso and Mahulikar [11, 12, 13] proposed the use of Brinkman number to explain the unusual behavior of laminar liquid flow in micro channels and experimentally verified that Brinkman number correlates the convection in microchannels in spite of its relatively low values, and also Brinkman number decides the fundamental limit for the reduction of the microchannel dimensions (optimum design) and is more important in the laminar regime compared to the transition and turbulent regime. Furthermore, Brinkman number plays a role in determining the flow transition points even when experimental data is obtained locally along the flow for the constant wall heat flux boundary condition.

Wang and Peng [14] investigated the heat transfer characteristics and cooling performance of rectangular shaped microgrooves machined into stainless steel plates, using methanol as the cooling fluid. They analyzed the influence of liquid velocity, subcooling, property variations and microchannel geometry configuration on the heat transfer behavior, cooling performance, and liquid flow mode transition experimentally. Measurements made to clarify the flow nucleate boiling attributes indicated an increased heat transfer rate and a behavior that was quite different from what typically occurs in longer tubes or channels due to the relatively large portion of the surface area associated with the thin film region. Furthermore, their results showed that the liquid velocity, liquid subcooling, liquid properties and geometry of the microchannels have significant influence on the heat transfer performance, cooling characteristics and liquid flow mode transition. They concluded that, if selected properly, the correct combination of these parameters can provide significant improvements in the thermal performance and heat removal rate for a wide variety of applications, particularly those where space is limited such as electronic circuits and devices.

Chen et al. [15] investigated the fluid flow and heat transfer in microchannels with different hydraulic diameters ranging from 57-267 μm experimentally, using methanol as the working fluid. Their experimental results indicated that the flow behavior was in the laminar regime when Reynolds number was between 50 and 850, and the surface roughness, viscosity and channel geometry had great effects on flow characteristics in microchannels. Furthermore, their results indicted that forced convection in microchannel heat sink exhibited excellent cooling performance, especially in the phase change regime.

Pfahler et al. [16] have experimentally investigated the fluid flow in rectangular microchannels with cross-section ranging in area from 80 to 7200 μm^2. Their objective was to determine the length scales at which the continuum assumptions

break down, and to estimate the adequacy of the Navier-Stokes equations for predicting the fluid flow behavior. They found that in the relatively large flow channels, their observations were in agreement with the predictions of the Navier-Stokes equations. However, in the smallest of their channels, a significant deviation from the Navier-Stokes predictions was observed.

Pfahler et al. [17, 18] measured the friction factor for liquids and gases in microchannels. Nitrogen gas and alcohol were used in channels with depths changing from 0.5 to 50 μm. They determined a lower friction factor which increased with Reynolds number for small Reynolds numbers and became independent of Reynolds number for large Reynolds numbers. In another analysis, they used nitrogen, helium, and isopropyl liquid and silicone oil to determine the flow characteristics in channels with hydraulic diameters varying from 0.5 to 50 μm. For both gases and liquids, they obtained smaller friction factor values than the conventional sizes. Isopropyl results showed a dependency on the channel size. Silicone oil results, on the other hand showed a Reynolds number dependency. They concluded that the small friction factor values for liquids are due to the reduction of viscosity with decreasing size, and for gases due to the rarefaction effects. Pfahler et al. [19] also reported after a study of liquid flow in microchannels that there is a critical dimension below which the Navier-Stokes equations cannot be used to obtain the characteristic flow properties.

Wu and Little [20] designed a microminiature Joule-Thompson refrigerator and investigated pressure drop for gas flow in microchannels. They found that the measured friction factor is much higher than the one expected from the classical theory. They found that transition Reynolds number was between 400 and 900 for various tested configurations. In their next study, Wu and Little [21] investigated the heat transfer for gas flow in microchannels. They observed a Reynolds number dependence for fully developed flow in laminar regime. Heat transfer coefficients

were found to be higher than expected from the classical theory, like friction coefficient. They concluded that deviations from the theory might be due the asymmetric wall roughness and non-uniform wall heating conditions.

Choi et al. [22] studied the convective heat transfer of dry nitrogen flow in circular microtubes, where the diameter ranged from 3 to 81 μm for laminar and turbulent regime. They avoided entrance effects by using long channels. Heat transfer was found to be a function of Reynolds number in the laminar regime and as much as seven times larger than the ones for turbulent flow regime. In laminar regime friction constant was found to be lower than predicted, while turbulent flow regime results were fairly scattered. They also investigated the roughness effect, and concluded that roughness does not affect the friction factor in laminar flow regime.

Arkilic et al. [23] investigated gaseous flow with slight rarefaction through long microchannels both analytically and experimentally. They demonstrated both compressibility and non-continuum effects by analyzing the two-dimensional Navier-Stokes equations with first order slip velocity boundary condition. They showed that experimental results obtained with the described mass flow measurement technique for stream wise helium mass flow through microchannels 52.25 μm wide, 1.33 μm deep and 7500 μm long for pressure range of 1.2 to 2.5 atmospheres (outlet pressures at atmospheric), agreed with the analytical analysis.

Xin and Zhang [24] investigated the flow characteristics of water and air flowing in the rectangular microchannels with 0.23-1.1 mm in the hydraulic diameter. They founded that critical and transition Reynolds numbers are lower than that of macrochannels for both water and air flow, and hydraulic diameter has some influences on them. They concluded that for water flow, friction factors for transition and turbulent flow cannot be predicted by the friction factor correlation for the macrochannel. They observed that air flow in microchannel consists of four flow

regimes; laminar flow, transition flow, turbulent flow and accelerating turbulent flow; and when hydraulic diameter is equal to and less than 0.225 mm, the transition and turbulent flow regime disappear.

Telles et al. [25] solved the laminar forced convection heat transfer problems inside ducts, with axial conduction at the wall, subjected to the three main types of boundary conditions exactly. The general method of solution involved the change of the dependent variable leading to square integrable function in real line. The form of solutions was presented for the flows inside circular pipes, annular space between pipes and between parallel plates.

Beskok and Karniadis [26] have developed a numerical model based on spectral element method to simulate unsteady two and three-dimensional incompressible flow in complex microdomains (e.g. microblades, microbearings, micromotors). Their method is valid for slip-flow regime (i.e. $Kn < 0.1$). They proposed the use of higher order velocity slip condition including the thermal creep effect which accounts for the induced flow due to the temperature gradient along the channel (from cold side to hot side) due to the micronsized channel size. They verified their method by comparing it to the analytical solutions for simple prototype flows. They noted the importance of the thermal creep on pressure distribution, and the importance of the accommodation coefficient. They explained the drag reduction phenomena apparent in microchannels by the slip-flow theory. They addressed the effect of compressibility for severe pressure drops. Later, they extended their analysis to combined effect of compressibility and rarefaction in gas flows [27]. Their analysis considers the flow regime up to Kn =0.3. They compared their results for flat channel with available experimental results. They concluded that compressibility is important for pressure driven flows and rarefaction is important for shear driven flows. They observed that viscous heating is an important mechanism in microscale. Additionally, they proposed benchmark experiments to systematically study

compressibility, rarefaction and viscous heating in microscales in order to provide validation to numerical models and the slip-flow theory.

In another study, Beskok and Karniadis [28] developed a simple physics-based unified model that predicts the velocity distribution, the volumetric and mass flow rates, as well as the pressure distribution in channel, pipe and duct flows of general aspect ratio for the entire flow regime (i.e. $0<Kn<\infty$). They proposed a general slip boundary condition which is second order in slip-flow regime, and which is used to represent the velocity distribution with a reasonable accuracy for the entire flow regime. Their model gave small deviations only in transition regime which they addressed to the growth of the Knudsen layer within the channel. They validated their model with comparisons against direct simulation Monte Carlo, linearized Boltzmann solutions and experimental data. They performed all of their simulations based on diffuse reflection (i.e. momentum accommodation coefficient is equal to 1), and they proposed to study unified model for non-diffuse reflection in foregoing studies.

Mikhailov and Cotta [29] developed a Mathematica package that computes the eigenvalues, the eigen functions, eigen integrals, the dimensionless temperature, the average dimensionless temperature and the Nuselt number for steady state and periodic heat transfer in microparallel plate channel and microtube taking into account the velocity slip and the temperature jump. They solved the steady state heat transfer in thermally developing, hydrodynamically developed forced laminar flow inside microconduits with uniform and periodic inlet temperature, and the steady-state heat transfer in thermally and hyrodynamically developed electro-osmotic flow inside microconduits with uniform wall heat flux and inlet temperature.

Barron et al [30] extended the original Graetz problem for thermally developing heat transfer in laminar flow through circular tube to include the effects of slip-flow. They

developed a new technique to evaluate the eigenvalues for the problem, which they were able to calculate only first four eigenvalues. Although they explicitly mentioned the temperature jump in the specification of boundary condition, they ignored this boundary condition in the calculation of the eigenvalues. Due to the misapplication of the temperature jump boundary condition, they found that Nusselt number increases with increasing Knudsen number, and suggested that slip-flow is one of the mechanisms being responsible for the enhancement of the heat transfer in gaseous convection in microtubes.

In another study, Barron et al. [31] discussed their new technique developed for the evaluation of the eigenvalues for the graetz problem extended to the slip-flow. They were able to determine first four eigenvalues with precision of about 4 digits. Moreover, they proposed a simplified relationship between the eigenvalues and Knudsen number. They concluded that an improved method with enhanced calculation speed would be of future interest.

Mikhailov and Cotta [32] proposed the use of Mathematica software in the calculation of the eigenvalues of the Graetz problem extended to slip-flow. They calculated the first five eigenvalues with precision of 16 digits and addressed some methods for higher order eigenvalues.

Ameel et al. [33] extended the work of Barron et al. [31] from isothermal case to the constant heat flux boundary condition in a microtube. They developed expressions for the temperature field and the Nusselt number. The Nusselt number was found to decrease with increasing Knudsen number, primarily as a result of an increase in the temperature jump at the wall with Knudsen number. They observed a reduction in Nusselt number of the order of 40% over the full slip-flow range. Furthermore, they found that the entrance length varies with Knudsen number, an increase in slip-flow resulting in a longer entrance length.

Larrode et al. [3] studied slip-flow heat transfer in circular tubes under the conditions that allowed us to exploit its similarities to the classical Graetz problem. They showed that heat transfer depends on two parameters; slip radius ρ_s, which is a measure of the degree of rarefaction, and β, which is a function of the surface accommodation coefficients. The effect of the temperature jump at the wall, which was ignored in previous study of Barron et al. [31], as determined to be essential in the heat transfer analysis. They found that heat transfer increase or decrease with increasing rarefaction effect depending on the value of the parameter β; on the other hand, for fixed degree of rarefaction heat transfer decreases with increasing value of the parameter β. Moreover, they developed a new uniform asymptotic approximation to the eigen-functions of the Graetz problem, a weighted asymptotic approximation that gave improved results with respect to the well known WKB approximation to be able to determine the heat transfer close to the entrance, a region where rarefaction effects were found to be more pronounced. They briefly discussed the method of evaluation of the eigen-function of the Graetz problem in another study [34].

Bayazitoglu and Kakac [35] discussed the flow regimes and the dimensionless parameters that effects the flow field in microchannel single phase gaseous fluid flow. They noted that viscous heating, compressibility and rarefaction is to be considered in gaseous flows in microchannels.

Tunc and Bayazitoglu [36] studied the convective heat transfer for steady state, hydrodynamically developed laminar flow in microtubes with uniform temperature and uniform heat flux boundary conditions by integral transform technique. Temperature jump at the wall and viscous heating within the medium were included. The solution method was verified for the cases where viscous heating is neglected. For uniform temperature case, with a given Brinkman number, which is the indication of the degree of the viscous heating, at specified axial lengths the effect of

viscous heating was investigated for developing range, reaching the fully developed Nusselt number. The effect of viscous heating was investigated for both of the cases where the fluid was being heated or cooled. They showed the combined effects of Knudsen number, Brinkman number and Prandtl number on the heat transfer. They underestimated the fully developed Nusselt number, since they considered only the first four eigenvalues during their calculations. They concluded that temperature jump gives a rise to the Nusselt number, but its effect diminishes with increasing Prandtl number. They also showed that viscous heating has different effects for different cases.

Tunc and Bayazitoglu [37] solved the transient heat convection in a circular microchannel for hydrodynamically developed and thermally developing flow conditions with constant wall temperature by the integral transform and Laplace transform techniques analytically. The effects of slip velocity, temperature jump and viscous heating were investigated. Their results confirmed that the viscous heating effects increase the Nusselt number for the specified conditions. They used more than four eigenvalues to calculate Nusselt number, and they corrected their results from their previous work [36]. They also discussed the effect of considered numbers of eigenvalues on the value of the fully developed Nusselt number.

Li et al. [38] investigated the effect of channel size on the laminar flow characteristics of gas flowing through microtubes, analytically. They proposed a new theoretical model, called wall-adjacent layer model to account for the wall effect. They found that the change in viscosity of fluid in a very thin layer near the wall-adjacent layer, which is about 5 times of the mean free path, result in significant influence on the flow characteristics. The variation of viscosity was obtained by the kinetic theory of gases. They discussed the applicability of their model, and concluded that it is valid for Kn <0.1. They derived the velocity profile and pressure drop for laminar gas flow inside microtube, and concluded that friction factor is less

that that in macropassages at a specified value of Reynolds number, the velocity is greater than that is determined from the conventional theory.

Guo and Wu [39] studied the compressibility effect on the gas flow and heat transfer in a microtube. They used a finite difference, forward marching numerical procedure with upwind scheme for the axial direction and power law for the lateral direction. They imposed no-slip and no-temperature jump boundary conditions. They validated their results with calculation of the friction factor for low Mach number flow. They founded that compressibility cause an increase in the mean velocity, an additional pressure drop in flow direction and the change of the shape of dimensionless velocity profile. Furthermore, they founded that for high Mach number, friction factor increases with increasing Mach number and Nusselt number increases with increasing dimensionless tube length (i.e. fully developed conditions are unachievable).

Xu et al. [40] analyzed the effects of viscous dissipation on the characteristics of liquid flow in microchannels, numerically. They solved the combined entrance region problem with no-slip velocity and adiabatic wall boundary conditions by treating the heat conductivity and viscosity as functions of temperature. They found that effects of viscous dissipation became significant and influence the temperature, pressure and velocity distributions in the flow. Therefore, relationships between the average friction factor and Reynolds number change when the hydraulic diameter of the microchannel is very small. They established a criterion to evaluate the possibilities of the viscous dissipation effects on flows in microgeometries.

Barber and Emerson [41] conducted an investigation of low Reynolds number rarefied gas behavior at the entrance of a parallel plate microchannel using a specially adapted two-dimensional Navier-Stokes solver within the slip-flow regime (i.e. $0< Kn<0.1$) implementing tangential slip velocity boundary condition along the

walls of the flow domain. The numerical model indicated that Knudsen number has a significant effect on the hydrodynamic development length at the entrance to parallel plates. They found that at the upper limit of the slip-flow regime (Kn ~0.1), entrance lengths are approximately 25% longer than those experienced in the continuum regime.

Kavehpour et al. [42] studied gas compressibility and rarefaction in microchannels using a two dimensional flow and heat transfer model assuming slip-flow regime by solving the compressible form of momentum and energy equations with slip velocity and temperature jump boundary conditions in a parallel plate channel for both uniform wall temperature and uniform wall heat flux, numerically. Their numerical methodology was based on finite difference scheme. To verify the model, the mass flow rate as compared with experimental results of helium through microchannels, normalized friction coefficient was compared with the experiments of nitrogen and helium flows in microchannels, and axial pressure distribution was compared with the experimental results for nitrogen flow in microchannel. They found that Nusselt number and friction coefficient were substantially reduced for slip flows compared with the continuum flows. Also, the velocity and temperature distributions were found to be flattened compared with the continuum flows, and the axial pressure variation was found to become nonlinear. They showed that the effect of compressibility is important for high Reynolds numbers and that the effect of rarefaction is significant for low Reynolds numbers.

Hadjiconstantinou and Simek [43] investigated the constant wall temperature convective heat transfer characteristics of a model gaseous flow between parallel plates under hydrodynamically and thermally fully developed conditions. In the calculation of the Nusselt number, they used slip-flow theory in the presence of axial conduction for microchannels, and a stochastic molecular simulation technique known as the direct simulation Monte Carlo (DSMC) for nanochannels. They

showed that the Nusselt number decreases monotonically with increasing Knudsen number in the fully accommodating case, and that axial heat conduction increases the Nusselt number. Their results showed a good agreement between slip-flow prediction and the DSMC results for Kn <0.1, and a good approximation beyond its expected range of applicability.

Zu et al. [44] conducted an analysis of the heat transfer characteristics between two asymmetrically heated parallel plates with microspacing. They solved the momentum and energy equation with the boundary conditions of the slip velocity and the temperature jump in order to obtain the dimensionless temperature distribution, heat transfer and Nusselt number. They concluded that, as Knudsen number increases, the temperature jump near the heating wall increases; the dimensionless temperature in the microchannel decreases under the same heat flux ratio, and the Nusselt rates for the asymmetrically heated wall decreases at a fixed heat flux ratio. They also concluded that Nusselt number rates for the heated walls increase with increasing thermal accommodation coefficient and with decreasing tangential accommodation coefficient.

Mayes and Webb [45] analyzed the thermally fully developed, electro-osmotically generated convective transport for a parallel plate microchannel and circular microtube under imposed constant wall heat flux and constant wall temperature boundary conditions. The exact solution for the fully developed, dimensionless temperature profile and corresponding Nusselt number have been determined for both geometries and both thermal boundary conditions. The fully developed temperature profiles and Nusselt number are found to depend on the relative duct radius and the magnitude of the dimensionless volumetric source.

Yu and Ameel [46] studied the laminar slip-flow forced convection in rectangular microchannels analytically by applying a modified generalized integral transform

technique which is a hybrid solution method that uses both analytical and numerical procedures to solve the energy equation, assuming hydrodynamically fully developed flow. Results were given in terms of the fluid mixed mean temperature, and both local and fully developed mean Nusselt numbers. Heat transfer was found to be increase, decrease or remain unchanged compared to non-slip flow, depending on two dimensionless parameters that include effect of rarefaction and fluid-wall interaction. The transition point at which the switch from heat transfer enhancement to reduction occurs was identified for different aspect ratios. Furthermore; for a given aspect ratio, they found that increasing temperature jump always reduces heat transfer and shortens thermal entrance region.

In their foregoing study, Yu and Ameel [47] found a universal finite Nusselt number for laminar slip flow heat transfer at the entrance of a conduit which is valid for both isothermal and isoflux thermal boundary conditions, and for any conduit geometry, by using the same method. They calculated the local Nusselt number at the axial location very close to the entrance and then extrapolated their results to found the finite entrance Nusselt number value, which is infinite for the macroconduits.

Tunc and Bayazitoglu [48] investigated the convection heat transfer in a rectangular microchannel assuming fully developed flow both thermally and hydrodynamically for the constant axial and peripheral heat flux boundary condition. They applied integral transform technique for both momentum and energy equations. First, the fully developed velocity profile was determined, and then substituted into the energy equation to determine the Nusselt number. They verified the method by comparing the results for zero Knudsen number, which corresponds to a macrosize channel, to the data from previous studies. They discussed the effects of rarefaction and channel size on the velocity distribution and heat transfer. They concluded that Nusselt number decreases with increasing Knudsen number, regardless of the value of the aspect ratio; however Nusselt number decreases significantly for smaller values of

aspect ratio which was explained by the increasing rarefaction. Furthermore, Nusselt number was found to increase with Prandtl number by reducing the temperature jump, and the change in Nusselt number due to Prandtl number was found to be amplified with decreasing aspect ratio. Although they did not consider the viscous heating, they concluded that effects of viscous heating in a rectangular channel might be the same as the effect in a microtube, which they discussed in their one of the previous studies [36].

Papautsky et al. [49] described fluid behavior in rectangular microchannels using a numerical model based on the micropolar fluid theory that augments the laws of classical continuum mechanics including the micro-rotational effects of fluid molecules and variations in the apparent fluid viscosity in the region close to the walls of the channels. Their numerical model used the finite difference method with a successive relaxation solution technique, for fully developed fluid flow in microchannels, and provided a means of predicting flow characteristics, such as volumetric mass flow rate, average velocity, pressure drop and Darcy friction factor for incompressible fluids operating in microchannels. The simulated widths varied from 50 to 800 μm, while channel heights ranged from 25 to 50 μm. Moreover, they verified their model using experimental data collected for flows through micromachined channels. They represented their results with the available experimental data and predictions from Navier-Stokes equations, and the numerical model provided a better approximation of the experimental data than the Navier-Stokes theory, which is an essential conclusion to the successful design and development of future microscale microfludic devices.

Ryu et al. [50] developed a tree dimensional analysis procedure for the thermal performance of a manifold microchannel heat sink, using water as the coolant and the silicon as heat sink material. They solved the system of fully elliptic equations that govern the flow and thermal fields by a SIMPLE-type finite volume method in

which an upwind differencing scheme was used for convective derivatives. They obtained the optimal design variables (channel depth, channel width, fin thickness and inlet/outlet width ratio) that minimize the thermal resistance for a given pumping power and a specified number of manifolds.

Qu and Mudawar [51] analyzed the three-dimensional fluid flow and heat transfer in a rectangular microchannel heat sink numerically using water as the cooling fluid. Their numerical code is based on finite difference method and the SIMPLE algorithm. They compared their numerical results with analytical solutions and available experimental data. For their microchannel heat sink, they founded that the temperature rise along the flow direction in the solid and fluid regions could be approximate as linear and the temperature along the transverse direction at a given longitudinal location was nearly constant. They also found that increasing Reynolds number increases the length of the developing region and fully developed flow might not be achieved inside the heat sink for high Reynolds numbers, which resulted in enhanced heat transfer and higher pressure drop.

In the study of Fan et al. [52] carried out the numerical simulation on the gaseous micro channel using the DMSC. After normalizing the velocities by the area-averaged stream wise velocity at the channel exit, the result of DSMC was presented. Several unique features were obvious: for maintaining a constant mass flow, the mean stream wise velocity at the walls was found to increase to make up for the density drop caused by the decrease of the pressure in the channel direction. This was in contrast to the classical Poisueille flow. In addition, the velocities at the walls were found to be non-zero and increase in the stream wise direction, which demonstrates the slip flow effect due to rarefaction. The results of DSMC were validated by analytic solution in slip-flow regime, and the two solutions were compared. They noted remarkable agreements between the two results.

Toh et al. [53] investigated the three-dimensional fluid flow and heat transfer phenomena inside the heated microchannels. Steady, laminar flow and heat transfer equations are solved using finite volume method. The numerical procedure was validated by comparing the predicted local thermal resistances with available experimental data. The friction factor was also predicted in their study. It was found that the heat input lowered the friction losses, particularly at lower Reynolds numbers. They concluded that at lower Reynolds number the temperature of the water increased, leading to a decrease in the viscosity and hence smaller friction losses.

Guo and Li [54] reviewed and discussed the size effect on microscale single phase fluid flow and heat transfer. They classified the physical mechanisms for the size effect on the microchannel flow and heat transfer as the gas rarefaction effect and the variations of the predominant factors influence the relative importance various phenomena on the flow and heat transfer as the characteristic length decreases. They concluded that due to the high surface to volume ratio in microchannel flows, factors which are related to the surface area become more important and even dominant over factors related to the volume effect among which are (a) surface friction induced flow compressibility, which makes the fluid velocity profiles flatter and leads to higher friction factors and Nusselt numbers, (b) surface roughness which is likely responsible for the early transition from laminar to turbulent flow and increased friction factor and Nusselt number, (c) other surface related effects which include the axial heat conduction in the channel wall and the surface geometry. They also concluded that the discrepancies among different friction factor and heat transfer correlations proposed by various investigators might be, at least in part, attributed to the uncertainties of the experimental data.

Papautsky et al. [55] compiled a comprehensive study of the results of microscale single-phase internal flow. The only definite conclusion that they reached from the

currently available data was that the slip-flow gas data indicated an approximately 60% reduction in friction factor compared to macroscale theory at the same Reynolds number. They concluded that the currently available experimental data for other types of flows were inconclusive as they appear both above and below the theoretical predictions. They attributed these results to roughness of the channels, to uncertainty in the determination of channel dimensions, and to the lack of a well-controlled surface structure, as the bonding of silicon and glass was the predominant method for microchannel fabrication. They made some preliminary conclusions regarding non-slip fluid flows such as; microchannel surface appeared to increase friction factor, laminar friction constant appeared to be approximately 20% higher that the theoretical predictions for flow of water, and some data seemed to suggest lower transition Reynolds number. They reported that, there is a clear need for additional experimental investigations over a wider Reynolds number range using microchannels with well-characterized dimensions and surface roughness, and well designed experimental methods in order to understand microscale single-phase internal fluid flow.

More information on various topics of Steady State and Transient, Single Phase, Two Phase, Microchannel Heat Transfer, Microscale and Nanoscale Phenomena, Microfluidics Applications, Computational Methods, Heat Pipes, Heat Exchanger Applications, Microscale Heat Transfer at Low Temperature and Some Biomedical Applications among others can be found in the proceedings of NATO-ASI on Microscale Heat Transfer- Fundamentals and Applications in Biological and MEMS [56].

CHAPTER 3

SINGLE PHASE HEAT TRANSFER IN MICROTUBES WITHOUT VISCOUS DISSIPATION

3.1. Introduction

In this section, heat transfer analysis of hydrodynamically developed and thermally developing single phase laminar flow of a viscous fluid in microtubes is performed. The thermo-physical properties are assumed to be constant. Viscous dissipation term is neglected. The momentum equation is solved analytically to determine the fully developed velocity profile. Substituting the fully developed velocity profile, energy equation is solved by using numerical methods for constant wall temperature and constant wall heat flux thermal boundary conditions for slip-flow regime, which is the flow regime for most of the gaseous flows in microchannels.

3.2. Fully Developed Velocity Distribution in Microtubes

The geometry of the problem considered in this section is shown in Figure 3.1. The coordinate system is located at the center of the microtube. There is an unheated section at the inlet to be able to have a fully developed velocity profile.

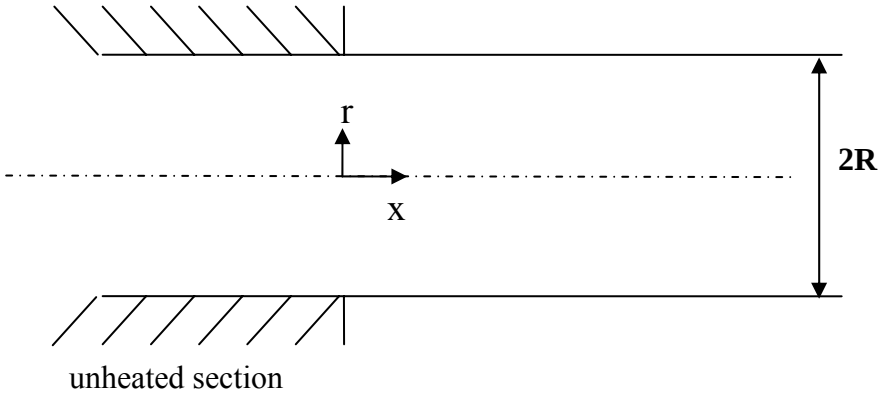

Figure 3.1. The Geometry of the Microtube Problem

For the flow conditions considered, the governing equations can be written as [57],

Continuity:

$$\frac{1}{r}\frac{\partial(rv)}{\partial r}+\frac{\partial u}{\partial x}=0 \tag{3.1}$$

Momentum equations:

x-component:

$$u\frac{\partial u}{\partial x}+v\frac{\partial u}{\partial r}=-\frac{1}{\rho}\frac{\partial p}{\partial x}+\nu\left(\frac{1}{r}\frac{\partial}{\partial r}\left(r\frac{\partial u}{\partial r}\right)+\frac{\partial^2 u}{\partial x^2}\right) \tag{3.2}$$

r-component:

$$u\frac{\partial v}{\partial x}+v\frac{\partial v}{\partial r}=-\frac{1}{\rho}\frac{\partial p}{\partial r}+\nu\left\{\frac{\partial}{\partial r}\left(\frac{1}{r}\frac{\partial(rv)}{\partial r}\right)+\frac{\partial^2 v}{\partial x^2}\right\} \tag{3.3}$$

where u and v are the velocity components in x and r directions, respectively.

For steady and fully developed flow $u = u(r)$, and the velocity component v is zero everywhere. Therefore; continuity equation, Eq. (3.1) is satisfied identicaly and the Navier-Stokes Equations, Eqs. (3.2) and (3.3) reduce to

$$-\frac{1}{\rho}\frac{\partial p}{\partial x}+\nu\frac{d^2u}{dr^2}=0 \tag{3.4}$$

$$-\frac{1}{\rho}\frac{\partial p}{\partial r}=0 \tag{3.5}$$

From Eq. (3.5), it is concluded that the pressure, p must be constant across any section perpendicular to flow (i.e. $p = p(x)$ only). Hence, Eq. (3.4) can be written as;

$$\frac{dp}{dx}=\mu\frac{d^2u}{dr^2} \tag{3.6}$$

Since the left hand side of the Eq. (3.6) is function of x only and the right hand side is function of r only, the only possible solution, both should be equal to a constant.

$$\frac{dp}{dx}=const.=-\frac{\Delta P}{L} \tag{3.7}$$

where ΔP is pressure drop over a length L of the tube. Hence, Eq.(3.6) becomes,

$$\frac{d^2u}{dr^2}=-\frac{\Delta P}{\mu L} \tag{3.8}$$

Eq. (3.8) is the ordinary differential equation to be solved to determine the fully developed velocity profile with the appropriate boundary conditions given below,

$$r = 0 \quad u = finite \tag{3.9-a}$$

$$r = R \quad u = U_s \tag{3.9-b}$$

where U_s is the slip velocity, which is defined as, by taking $F_m=1$ in Eq. (1.3),

$$U_s = -\lambda\left(\frac{du}{dr}\right)_{r=R} \tag{3.10}$$

where λ is the mean free path.

Integrating the Eq. (3.8) twice yields,

$$u(r) = -\frac{1}{\mu}\frac{\Delta P}{L}\frac{r^2}{4} + c_1 \ln r + c_2 \tag{3.11}$$

Applying the boundary conditions, c_1 and c_2 can be determined. Substituting c_1 and c_2 into the Eq. (3.11) yields,

$$u(r) = \frac{1}{4\mu}\frac{\Delta P}{L}(R^2 - r^2 + 4KnR^2) \tag{3.12}$$

Using the definition of the mean velocity for an incompressible fluid [57], the velocity profile can be represented in terms of the mean velocity yields,

$$\frac{u}{u_m} = \frac{2(1-(\frac{r}{R})^2) + 8Kn}{1+8Kn} \tag{3.13}$$

Defining dimensionless radius as,

$$\eta = \frac{r}{R} \tag{3.14}$$

Eq. (3.13) can be written as,

$$\frac{u}{u_m} = \frac{2(1-\eta^2)+8Kn}{1+8Kn} \tag{3.15}$$

Velocity profile also depends on the Knudsen number. Note that, by setting *Kn=0* Eq. (3.15) is identical to the fully developed velocity profile of a flow in a macrotube, which is

$$\frac{u}{u_m} = 2(1-\eta^2) \tag{3.16}$$

The terms containing Knudsen number in Eq. (3.15) introduce the slip velocity at the wall.

The fully developed velocity profile is plotted as a function of η and Kn number in Figure 3.2. Kn number changes between 0 and 0.1. Kn=0 represents the flow in macrotubes, and Kn=0.1 is the applicability limit of the slip flow theory. As seen from the figure, as rarefaction increases (i.e. Kn number increases), the slip at the wall increases from zero for Kn=0 to 0.444 for Kn=0.1. This increase in the slip velocity leads to a decrease in the gradient of the velocity at the wall, which is the reason for the reduction in the friction factor in gaseous flows in microchannels. As Kn number increases from 0 to 0.1, the maximum dimensionless velocity located at the center, decreases from 2.000 for Kn=0 to 1.556 for Kn=0.1.

The location where the velocity is equal to mean velocity (i.e. $u=u_m$) is independent of Kn number. The location of that point can be determined by equating Eq. (3.15) to unity. This independence is seen as a knot point in the graph, which is around $\eta=0.7$.

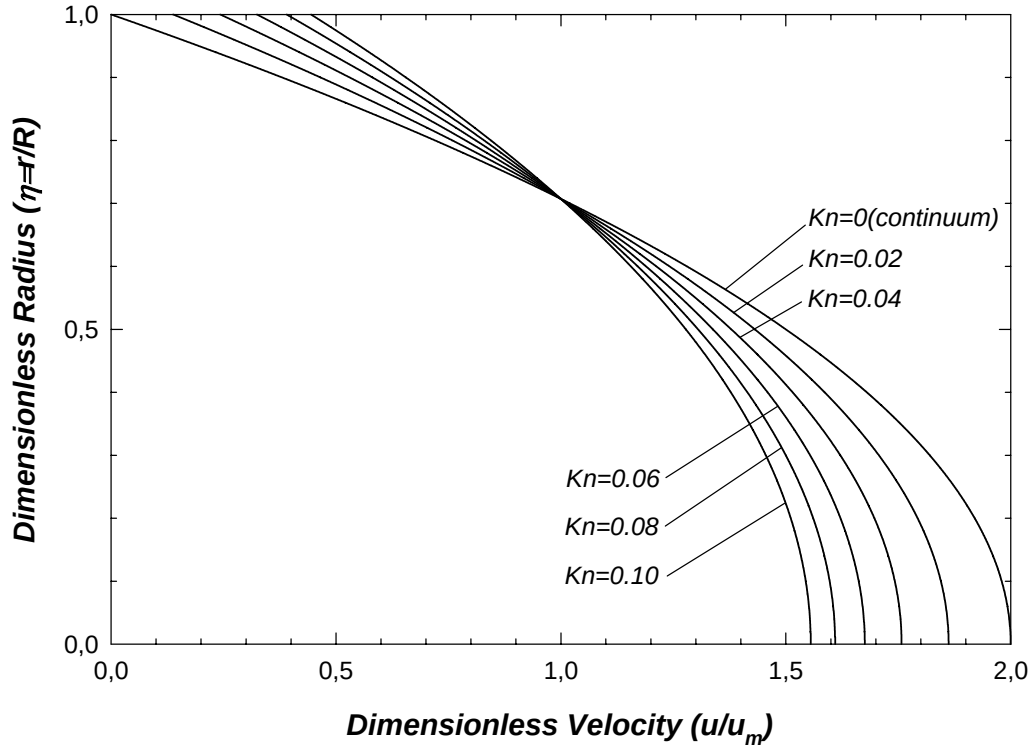

Figure 3.2. Fully Developed Velocity Profile Inside a Microtube

3.3. Heat Transfer Analysis

3.3.1. Formulation

Two dimensional energy equation in cylindrical coordinates with constant properties, negligible axial conduction and negligible viscous dissipation term can be written as [57];

$$u\frac{\partial T}{\partial x}=\frac{\alpha}{r}\frac{\partial}{\partial r}\left(r\frac{\partial T}{\partial r}\right) \tag{3.17}$$

The case of constant wall temperature, boundary conditions are,

$$\text{at } r = R \qquad T = T_s \tag{3.18-a}$$

$$\text{at } \ r = 0 \qquad \frac{\partial T}{\partial r} = 0 \tag{3.18-b}$$

$$\text{at } \ x = 0 \qquad T = T_i \tag{3.18-c}$$

where T_i and T_s are the temperatures of the gas at the inlet and at the surface, respectively.

In the case of constant wall heat flux, boundary conditions are,

$$\text{at } r = R \qquad \frac{\partial T}{\partial r} = \frac{q''}{k} \tag{3.19-a}$$

$$\text{at } \ r = 0 \qquad \frac{\partial T}{\partial r} = 0 \tag{3.19-b}$$

$$\text{at } \ x = 0 \qquad T = T_i \tag{3.19-c}$$

The energy equation is non-dimensionalized by the following dimensionless quantities,

$$\theta = \frac{T - T_w}{T_i - T_w} \quad \text{(for constant wall temperature)} \tag{3.20-a}$$

$$\theta = \frac{T - T_i}{q'' R / k} \quad \text{(for constant wall heat flux)} \tag{3.20-b}$$

$$\eta = \frac{r}{R} \tag{3.20-c}$$

$$\xi = \frac{x}{R \,\mathrm{Re}\,\mathrm{Pr}} \tag{3.20-d}$$

$$\bar{u} = \frac{u}{u_m} \tag{3.20-e}$$

Introducing the dimensionless quantities, Eqs (3.24-a) through (3.24-e) the energy equation becomes,

$$\frac{\bar{u}}{2}\frac{\partial\theta}{\partial\xi} = \frac{\partial^2\theta}{\partial\eta^2} + \frac{1}{\eta}\frac{\partial\theta}{\partial\eta} \tag{3.21}$$

Using the dimensionless quantities, Eqs. (3.20-a) through (3.20-e) and the temperature jump boundary condition, Eq. (1.5), the boundary conditions for constant wall temperature become,

$$\text{at } \eta = 1 \qquad \theta = -2\kappa Kn\left(\frac{\partial\theta}{\partial\eta}\right)_{\eta=1} \tag{3.22-a}$$

$$\text{at } \eta = 0 \qquad \frac{\partial\theta}{\partial\eta} = 0 \tag{3.22-b}$$

$$\text{at } \xi = 0 \qquad \theta = 1 \tag{3.22-c}$$

$$\text{where} \quad \kappa = \frac{2 - F_T}{F_T}\frac{2\gamma}{\gamma + 1}\frac{1}{\mathrm{Pr}} \tag{3.23}$$

The boundary conditions for the constant wall heat flux case,

$$\text{at } \eta = 1 \qquad \frac{\partial\theta}{\partial\eta} = 1 \tag{3.24-a}$$

$$\text{at } \eta = 0 \qquad \frac{\partial\theta}{\partial\eta} = 0 \tag{3.24-b}$$

$$\text{at } \xi = 0 \qquad \theta = 0 \tag{3.24-c}$$

Local heat transfer coefficient is written as,

$$h_x = -\frac{k}{(T_m - T_w)}(\frac{\partial T}{\partial r})_{r=R} \tag{3.25}$$

Introducing dimensionless quantities into Eq. (3.25), the Nusselt number is determined for constant wall temperature as,

$$Nu_x = \frac{h_x D}{k} = -\frac{2(\frac{\partial \theta}{\partial \eta})_{\eta=1}}{\theta_m} \tag{3.26}$$

Introducing dimensionless quantities and the temperature jump boundary condition, Eq. (1.5) into the Eq. (3.25), the Nusselt number is determined for constant wall heat flux as,

$$Nu_x = \frac{h_x D}{k} = \frac{2}{\theta_m - \theta_s - 2\kappa Kn} \tag{3.27}$$

where θ_m is the dimensionless mean temperature, and it is defined as,

$$\theta_m = 2\int_0^1 (\frac{u}{u_m})\theta(\eta,\xi)\eta d\eta \tag{3.28}$$

To determine the local Nusselt number, the energy equation, Eq. (3-21) should be solved with indicated boundary conditions to obtain the temperature distribution. The energy equation, Eq. (3-21) is a well-known second order partial diferrential equation, which has solutions for both constant wall temperature and constant wall heat flux cases for flows in macrochannels (i.e. *Kn=0*) [57]. However, for flows in microchannels, there are additional terms in the fully developed velocity profile and at the wall thermal boundary conditions. These extensions in the problem introduce some difficulties in the analytical solution. Although the analytical solution was

obtained for constant wall temperature [3, 30, 36] and for constant wall heat flux [29, 33, 36] cases for flow in microchannels; with some further extensions such as; variation of thermophysical properties, compressibility, the effect of axial conduction etc., analytical solution can become unachievable. Therefore, using numerical methods for the solution of this partial differential equation is an appropriate way to handle these difficulties, and improve the solution for further extensions in the problem.

3.3.2. Numerical Solution

The energy equation, Eq (3.21) is a second order partial differential equation. The momentum equation and energy equation are decoupled, since the thermo-physical properties are assumed to be constant. So, the coefficients of the algebraic form of differential equation will be constant for a predescribed location in the domain. The boundaries of the solution domain are regular, since it is the interior region of a microtube. The most convenient way to solve a partial differential equation with these conditions is the finite difference scheme due to its simplicity for regular boundaries and constant coefficients.

The finite difference scheme divides the solution domain into nodes as shown in Figure 3.3. The underlying partial differential equation is written for each of these nodes. Finite-difference approximations are then substituted for the derivatives to convert the equations to an algebraic form [58].

The energy equation is a steady state problem. It is not bounded in the increasing x-direction. But, from the physics of the problem, it is known that the temperature of the fluid reaches the wall temperature as x goes to infinity. By introducing this aspect, the energy equation becomes a boundary value problem. Therefore, the energy equation is characterized as an elliptic partial differential equation.

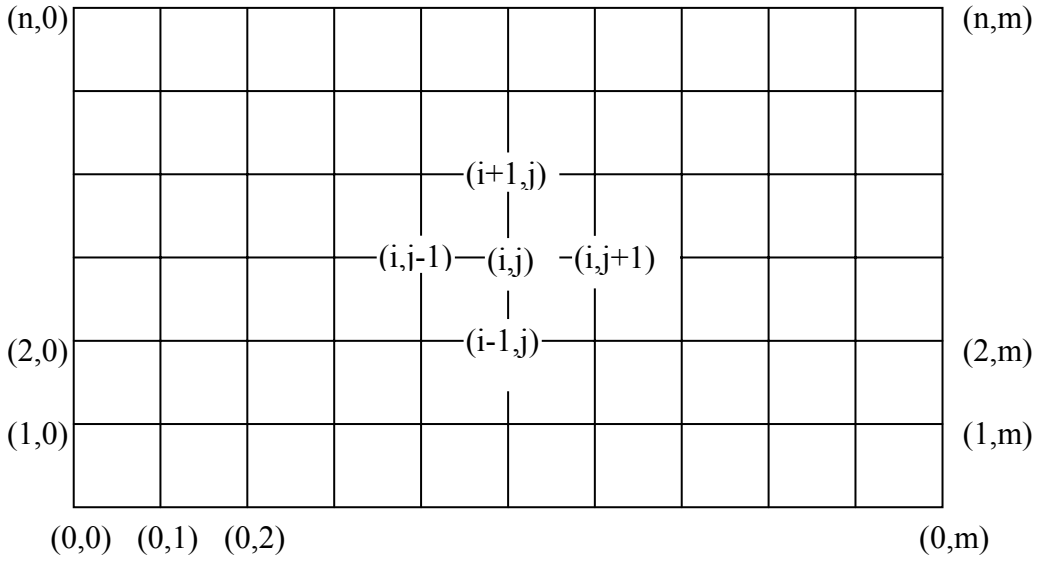

Figure 3.3. Solution Domain of the Problem

The solution of the elliptic partial differential equations includes the simultaneous solution of algebraic equations either by implicit or explicit methods. Explicit method includes matrix inversion procedure. Matrix inversion procedure can be problematic for large matrixes. Implicit methods include some iterative procedures in which convergence needs to be controlled. Not to face up with these problems, the steady state problem is transformed into a transient problem (i.e. elliptic partial differential equation is transformed into a parabolic differential equation) as follows;

$$\frac{\partial\theta}{\partial\tau}+\frac{\bar{u}}{2}\frac{\partial\theta}{\partial\xi}=\frac{\partial^2\theta}{\partial\eta^2}+\frac{1}{\eta}\frac{\partial\theta}{\partial\eta} \tag{3.29}$$

By defining the dimensionless time as,

$$\tau = \frac{\alpha t}{R^2} \tag{3.30}$$

Solution of the parabolic differential equations includes the evaluation of the property of a node for the next time step by substituting the previous time step properties of the related nodes. As time goes to infinity, the solution also reaches the steady state solution, which is the desired solution of the elliptic differential equation, Eq. (3.21). Since, the solution procedure of the parabolic differential equation also includes numerical methods, it has also a stability problem which can be handled easily, which is mentioned in the foregoing sections.

To initiate the substitution process of the parabolic differential equation, an initial value should be assigned. To fasten the solution procedure to obtain the steady state results, expected steady state temperature distribution can be the initial value of the differential equation, since the parabolic differential equations reach their steady state solutions independent of their initial value [58]. But, to obtain the solution of the transient problem, the temperature in the domain at $t=0$ is assigned as the inlet temperature of the fluid for this study.

In spite of fastening the solution procedure of the parabolic partial differential equation, computation time can be as long as the computation time of the elliptic differential equation; but surely, it is a simple, non-problematic algorithm by satisfying the required stability criteria. The advantage of solving the parabolic partial differential equation instead of the elliptic partial differential equation is the simplicity.

Introducing the dimensionless time also, the initial and the boundary conditions of the transient energy equation, Eq. (3.29) become,

$$\text{at } \tau = 0 \qquad \theta = 1 \tag{3.31-a}$$

$$\text{at } \eta = 1 \qquad \theta = -2\kappa Kn\left(\frac{\partial \theta}{\partial \eta}\right)_{\eta=1} \tag{3.31-b}$$

$$\text{at } \eta = 0 \qquad \frac{\partial \theta}{\partial \eta} = 0 \tag{3.31-c}$$

$$\text{at } \xi = 0 \qquad \theta = 1 \tag{3.31-d}$$

for constant wall temperature; and,

$$\text{at } \tau = 0 \qquad \theta = 0 \tag{3.32-a}$$

$$\text{at } \eta = 1 \qquad \frac{\partial \theta}{\partial \eta} = 1 \tag{3.32-b}$$

$$\text{at } \eta = 0 \qquad \frac{\partial \theta}{\partial \eta} = 0 \tag{3.32-c}$$

$$\text{at } \xi = 0 \qquad \theta = 0 \tag{3.32-d}$$

for constant wall heat flux boundary condition.

For the calculation of the Nusselt number, the first derivative at the wall for the constant wall temperature case, and the dimensionless mean temperature for both cases should be computed. The derivative at the wall is computed by using same finite difference approximation that is used in the discretization of the Eq. (3.29). The evaluation of the dimensionless mean temperature needs the computation of the integral given by Eq. (3.28), which is computed numerically by using Simpson' s 1/3 rule [58].

3.3.2.1. Domain Discretization

The solution domain is divided into finite number of meshes as shown in Figure 3.3. The nodes are located at the corners of the meshes. Due to the symmetry of the

solution domain, only one half of the solution domain is considered. For constant wall temperature case, 100x100 grids; and for constant wall heat flux case, 250x250 grids which are distributed uniformly in the radial and longitudinal directions are used for the computation. The solution domain is bounded in the radial direction, but open ended in the longitudinal direction. It is known from the physics of the problem that flow becomes thermally fully developed beyond an axial location. Beyond this location, there is no need to find the temperature distribution. Therefore, a reasonable value for the length of the tube which allows the flow to be thermally fully developed, is assigned. For these two boundary conditions, the length of the tube is assigned as the dimensionless longitudinal coordinate, $\xi=1$.

3.3.2.2. Equation Discretization

Discretization of the Eq. (3.29) and the related boundary conditions requires second and first derivatives in space and first derivative in time. Centered, forward and backward $o(h^2)$ finite-divided differences are used to approximate the space derivatives depending on the location of the node; only forward finite difference is used to approximate the time derivative. The approximate derivatives are given below;

$$\frac{\partial^2\theta}{\partial\eta^2}=\frac{-\theta^k_{i+3,j}+4\theta^k_{i+2,j}-5\theta^k_{i+1,j}+2\theta^k_{i,j}}{(\Delta\eta)^2} \quad \text{(forward)} \qquad (3.33\text{-a})$$

$$\frac{\partial^2\theta}{\partial\eta^2}=\frac{2\theta^k_{i,j}-5\theta^k_{i-1,j}+4\theta^k_{i-2,j}-\theta^k_{i-3,j}}{(\Delta\eta)^2} \quad \text{(backward)} \qquad (3.33\text{-b})$$

$$\frac{\partial^2\theta}{\partial\eta^2}=\frac{\theta^k_{i+1,j}-2\theta^k_{i,j}+\theta^k_{i-1,j}}{(\Delta\eta)^2} \quad \text{(central)} \qquad (3.33\text{-c})$$

$$\frac{\partial\theta}{\partial\eta}=\frac{-\theta^k_{i+2,j}+4\theta^k_{i+1,j}-3\theta^k_{i,j}}{2\Delta\eta} \quad \text{(forward)} \qquad (3.33\text{-d})$$

$$\frac{\partial \theta}{\partial \eta} = \frac{3\theta_{i,j}^{k} - 4\theta_{i-1,j}^{k} + \theta_{i-2,j}^{k}}{2\Delta\eta} \quad \text{(backward)} \quad \text{(3.33-e)}$$

$$\frac{\partial \theta}{\partial \eta} = \frac{\theta_{i+1,j}^{k} - \theta_{i-1,j}^{k}}{2\Delta\eta} \quad \text{(central)} \quad \text{(3.33-f)}$$

$$\frac{\partial \theta}{\partial \xi} = \frac{-\theta_{i,j+2}^{k} + 4\theta_{i,j+1}^{k} - 3\theta_{i,j}^{k}}{2\Delta\xi} \quad \text{(forward)} \quad \text{(3.33-g)}$$

$$\frac{\partial \theta}{\partial \xi} = \frac{3\theta_{i,j}^{k} - 4\theta_{i,j-1}^{k} + \theta_{i,j-2}^{k}}{2\Delta\xi} \quad \text{(backward)} \quad \text{(3.33-h)}$$

$$\frac{\partial \theta}{\partial \xi} = \frac{\theta_{i,j+1}^{k} - \theta_{i,j-1}^{k}}{2\Delta\xi} \quad \text{(central)} \quad \text{(3.33-i)}$$

$$\frac{\partial \theta}{\partial \tau} = \frac{\theta_{i,j}^{k+1} - \theta_{i,j}^{k}}{\Delta\tau} \quad \text{(forward)} \quad \text{(3.33-j)}$$

where *i* denotes the radial location, *j* denotes the longitudinal location and *k* denotes the location in time.

In forward and backward differencing formulas, three nodes are used in order to reach the same order of accuracy as the central differencing formula.

3.3.2.2.1. Nodes at the Interior Region

For an interior node, central differences for space; Eqs (3.33-c), (3.33-f), (3.33-i) and forward difference for time, Eq. (3.33-j) are substituted into the energy equation, Eq. (3.29). The algebraic form of the energy equation becomes;

$$\theta_{i,j}^{k+1} = \theta_{i,j}^{k} + C_1(\theta_{i+1,j}^{k} - 2\theta_{i,j}^{k} + \theta_{i-1,j}^{k}) + C_2 \frac{1}{\eta_i}(\theta_{i+1,j}^{k} - \theta_{i-1,j}^{k}) - C_3\overline{u}(\eta_i)(\theta_{i,j+1}^{k} - \theta_{i,j-1}^{k}) \quad (3.34)$$

where C_1, C_2, C_3 are the coefficients and defined as,

$$C_1 = \frac{\Delta\tau}{(\Delta\eta)^2} \tag{3.35}$$

$$C_2 = \frac{\Delta\tau}{2\Delta\eta} \tag{3.36}$$

$$C_3 = \frac{\Delta\tau}{4\Delta\xi} \tag{3.37}$$

and $\overline{u}(\eta)$ is the dimensionless fully developed velocity profile, given by Eq. (3.15).

3.3.2.2.2. Nodes at the Inlet

The temperature of an inlet node is prescribed, which is the boundary condition.

$$\theta_{0,j}^{k+1} = 1 \tag{3.38-a}$$

$$\theta_{0,j}^{k+1} = 0 \tag{3.38-b}$$

which are for constant wall temperature and constant wall heat flux cases, respectively.

3.3.2.2.3. Nodes at the Exit

For an exit node, central differences in radial direction, Eqs. (3.33-c), (3.33-f), backward difference in longitudinal direction, Eq. (3.33-h) and forward difference in time, Eq. (3.33-j) are substituted into the energy equation, Eq. (3.29). The algebraic form of the energy equation becomes;

$$\theta_{i,j}^{k+1} = \theta_{i,j}^{k} + C_1(\theta_{i+1,j}^{k} - 2\theta_{i,j}^{k} + \theta_{i-1,j}^{k}) + C_2\frac{1}{\eta_i}(\theta_{i+1,j}^{k} - \theta_{i-1,j}^{k})$$
$$-C_3 u^*(\eta_i)(3\theta_{i,j}^{k} - 4\theta_{i,j-1}^{k} + \theta_{i,j-2}^{k}) \tag{3.39}$$

where C_1, C_2, C_3 are the coefficients that are given in Eqs. (3.35), (3.36) and (3.37).

3.3.2.2.4. Nodes at the Centerline

For a centerline node, central differences in longitudinal direction, Eq. (3.33-i), forward difference in time, Eq. (3.33-j) are substituted into the energy equation, Eq. (3.29). For the second derivative in radial direction, following approximation is used;

$$\frac{\partial^2\theta}{\partial\eta^2} = \frac{\theta^k_{1,j} - 2\theta^k_{0,j} + \theta^k_{-1,j}}{(\Delta\eta)^2} \tag{3.40}$$

where $\theta^k_{-1,j}$ is a fictitious quantity and is equal to $\theta^k_{1,j}$ due to the symmetry of the solution domain. Thus Eq. (3.40) becomes,

$$\frac{\partial^2\theta}{\partial\eta^2} = \frac{2(\theta^k_{1,j} - \theta^k_{0,j})}{(\Delta\eta)^2} \tag{3.41}$$

At the center, first derivative term becomes indetermined, therefore limit of this term should be calculated. By using l' Hospital' s rule, it can be approximated as,

$$\lim_{\eta\to 0}\frac{1}{\eta}\frac{\partial\theta}{\partial\eta} = \frac{\partial^2\theta}{\partial\eta^2} = \frac{2(\theta^k_{1,j} - \theta^k_{0,j})}{(\Delta\eta)^2} \tag{3.42}$$

Substituting Eqs. (3.33-i), (3.33-j), (3.41), (3.42) into energy equation, Eq. (3.29), the algebraic form of the energy equation becomes;

$$\theta^{k+1}_{i,j} = \theta^k_{i,j} + 4C_1(\theta^k_{1,j} - \theta^k_{0,j}) - C_3 u^*(\eta_0)(\theta^k_{0,j+1} - \theta^k_{0,j-1}) \tag{3.43}$$

where C_1, C_3 are the coefficients that are given in Eqs. (3.35) and (3.37).

3.3.2.2.5. Nodes at the Boundary

Since thermal wall boundary conditions are different for constant wall temperature and constant wall heat flux cases, the discretization at the boundaries are discussed in different sections for these two cases.

3.3.2.2.5.1. Constant Wall Temperature

Boundary condition at the wall, Eq. (3.31-a) should be discretised for a boundary node. Boundary condition includes the first derivative in radial direction. Since there is no node in the forward direction, backward differencing is used to approximate the first derivative. By substituting the Eq. (3.33-c) into the Eq. (3.31-a), the algebraic form of the boundary condition becomes,

$$\theta_{n,j} = \kappa \frac{4\theta_{n-1,j} - \theta_{n-2,j}}{2\Delta\eta(1 + \frac{3\kappa}{2\Delta\eta})} \tag{3.44}$$

It should be noted that, when $\kappa=0$, dimensionless temperature becomes zero, which means no temperature jump at the wall (i.e. flow in macrotubes).

Substituting Eq. (3.44) into the Eq. (3.34), the algebraic form of the energy equation for a node near the wall which includes the effect of the boundary condition for the constant wall temperature case becomes,

$$\theta_{n-1,j}^{k+1} = \theta_{n-1,j}^{k} + C_1(\kappa \frac{4\theta_{n-1,j}^{k} - \theta_{n-2,j}^{k}}{2\Delta\eta(1+\frac{3\kappa}{2\Delta\eta})} - 2\theta_{n-1,j}^{k}$$
$$+\theta_{n-2,j}^{k}) + C_2 \frac{1}{\eta_i}(\kappa \frac{4\theta_{n-1,j}^{k} - \theta_{n-2,j}^{k}}{2\Delta\eta(1+\frac{3\kappa}{2\Delta\eta})} - \theta_{n-2,j}^{k}) - C_3 u^*(\eta_i)(\theta_{i,j+1}^{k} - \theta_{i,j-1}^{k}) \quad (3.45)$$

where C_1, C_2, C_3 are the coefficients that are given in Eqs. (3.35), (3.36) and (3.37).

3.3.2.2.5.2. Constant Wall Heat Flux

Boundary condition at the wall, Eq. (3.32-a) should be discretised for a boundary node. Boundary condition includes the first derivative in radial direction. Since there is no node in the forward direction, backward differencing is used to approximate the first derivative. By substituting the Eq. (3.33-c) into the Eq. (3.32-a), the algebraic form of the boundary condition becomes,

$$\theta_{n,j} = \frac{2\Delta\eta + 4\theta_{n-1,j} - \theta_{n-2,j}}{3} \quad (3.46)$$

Substituting Eq. (3.46) into the Eq. (3.29), the algebraic form of the energy equation for a node near the wall which includes the effect of the boundary condition for the constant wall temperature case becomes,

$$\theta_{n-1,j}^{k+1} = \theta_{n-1,j}^{k} + C_1(\frac{2\Delta\eta + 4\theta_{n-1,j} - \theta_{n-2,j}}{3} - 2\theta_{n-1,j}^{k}$$
$$+\theta_{n-2,j}^{k}) + C_2 \frac{1}{\eta_i}(\frac{2\Delta\eta + 4\theta_{n-1,j} - \theta_{n-2,j}}{3} - \theta_{n-2,j}^{k}) - C_3 u^*(\eta_i)(\theta_{i,j+1}^{k} - \theta_{i,j-1}^{k}) \quad (3.47)$$

where C_1, C_2, C_3 are the coefficients that are given in Eqs. (3.35), (3.36) and (3.37).

3.3.2.3. Stability and Convergence

In the solution of the parabolic partial differential equation, step size in time is a critical choice to obtain a stable solution. The step size in time should satisfy the stability criterian for stable solution [58]. It can be written as,

$$C_1 < \frac{1}{2} \tag{3.48}$$

where C_1 is the coefficient that is given in Eq. (3.35).

It has been observed that by choosing a proper value for $\Delta\tau$, a stable solution is reached; otherwise the numerical solution diverges. By trial and error, it is determined that

$$\Delta\tau = 0.4\Delta\eta^2 \tag{3.49}$$

is a safe choice for this study to obtain a stable solution.

This numerical calculation is open ended in the time domain, so a convergence criterian is needed to stop the computation. For this study, the convergence criterian is that the difference between the two fully developed Nu values of two successive time steps, is less than 10^{-3}. To satisfy this criterian, dimensionless time is chosen as $\tau = 2$ for constant wall temperature and $\tau = 4$ for constant wall heat flux cases, respectively. The mesh sizes are chosen in order to get sufficiently accurate Nusselt value for the flows in macrochannels (i.e. Kn = 0), which have available analytical solutions [57].

3.4. Results and Discussion

The dimensionless transient temperature distribution inside a microtube is determined by solving the Eq. (3.29) numerically with the appropriate boundary conditions. Once the dimensionless temperature distribution is determined, local Nusselt number, being the main interest of the heat transfer problems, is determined as a function of dimensionless axial coordinate and dimensionless time from Eqs. (3.26) and (3.27) for different Kn number values. Since, the slip flow modelling is valid for Kn<0.1, analysis is done for Kn =0, 0.02, 0.04, 0.06, 0.08, 0.10. Notice that, Kn =0 is the no-slip condition (i.e. flow in macrochannels), which is the validification of the accuracy of the numerical solution.

It is clear from the formulation that temperature distributions in slip-flow regime are functions of Kn number and the parameter κ. Kn number includes the effect of rarefaction and the parameter κ includes the effect of gas and surface properties. κ =0 and κ =10 are two limiting cases of this study as stated Larrode et al [3]. κ =0 is a fictitious, but a useful case to observe the effect of slip velocity without temperature jump on heat transfer. κ =10 is the other limit, which accounts for a very large temperature jump at the wall. κ =1.667 is the typical value for air, which is the working fluid for various engineering applications. Dimensionless fully developed temperature distribution and local Nu numbers are plotted for different Kn number and κ values for constant wall temeprature and constant wall heat flux boundary condition cases.

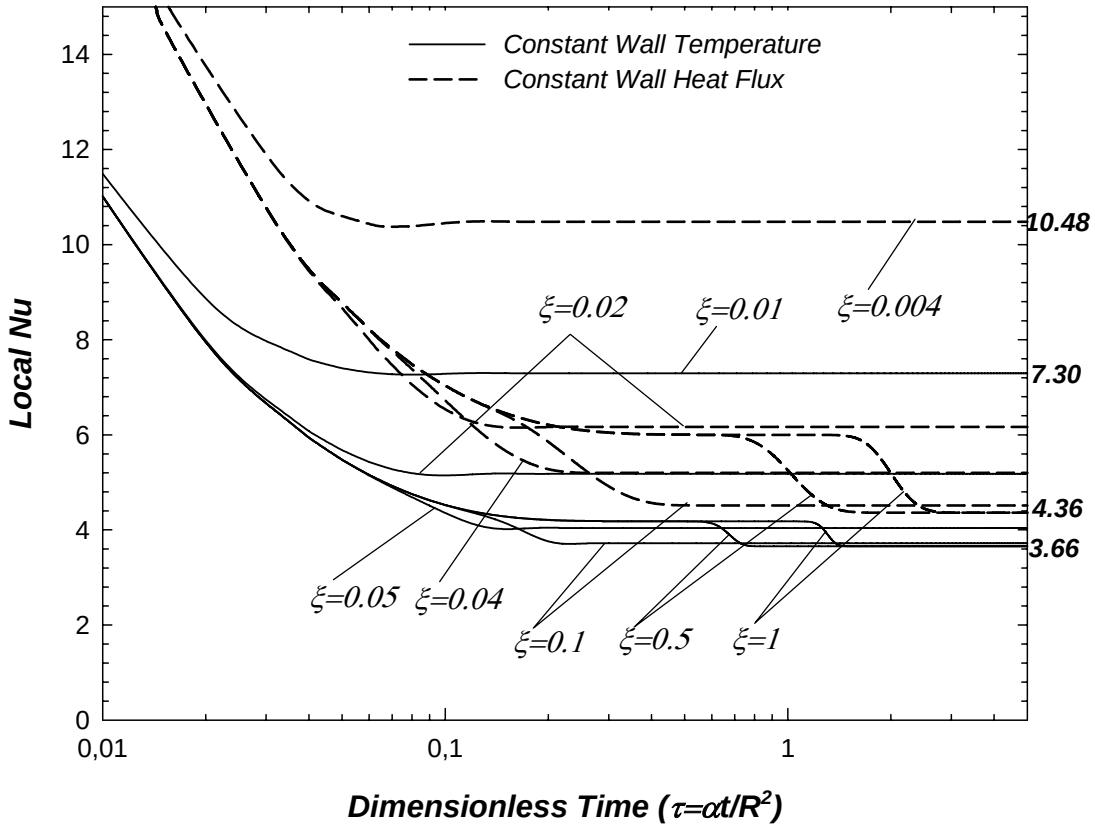

Figure 3.4. Variation of Local Nu with Dimensionless Time
at Different Axial Locations, Microtube (Kn =0)

Figure 3.4. shows the variation of local Nu with dimensionless time, τ at different axial locations, for Kn =0 for both constant wall temperature and constant wall heat flux cases. After sufficiently long time, Nu number values reach to a steady-state value which is 3.66 for constant wall temperature, and 4.36 for constant wall heat flux cases. As the dimensionless axial coordinate, ξ increases, the time required to reach the steady state conditions increases. Beyond an axial location, all curves reach the same local Nu value, which is the indication of the thermal entrance region. This axial location is between ξ =0.1 and ξ =0.5 for both cases. Figure 3.4. is generated

only for Kn =0, since for different Kn number and κ values, the behavior of the curves does not change. The only differences would be the fully developed Nu values, the time required for steady state conditions, and the length of the thermal entrance region.

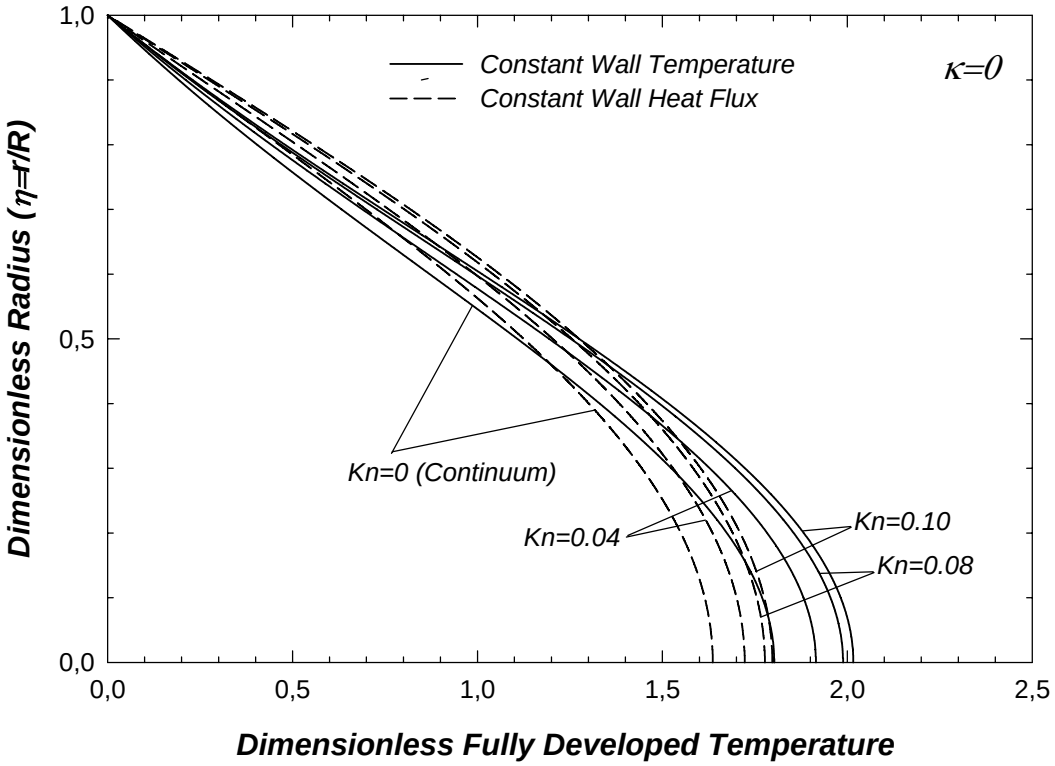

Figure 3.5. Dimensionless Fully Developed Temperature Profile as a Function of Kn Number, Microtube (κ =0)

Figures 3.5 and 3.6 show the dimensionless fully developed temperature profile as a function of Kn number for κ =0 and κ =1.667 for both constant wall tempearture and constant wall heat flux cases. From the figures, it is apparent that when Kn=0

independent of κ value, there is no temperature jump at the wall, which stands for the flow in macrochannel.

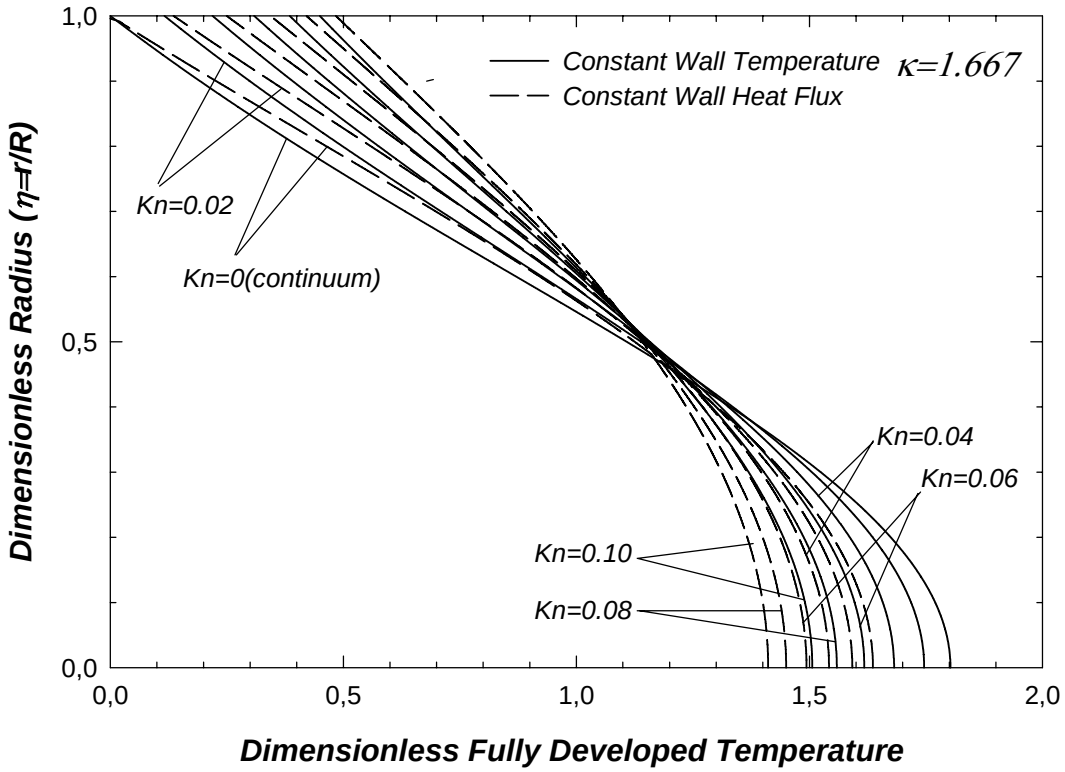

Figure 3.6. Dimensionless Fully Developed Temperature Profile as a Function of Kn Number, Microtube (κ =1.667)

For κ =0, there is no temperature jump at the wall, but there is a velocity slip at the wall due to Kn number dependence of the velocity profile, which leads to different temperature profiles for different Kn numbers. As seen from the Figure 3.5, the gradient at the wall increases for both cases, which will lead to an increase in Nu number. As rarefaction increases, the maximum dimensionless temperature located at the center, also increases from 1.803 for Kn =0 to 2.017 for Kn =0.1, which

indicates 12% increase for constant wall temperature, and from 1.636 Kn =0 to 1.797 for Kn =0.1, which indicates 9% increase for constant wall heat flux case.

For κ =1.667, temperature jump exists at the wall, and increases as rarefaction increases. Dimensionless fully developed temperature is zero at the wall for Kn =0, for both cases; and increases to 0.450 for constant wall temperature case, and 0.484 for constant wall heat flux case for Kn=0.1. Unlike κ =0 case, as rarefaction increases, the gradient at the wall decreases, and the maximum dimensionless temperature decreases for both cases. Larger values of κ will lead to more increase in temperature jump, and more decrease in maximum dimensionles temperature.

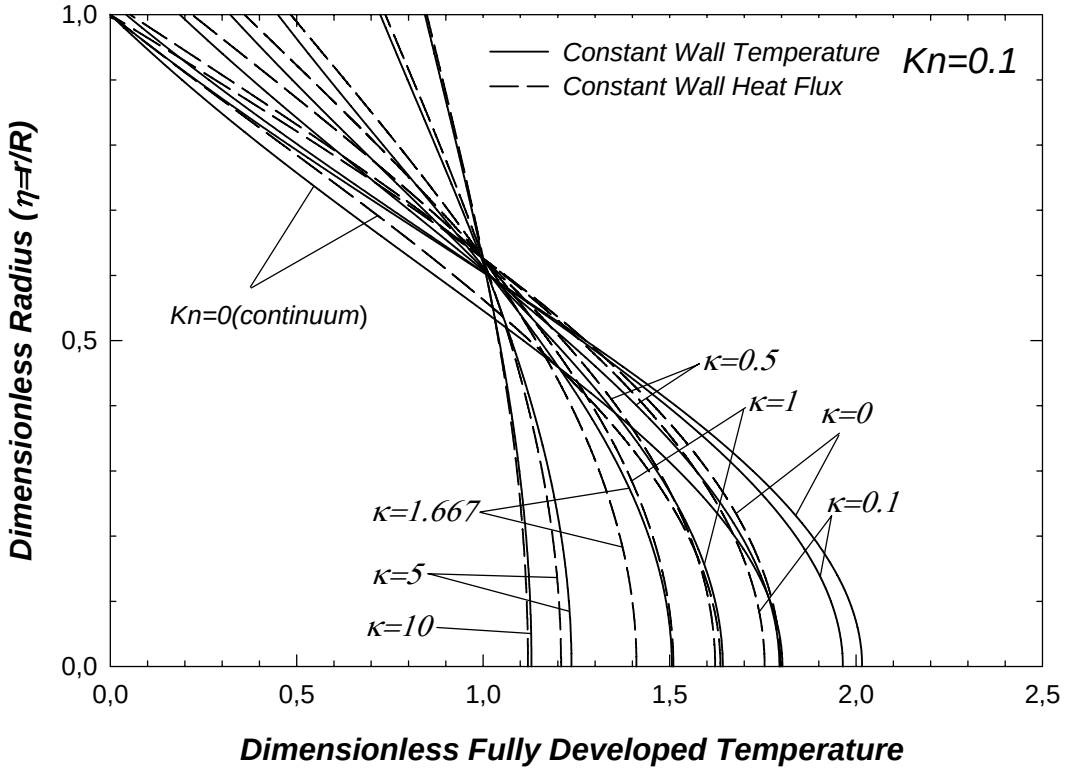

Figure 3.7. Dimensionless Fully Developed Temperature Profile as a Function of κ Parameter, Microtube (Kn=0.1)

Figure 3.7 shows the dimensionless fully developed temperature profile as a function of κ parameter for Kn =0.1 for both constant wall temperature and constant wall heat flux cases. As κ increases, the temperature jump increases; the amount of temperature jump at the wall approaches to each other for both boundary conditions, and the dimensionless fully developed temperature profile approaches to a uniform distribution for both boundary conditions. The maximum dimensionless temperature also decreases as κ increases. The decrease which is 44 % for constant wall temperature, and 36 % for constant wall heat flux, is more significant for constant wall temperature case.

Figures 3.8, 3.9 and 3.10 show the steady state results of local Nu number as a function of dimensionless axial coordinate for different Kn numbers, where κ =0 (Figure 3.8), κ =1.667 (Figure 3.9) and κ =10 (Figure 3.10) for both constant wall temperature and constant wall heat flux cases. From the figures, it can be concluded that for Kn=0, independent from the κ value, all curves reach the well known fully developed Nu of 3.66 for constant wall temperature case, and of 4.36 for constant wall heat flux case asymptotically. Furthermore, all the curves approach to a fully developed Nu value asymptotically around ξ =0.1 for constant wall temperature and ξ =0.2 for constant wall heat flux case, which means that the flow is thermally developed beyond that location.The results deviate from the continuum case by the introduction of the rarefaction, and this deviation increases with increasing rarefaction. As κ increases, the deviation from the continuum for a prescribed Kn increases.

As seen from the Figure 3.8, for the limiting case, when κ=0, our numerical results agree with the results of Barron et al [30] for constant wall temperature case. Nu number gradually increases from 3.66 to 4.38 for constant wall temperature, and from 4.36 to 5.63 for constant wall heat flux, as the Kn increases by neglecting the

temperature jump at the wall for both cases. This is the same conclusion as Barron et al [30], due to the misapplication of the temperature jump boundary condition.

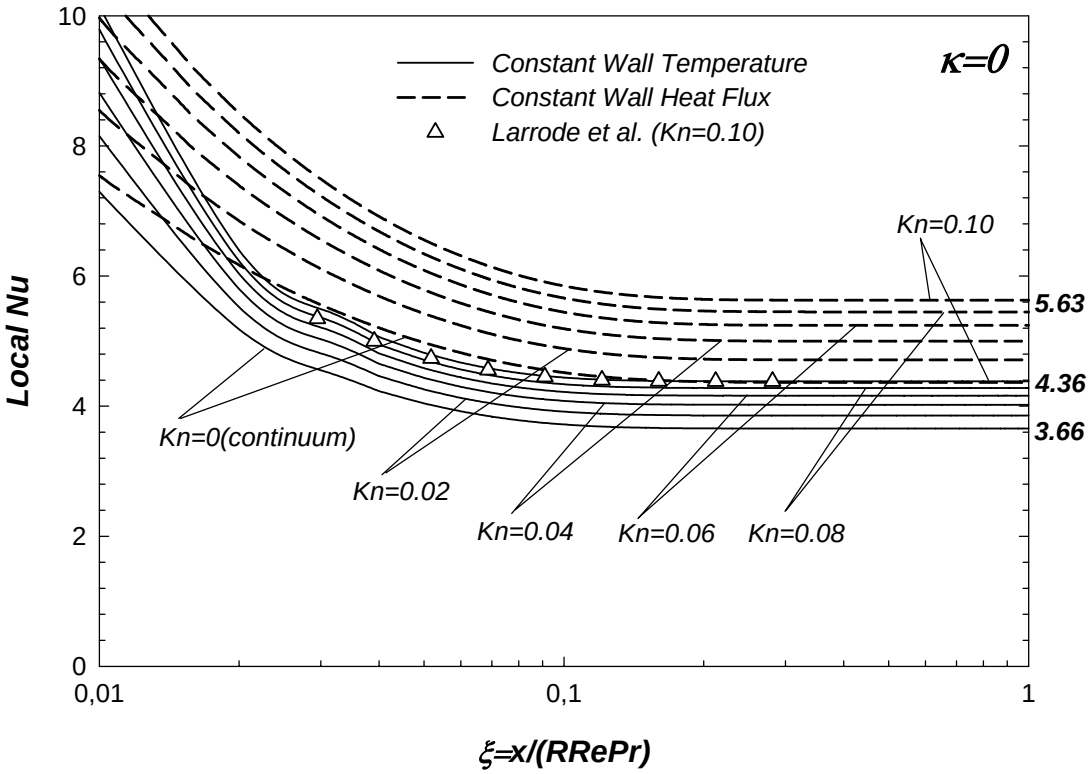

Figure 3.8. Variation of Local Nu as a Function of
Dimensionless Axial Coordinate for Different Kn Numbers, Microtube (κ =0)

In Figure 3.9, the curves corresponding to constant wall temperature case, are not so smooth at the entrance region because of the number of meshes. Since 100x100 meshes are used for constant wall temperature case, the results close to the entrance region are not so accurate. Increasing the number of meshes leads to more accurate results for entrance region which will also increase the computational time. Since

microchannels have large (L/D) ratios in practice, the entrance region results of this study are accepted as accurate enough.

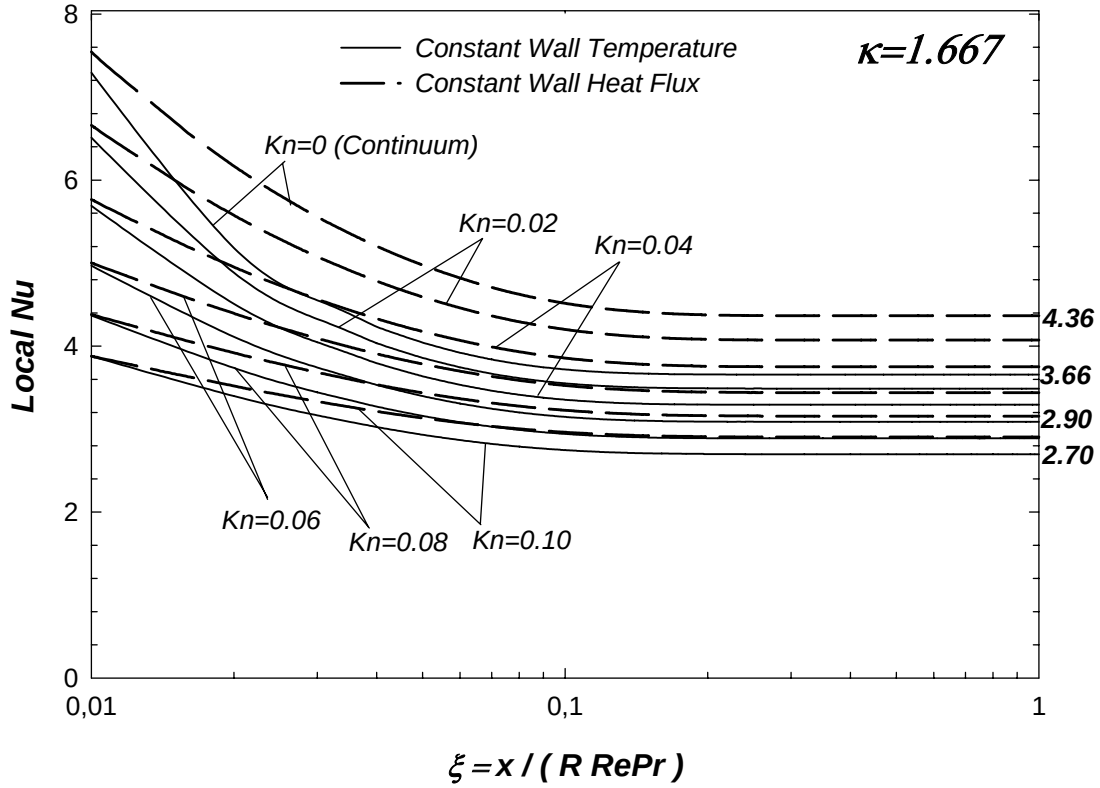

Figure 3.9. Variation of Local Nu as a Function of
Dimensionless Axial Coordinate for Different Kn Numbers, Microtube (κ =1.667)

Figure 3.9 shows the behavior of the air, as rarefaction increases for both cases. As seen from the figure, as Kn increases, local Nu decreases from 3.66 to 2.70 for constant wall temperature, and from 4.36 to 2.90 for constant wall heat flux. This is in contrast with the previous case; the temperature jump at the wall increases, the gradient at the wall decreases; therefore, the fully developed Nu number decreases for both cases.

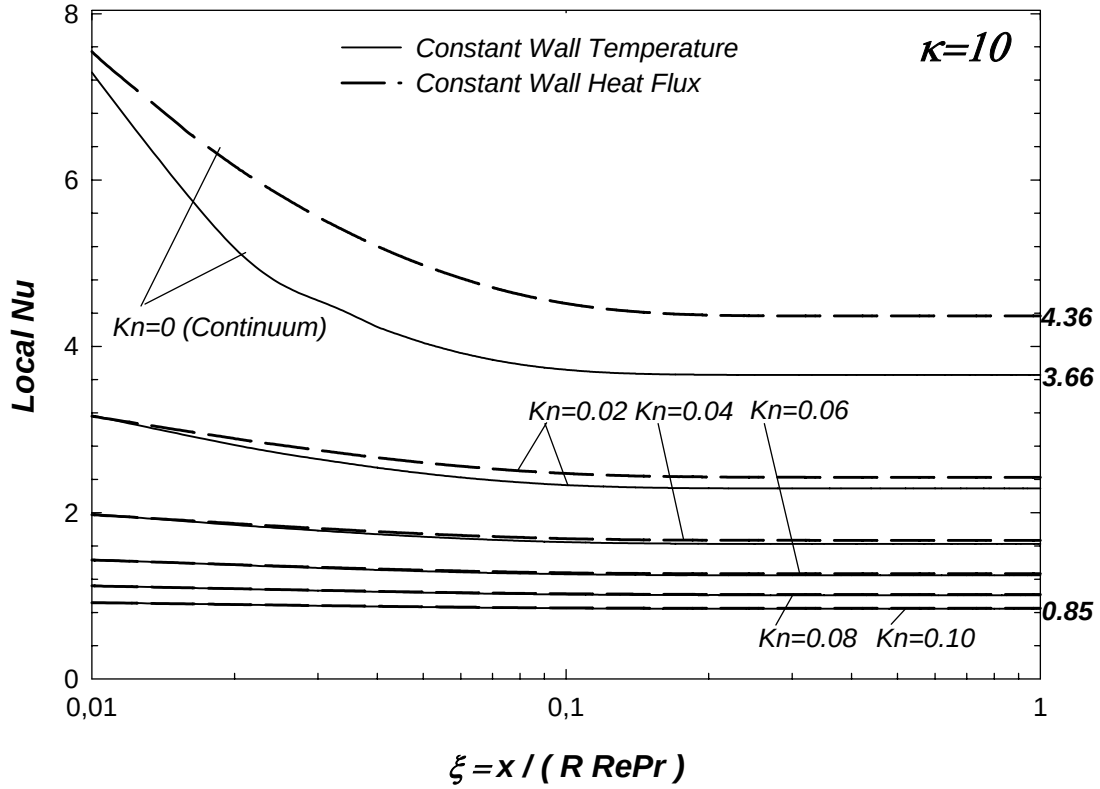

Figure 3.10. Variation of Local Nu as a Function of
Dimensionless Axial Coordinate for Different Kn Numbers, Microtube (κ =10)

Figure 3.10 shows the behavior of a gas with a large temperature jump. For large Kn number values, the local Nu curves coincide for both cases. Again, local Nu decreases from 3.66 to 0.84 for constant wall temperature, and from 4.36 to 0.85 for constant wall heat flux with increasing Kn number. But; this time, the effect of rarefaction is very dominant; even for Kn =0.02, the deviation from continuum is significant for both cases.

The results of the Figures 3.8, 3.9 and 3.10 are tabulated in Tables 3.1 and 3.2.

Table 3.1. Variation of Local Nu as a Function of Dimensionless Axial Coordinate for Different Kn Numbers and κ Values for Constant Wall Temperature, Microtube

ξ	Kn=0	Kn=0.02	Kn=0.04	Kn=0.06	Kn=0.08	Kn=0.10	
0.01	7.295	8.153	8.820	9.353	9.789	10.151	K=0
0.05	4,042	4.257	4.434	4.583	4.710	4.189	
0.10	3.718	3.915	4.080	4.218	4.336	4.439	
0.50	3.656	3.855	4.020	4.160	4.279	4.382	
1.00	3.656	3.855	4.020	4.160	4.279	4.382	
0.01	7.295	6.511	5.690	4.968	4.368	3.877	K=1.667
0.05	4.042	3.858	3.636	3.397	3.158	2.931	
0.10	3.718	3.550	3.353	3.146	2.941	2,746	
0.50	3.656	3.488	3.292	3.087	2.887	2,697	
1.00	3.656	3.488	3.292	3.087	2.887	2.697	
0.01	7.295	3.169	1.983	1.435	1.121	0.919	K=10
0.05	4.042	2.471	1.710	1.295	1.038	0.864	
0.10	3.718	2.331	1.645	1.259	1.015	0.849	
0.50	3.656	2.291	1.624	1.247	1.008	0.844	
1.00	3.656	2.291	1.624	1.247	1.008	0.844	

Table 3.2. Variation of Local Nu as a Function of Dimensionless Axial Coordinate for Different Kn Numbers and κ Values for Constant Wall Heat Flux, Microtube

ξ	Kn=0	Kn=0.02	Kn=0.04	Kn=0.06	Kn=0.08	Kn=0.10	
0.004	10.479	12.371	13.796	14.902	15.786	16.506	K=0
0.02	6.166	6.845	7.389	7.831	8.196	8.502	
0.04	5.203	5.690	6.085	6.411	6.684	6.915	
0.10	4.515	4.884	5.189	5.444	5.661	5.847	
0.50	4.364	4.710	4.998	5.241	5.448	5.627	
1.00	4.364	4.710	4.998	5.241	5.448	5.627	
0.004	10.479	8.758	7.186	5.984	5.084	4.400	K=1.667
0.02	6.166	5.573	4.950	4.391	3.916	3.517	
0.04	5.203	4.782	4.329	3.906	3.534	3.212	
0.10	4.515	4.200	3.855	6.525	3.226	2.961	
0.50	4.364	4.071	3.749	3.438	3.155	2.903	
1.00	4.364	4.071	3.749	3.438	3.155	2.903	

ξ	Kn=0	Kn=0.02	Kn=0.04	Kn=0.06	Kn=0.08	Kn=0.10	
0.004	10.479	3.561	2.116	1.499	1.158	0.943	
0.02	6.166	2.889	1.868	1.374	1.085	0.895	
0.04	5.203	2.661	1.772	1.323	1.053	0.874	*K=10*
0.10	4.515	2.471	1.687	1.276	1.024	0.854	
0.50	4.364	2.425	1.666	1.265	1.017	0.849	
1.00	4.364	2.425	1.666	1.265	1.017	0.849	

Figure 3.11 illustrates the effect of κ on local Nu for a fixed value of Kn =0.1. For large κ values, local Nu curves coincide for both cases. Besides the large deviation from continuum for large κ values, local Nu curves also become flat for large κ values. Fully developed Nu values change between 4.38 and 0.84 for constant wall temperature and between 5.63 and 0.85 for constant wall heat flux. The results of the Figure 3.11 are tabulated in Tables 3.3 and 3.4.

Table 3.3. Variation of Local Nu as a Function of Dimensionless Axial Coordinate for Different κ Values for Constant Wall Temperature, Microtube (Kn=0.10)

ξ	κ=0	κ=0.1	κ=0.5	κ=1	κ=1.667	κ=5	κ=10
0.01	10.151	9.303	6.912	5.189	3.877	1.698	0.919
0.05	4.189	4.678	4.135	3.544	2.931	1.511	0.864
0.10	4,439	4.299	3.797	3.279	2.746	1.464	0.849
0.50	4.382	2.240	3.732	3.218	2.697	1.448	0.844
1.00	4.382	4.240	3.732	3.218	2.697	1.448	0.844

Table 3.4. Variation of Local Nu as a Function of Dimensionless Axial Coordinate for Different κ Values for Constant Wall Heat Flux, Microtube (Kn=0.10)

ξ	κ=0	κ=0.1	κ=0.5	κ=1	κ=1.667	κ=5	κ=10
0.004	16.506	14.168	9.043	6.227	4.400	1.784	0.943
0.02	8.502	7.836	5.966	4.595	3.517	1.619	0.895
0.04	6.915	6.468	5.138	4.088	3.212	1.551	0.874
0.10	5.847	5.524	4.524	3.690	2.961	1.490	0.854
0.50	5.627	5.327	4.391	3.601	2.903	1.476	0.849
1.00	5.627	5.327	4.391	3.601	2.903	1.476	0.849

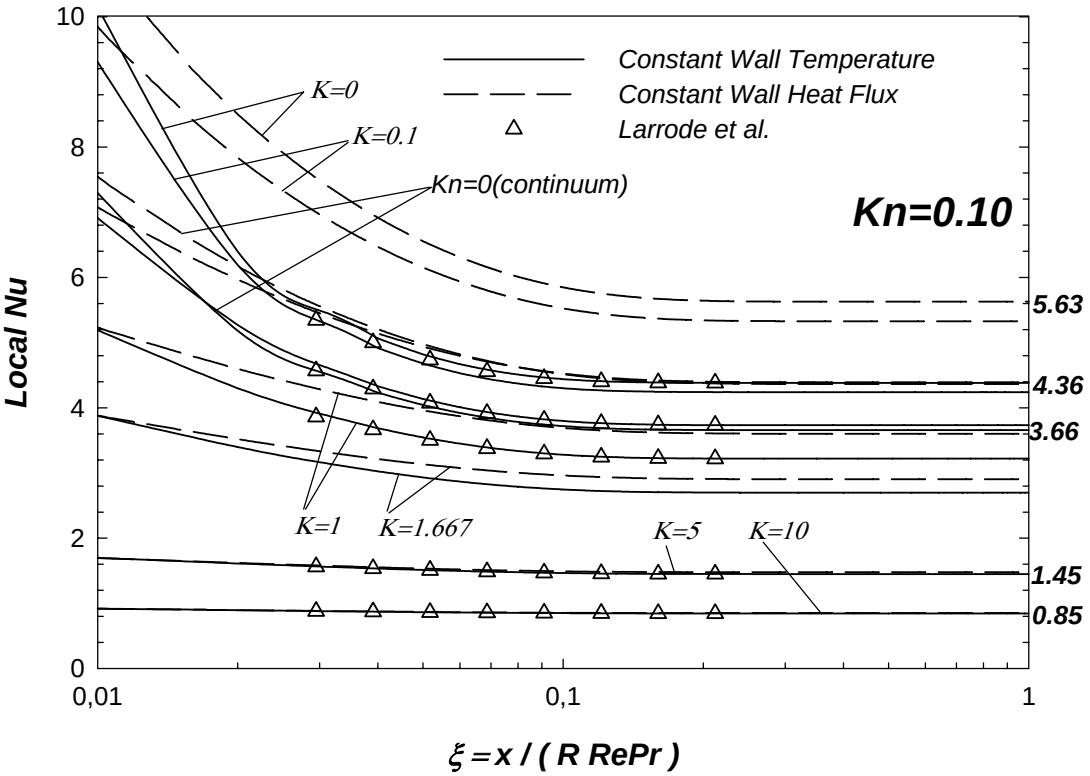

Figure 3.11. Variation of Local Nu as a Function of Dimensionless Axial Coordinate for Different κ Values, Microtube (Kn=0.10)

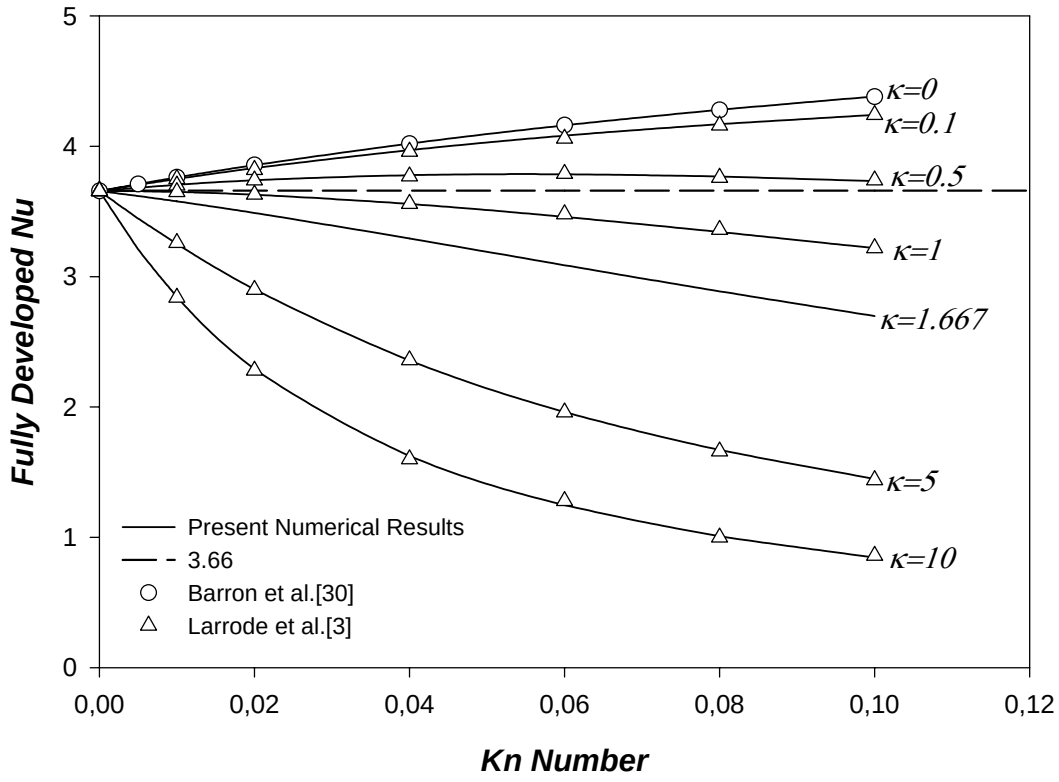

Figure 3.12. Fully Developed Nu as a Function of Kn Number and κ for Constant Wall Temperature, Microtube

Figures 3.12 and 3.13 illustrate the fully developed Nu as a function of Kn for different κ values for both constant wall temperature and constant wall heat flux cases. The results of Barron et al. [30], Larrode et al. [3] and Ameel et al [33] are also plotted in figures, to show the accuracy of the method. The important conclusion of these graphs is that, as κ increases, Nu number decreases. But depending on κ value, Nu number can be higher or lower than the continuum case. This effect is due to the small temperature gradient in radial direction at the wall.

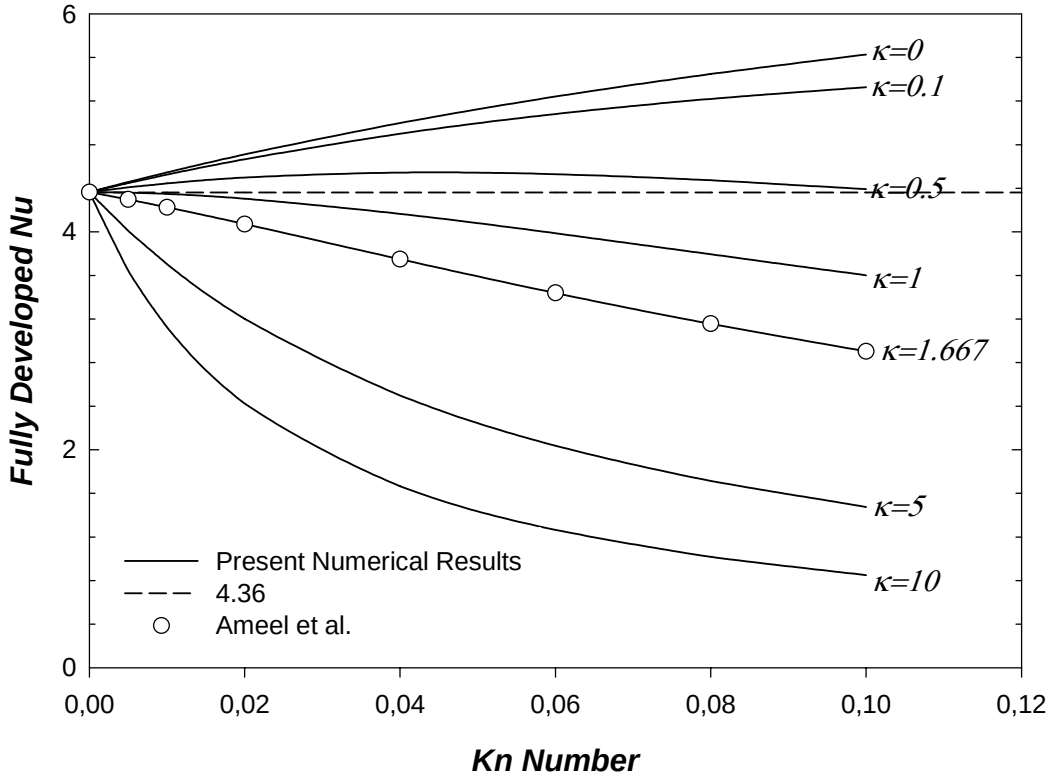

Figure 3.13 Fully Developed Nu as a Function of Kn Number and κ for Constant Wall Heat Flux, Microtube

The results of the Figures 3.12 and 3.13 are taulated in Tables 3.5 and 3.6 below.

Table 3.5. Fully Developed Nu as a Function of Kn Number and κ for Constant Wall Heat Temperature, Microtube

Kn	κ=0	κ=0.1	κ=0.5	κ=1	κ=1.667	κ=5	κ=10
0,00	3.656	3.656	3.656	3.656	3.656	3.656	3.656
0,005	3.710	3.704	3.682	3.655	3.618	3.445	3.209
0,01	3.761	3.749	3.704	3.649	3.577	3.250	2.843
0,02	3.855	3.832	3.739	3.628	3.488	2.902	2.291
0,04	4.020	3.970	3.778	3.557	3.292	2.356	1.624
0,06	4.160	4.081	3.785	3.458	3.087	1.961	1.247
0,08	4.279	4.136	3.767	3.342	2.887	1.670	1.008
0,10	4.382	4.240	3.732	3.218	2.697	1.448	0.844

Table 3.6. Fully Developed Nu as a Function of Kn Number and κ for Constant Wall Heat Flux, Microtube

Kn	κ=0	κ=0.1	κ=0.5	κ=1	κ=1.667	κ=5	κ=10
0,00	4.364	4.364	4.364	4.364	4.364	4.364	4.364
0,005	4.457	4.447	4.408	4.360	4.297	4.010	3.645
0,01	4.545	4.525	4.444	4.348	4.225	3.704	3.125
0,02	4.710	4.666	4.498	4.304	4.071	3.202	2.425
0,04	4.998	4.900	4.544	4.165	3.749	2.499	1.666
0,06	5.241	5.081	4.529	3.987	3.438	2.037	1.265
0,08	5.448	5.220	4.473	3.794	3.155	1.714	1.017
0,10	5.627	5.327	4.391	3.601	2.903	1.476	0.849

CHAPTER 4

SINGLE PHASE HEAT TRANSFER IN MICROCHANNELS BETWEEN PARALLEL PLATES WITHOUT VISCOUS DISSIPATION

4.1. Introduction

In this section, heat transfer analysis of hydrodynamically developed and thermally developing single phase laminar flow of a viscous fluid in microchannels between parallel plates is performed. The thermo-physical properties are assumed to be constant. Viscous dissipation term is neglected. The energy equation is solved numerically for constant wall temperature and constant wall heat flux thermal boundary conditions for slip-flow regime.

4.2. Fully Developed Velocity Distribution in Microchannels Between Parallel Plates

The geometry of the problem considered in this section is shown in Figure 4.1. The coordinate system is located at the center of the parallel plates. There is an unheated section at the inlet to be able to have a fully developed velocity profile.

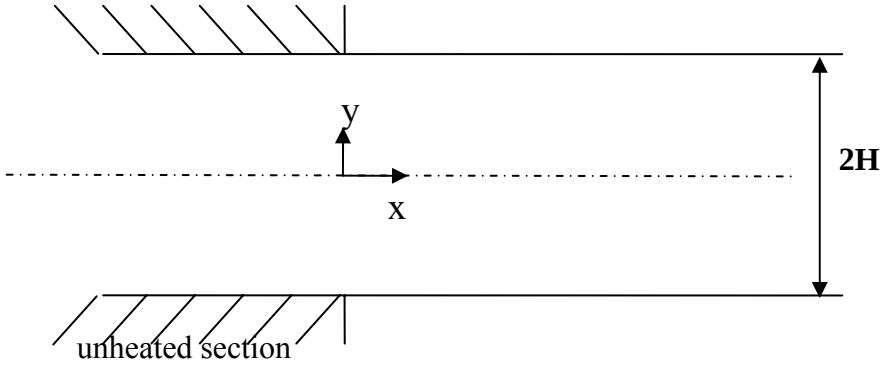

Figure 4.1. The Geometry of the Microchannel Problem

Using the governing equations and the slip velocity boundary condition, Eq. (1.2), the fully developed velocity profile is determined in terms of mean velocity as,

$$\frac{u}{u_m} = \frac{3}{2}\frac{1-(\frac{y}{H})^2 + 4Kn}{1+6Kn} \tag{4.1}$$

Defining dimensionless radius as,

$$\eta = \frac{y}{H} \tag{4.2}$$

the Eq. (4.1) can be written as,

$$\frac{u}{u_m} = \frac{3}{2}\frac{1-\eta^2 + 4Kn}{1+6Kn} \tag{4.3}$$

Fully developed velocity profile depends on the Knudsen number. Notice that, by setting Kn =0 in the Eq. (4.3) is identical to the fully developed velocity profile of a flow in a macrochannel between parallel plates, which is

$$\frac{u}{u_m} = \frac{3}{2}(1-\eta^2) \tag{4.4}$$

The terms containing Knudsen number in Eq. (4.4) introduce the slip velocity at the wall.

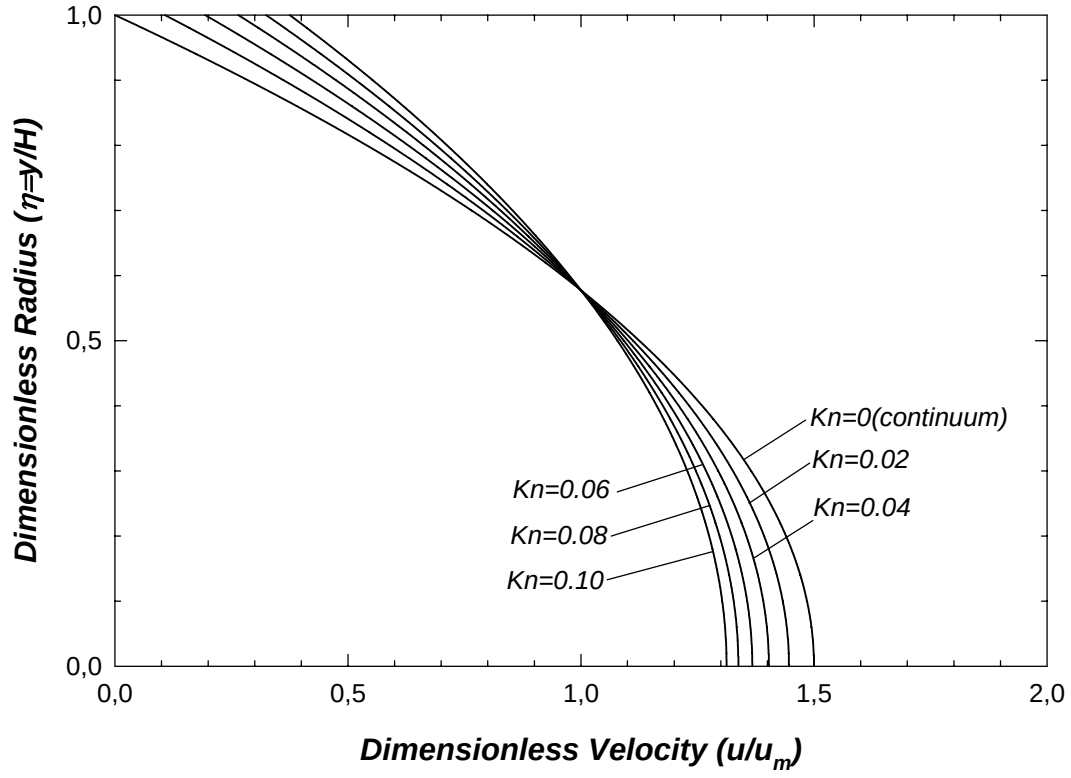

Figure 4.2. Fully Developed Velocity Profile Inside a Microchannel Between Parallel Plates

The fully developed velocity profile is plotted as a function of η and Kn number in Figure 4.2. Kn number changes between 0 and 0.1. Kn =0 represents the flow in macrochannels between parallel plates, and Kn =0.1 is the applicability limit of the slip flow theory. As seen from the figure, as rarefaction increases, the slip at the wall increases from zero for Kn =0 to 0.375 for 0.1. This increase in the slip velocity leads to a decrease in the gradient of the velocity at the wall, which is again the reason for the reduction in the friction factor in gaseous flows in microchannels. As Kn number increases, the maximum dimensionless velocity located at the center decreases from 1,5 for Kn =0 to 1.313 for Kn =0.1. There is also a knot point, where the velocity is equal to mean velocity around $\eta=0.58$.

4.3. Heat Transfer Analysis

4.3.1. Formulation

Two dimensional energy equation in cartesian coordinates with constant properties, negligible axial conduction and negligible viscous dissipation term can be written as [57];

$$u\frac{\partial T}{\partial x}=\alpha\frac{\partial^2 T}{\partial y^2} \tag{4.5}$$

The case of constant wall temperature, the boundary conditions are,

$$\text{at}\quad y=H \qquad T=T_s \tag{4.6-a}$$

$$\text{at}\quad y=0 \qquad \frac{\partial T}{\partial r}=0 \tag{4.6-b}$$

at $x = 0 \qquad T = T_i$ (4.6-c)

where T_i and T_s are the temperatures of the gas at the inlet and at the surface, respectively.

In the case of constant wall heat flux, the boundary conditions are,

at $y = H \qquad \frac{\partial T}{\partial y} = \frac{q^{"}}{k}$ (4.7-a)

at $y = 0 \qquad \frac{\partial T}{\partial r} = 0$ (4.7-b)

at $x = 0 \qquad T = T_i$ (4.7-c)

The energy equation is non-dimensionalized by the following dimensionless quantities,

$$\theta = \frac{T - T_w}{T_i - T_w} \quad \text{(for constant wall temperature)} \tag{4.8-a}$$

$$\theta = \frac{T - T_i}{q^{"} H / k} \quad \text{(for constant wall heat flux)} \tag{4.8-b}$$

$$\eta = \frac{y}{H} \tag{4.8-c}$$

$$\xi = \frac{x}{H \,\mathrm{Re}\,\mathrm{Pr}} \tag{4.8-d}$$

$$\overline{u} = \frac{u}{u_m} \tag{4.8-e}$$

Introducing the dimensionless quantities, Eqs (4.8-a) through (4.8-e) the energy equation becomes,

$$\frac{\overline{u}}{4}\frac{\partial\theta}{\partial\xi}=\frac{\partial^2\theta}{\partial\eta^2} \tag{4.9}$$

Using the dimensionless quantities, Eqs (4.8-a) through (4.8-e) and appropriate form of the temperature jump boundary condition, Eq. (1.4) for the considered geometry, the boundary conditions for constant wall temperature become,

$$\text{at} \quad \eta=1 \qquad \theta=-2\kappa Kn\left(\frac{\partial\theta}{\partial\eta}\right)_{\eta=1} \tag{4.10-a}$$

$$\text{at} \quad \eta=0 \qquad \frac{\partial\theta}{\partial\eta}=0 \tag{4.10-b}$$

$$\text{at} \quad \xi=0 \qquad \theta=1 \tag{4.10-c}$$

$$\text{where } \kappa=\frac{2-F_T}{F_T}\frac{2\gamma}{\gamma+1}\frac{1}{\mathrm{Pr}} \tag{4.11}$$

The boundary conditions for the constant wall heat flux case,

$$\text{at} \quad \eta=1 \qquad \frac{\partial\theta}{\partial\eta}=1 \tag{4.12-a}$$

$$\text{at} \quad \eta=0 \qquad \frac{\partial\theta}{\partial\eta}=0 \tag{4.12-b}$$

$$\text{at} \quad \xi=0 \qquad \theta=0 \tag{4.12-c}$$

Local heat transfer coefficient is written as,

$$h_x=-\frac{k}{(T_m-T_w)}\left(\frac{\partial T}{\partial r}\right)_{r=R} \tag{4.13}$$

Introducing dimensionless quantities into Eq. (4.13), the Nusselt number is determined for constant wall temperature as,

$$Nu_x = \frac{h_x D}{k} = -\frac{4(\frac{\partial \theta}{\partial \eta})_{\eta=1}}{\theta_m} \tag{4.14}$$

Introducing dimensionless quantities and the temperature jump boundary condition, Eq. (1.4) into the Eq. (4.13), the Nusselt number is determined for constant wall heat flux as,

$$Nu_x = \frac{h_x D}{k} = \frac{4}{\theta_m - \theta_s - 2\kappa Kn} \tag{4.15}$$

where θ_m is the dimensionless mean temperature, and defined as,

$$\theta_m = \int_0^1 (\frac{u}{u_m})\theta(\eta,\xi)d\eta \tag{4.16}$$

To determine the local Nusselt number, the energy equation, Eq. (4.9) should be solved with indicated boundary conditions to obtain the temperature distribution. The energy equation is solved by using numerical methods, due to the prescribed reasons mentioned in the previous chapter.

4.3.1.1. Numerical Solution

Like the problem in microtubes, the energy equation is transformed into a transient problem for the simplicity of the numerical solution.

$$\frac{\partial\theta}{\partial\tau}+\frac{\overline{u}}{4}\frac{\partial\theta}{\partial\xi}=\frac{\partial^2\theta}{\partial\eta^2} \tag{4.17}$$

By defining dimensionless time as,

$$\tau=\frac{\alpha t}{H^2} \tag{4.18}$$

Introducing dimensionless time also, the initial and boundary conditions of the transient energy equation become,

$$\text{at} \quad \tau=0 \qquad \theta=1 \tag{4.19-a}$$

$$\text{at} \quad \eta=1 \qquad \theta=-2\kappa Kn\left(\frac{\partial\theta}{\partial\eta}\right)_{\eta=1} \tag{4.19-b}$$

$$\text{at} \quad \eta=0 \qquad \frac{\partial\theta}{\partial\eta}=0 \tag{4.19-c}$$

$$\text{at} \quad \xi=0 \qquad \theta=1 \tag{4.19-d}$$

for constant wall temperature; and,

$$\text{at} \quad \tau=0 \qquad \theta=0 \tag{4.20-a}$$

$$\text{at} \quad \eta=1 \qquad \frac{\partial\theta}{\partial\eta}=1 \tag{4.20-b}$$

$$\text{at} \quad \eta=0 \qquad \frac{\partial\theta}{\partial\eta}=0 \tag{4.20-c}$$

$$\text{at} \quad \xi=0 \qquad \theta=0 \tag{4.20-d}$$

for constant wall heat flux boundary condition.

To calculate the Nusselt number, the first derivative of the dimensionless temperature at the wall and the dimensionless mean temperature should be computed. The derivative at the wall is computed by using the finite difference approximation. The evaluation of the dimensionless mean temperature needs the computation of the integral given by Eq. (4.16), which is computed numerically by using Simpson' s 1/3 rule [58].

4.3.1.1.1.Domain Discretization

The solution domain is divided into finite number of meshes as shown in Figure 3.3. The nodes are located at the corners of the meshes. Due to the symmetry of the solution domain, only one half of the solution domain is considered. For constant wall temperature case, 100x100 grids; and for constant wall heat flux case, 250x250 grids which are distributed uniformly in the vertical and longitudinal directions are used for the computation. The length of the tube is assigned as the dimensionless longitudinal coordinate, $\xi=1$, like the previous problem.

3.3.1.1.2.Equation Discretization

Discretization of the Eq. (4.17) and the related boundary conditions requires second and first derivatives in space and first derivative in time. Centered, forward and backward finite-divided differences, defined in Eqs. (3.33-a) through (3.33-j), are used to approximate the space derivatives and the time derivative.

4.3.1.1.2.1. Nodes at the Interior Region

For an interior node, central differences for space; Eq. (3.33-c), Eq. (3.33-i) and forward difference for time, Eq. (3.33-j) are substituted into the energy equation, Eqn (4.17). The algebraic form of the energy equation becomes;

$$\theta_{i,j}^{k+1} = \theta_{i,j}^{k} + C_1(\theta_{i+1,j}^{k} - 2\theta_{i,j}^{k} + \theta_{i-1,j}^{k}) - C_2\bar{u}(\eta_i)(\theta_{i,j+1}^{k} - \theta_{i,j-1}^{k}) \tag{4.21}$$

where C_1, C_2 are the coefficients and defined as,

$$C_1 = \frac{\Delta\tau}{(\Delta\eta)^2} \tag{4.22}$$

$$C_2 = \frac{\Delta\tau}{8\Delta\xi} \tag{4.23}$$

and $\bar{u}(\eta)$ is the dimensionless fully developed profile, given by Eq. (4.3).

4.3.1.1.2.2. Nodes at the Inlet

The temperature of an inlet node is prescribed, which is the boundary condition.

$$\theta_{0,j}^{k+1} = 1 \tag{4.24-a}$$

$$\theta_{0,j}^{k+1} = 0 \tag{4.24-b}$$

which are for constant wall temperature and constant wall heat flux cases, respectively.

4.3.1.1.2.3. Nodes at the Exit

For a exit node, central difference in radial direction, Eqs. (3.33-c), backward difference in longitudinal direction, Eq. (3.33-h) and forward difference for time, Eq. (3.33-j) are substituted into the energy equation, Eq.(4.17). The algebraic form of the energy equation becomes;

$$\theta_{i,j}^{k+1} = \theta_{i,j}^{k} + C_1(\theta_{i+1,j}^{k} - 2\theta_{i,j}^{k} + \theta_{i-1,j}^{k}) - C_2\overline{u}(\eta_i)(3\theta_{i,j}^{k} - 4\theta_{i,j-1}^{k} + \theta_{i,j-2}^{k}) \qquad (4.25)$$

where C_1, C_2 are the coefficients that are given in Eqs. (4.22) and (4.23).

4.3.1.1.2.4. Nodes at the Centerline

For a centerline node, central difference in longitudinal direction, Eq. (3.33-i), forward difference for time, Eq. (3.33-j) are substituted into the energy equation, Eq.(4.17). For the second derivative in radial direction, Eq. (3.41) is substituted. The algebraic form of the energy equation becomes;

$$\theta_{i,j}^{k+1} = \theta_{i,j}^{k} + 2C_1(\theta_{1,j}^{k} - \theta_{0,j}^{k}) - C_2\overline{u}(\eta_0)(\theta_{0,j+1}^{k} - \theta_{0,j-1}^{k}) \qquad (4.26)$$

where C_1, C_2 are the coefficients that are given in Eqs. (4.22) and (4.23).

4.3.1.1.2.5. Nodes at the Boundary

4.3.2.2.5.1. Constant Wall Temperature

Substituting discritised boundary condition, Eq. (3.44) into the Eqn. (4.17), the algebraic form of the energy equation for a node near the wall which includes the effect of the boundary condition for the constant wall temperature case becomes,

$$\theta_{n-1,j}^{k+1} = \theta_{n-1,j}^{k} + C_1(\kappa \frac{4\theta_{n-1,j}^{k} - \theta_{n-2,j}^{k}}{2\Delta\eta(1+\frac{3\kappa}{2\Delta\eta})} - 2\theta_{n-1,j}^{k} + \theta_{n-2,j}^{k}) \\ -C_2\overline{u}(\eta_i)(\theta_{i,j+1}^{k} - \theta_{i,j-1}^{k}) \tag{4.27}$$

where C_1, C_2 are the coefficients that are given in Eqs. (4.22) and (4.23).

4.3.2.2.5.2. Constant Wall Heat Flux

Substituting Eq. (3.46) into the Eq. (4.17), the algebraic form of the energy equation for a node near the wall which includes the effect of the boundary condition for the constant wall heat flux case becomes,

$$\theta_{n-1,j}^{k+1} = \theta_{n-1,j}^{k} + C_1(\frac{2\Delta\eta + 4\theta_{n-1,j} - \theta_{n-2,j}}{3} - 2\theta_{n-1,j}^{k} + \theta_{n-2,j}^{k}) \\ -C_2\overline{u}(\eta_i)(\theta_{i,j+1}^{k} - \theta_{i,j-1}^{k}) \tag{4.28}$$

where C_1, C_2 are the coefficients that are given in Eqs. (4.22) and (4.23).

4.3.1.1.3. Stability and Convergence

Again, the step size in time should satisfy the stability criterian for stable solution [58]. Again, it can be written as,

$$C_1 < \frac{1}{2} \tag{4.29}$$

where C_1 is the coefficient that is given in Eq. (4.22). Like the previous case, by trial and error, it is seen that

$$\Delta\tau = 0.4\Delta\eta^2 \tag{4.30}$$

is a safe choice for this problem to get a stable solution.

This numerical calculation is open ended in the time domain, so a convergence criterian is needed to stop the computation. For this study, the convergence criterian is that the difference between fully developed Nu values of two successive time step is less than 10^{-3}. To satisfy this criteria dimensionless time is chosen as $\tau=2$ for constant wall temperature and $\tau=4$ for constant wall heat flux cases, respectively.

4.4. Results and Discussion

The dimensionless transient temperature distribution inside a microchannel between parallel plates is determined by solving Eq. (4.17) numerically with the appropriate boundary conditions. Once the dimensionless temperature distribution is determined, local Nusselt number is determined as a function of dimensionless axial coordinate and dimensionless time from Eqs. (4.14) and (4.15) for different Kn number values, varies between 0 and 0.1. Notice that, Kn =0 is the no-slip condition (i.e. flow in

macrochannels), which is again the validification of the accuracy of the numerical solution.

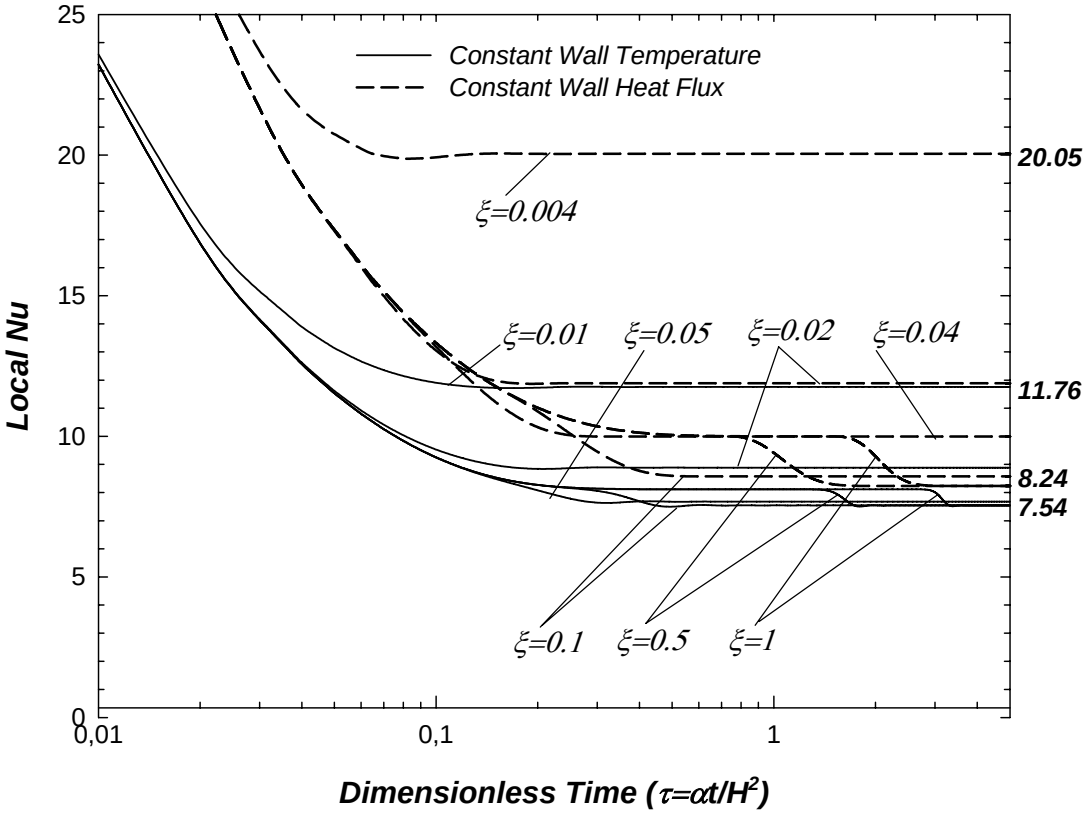

Figure 4.3. Variation of Local Nu with Dimensionless Time
at Different Axial Locations, Microchannel (Kn =0)

Figure 4.3 shows the variation of local Nu with dimensionless time, τ at different axial locations, for Kn=0 for both constant wall temperature and constant wall heat flux cases. After sufficiently long time, Nu number values reach to a steady state value which is 7.54 for constant wall temperature, and 8.24 for constant wall heat

flux cases. As the dimensiomless axial coordinate, ξ increases, the time required to reach the steady-state conditions increases. Beyond an axial location, all curves reach the same local Nu value, which is the indication of the thermal entrance region. This axial location is between ξ =0.1 and ξ =0.5 for both cases.

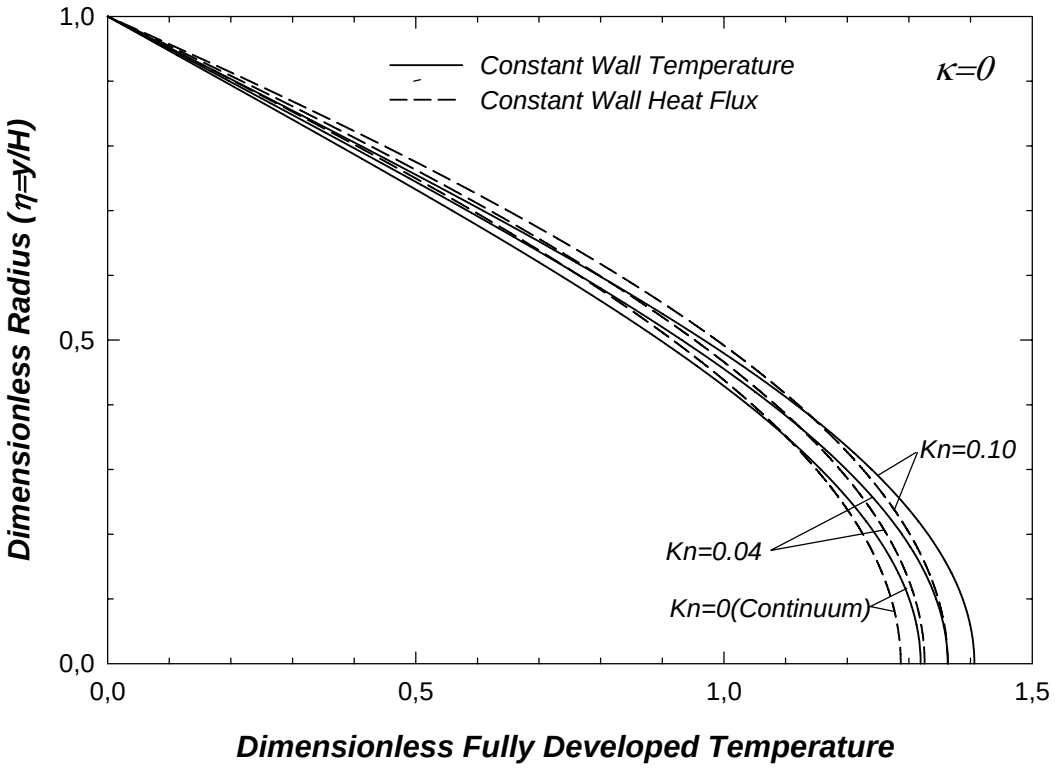

Figure 4.4. Dimensionless Fully Developed Temperature Profile as a Function of Kn Number, Microchannel (κ =0)

Figures 4.4 and 4.5 show the dimensionless fully developed temperature profile as a function of Kn number for κ =0 and κ =1.667 for both constant wall tempearture and constant wall heat flux cases. When Kn=0 independent of κ value, there is no

temperature jump at the wall, which stands for the flow in macrochannels. For κ =0, there is no temperature jump at the wall; but, there exists a velocity slip at the wall, which leads to different Nu values for different Kn numbers. As seen from the Figure 4.4, the gradient at the wall increases for both cases, which will lead to an increase in Nu number. As rarefaction increases, the maximum dimensionless temperature located at the center, also increases from 1.319 for Kn =0 to 1.406 for Kn =0.1, which indicates 25% increase for constant wall temperature, and from 1.287 Kn =0 to 1.363 for Kn =0.1, which indicates 6% increase for constant wall heat flux case.

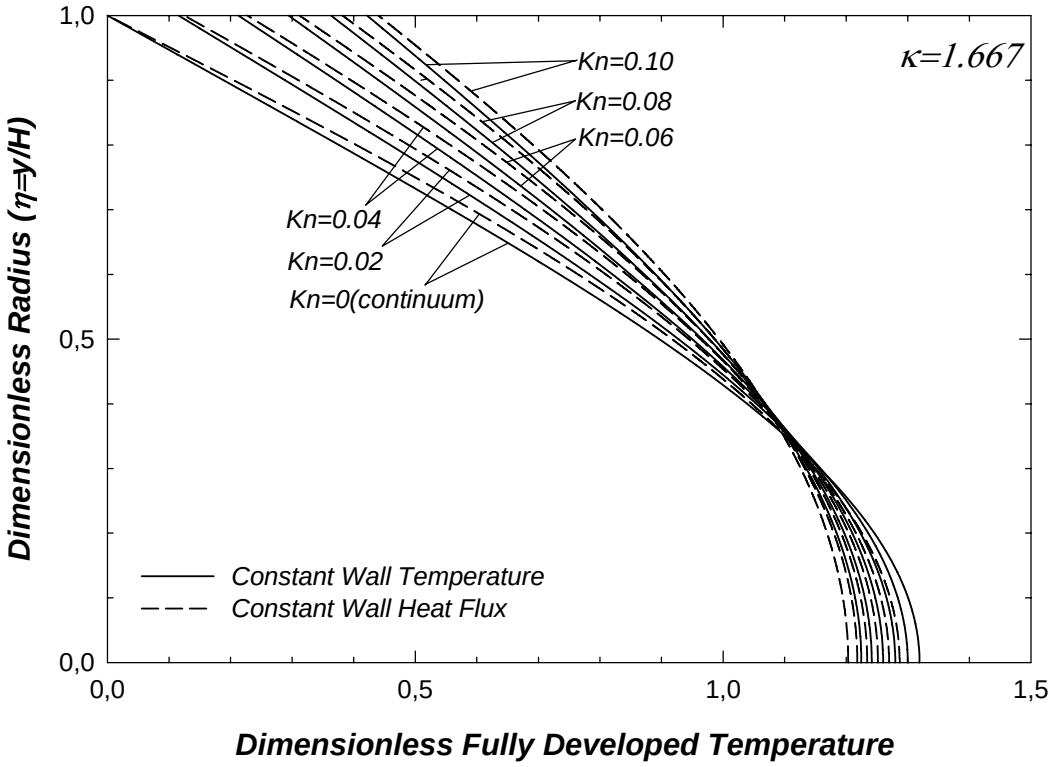

Figure 4.5. Dimensionless Fully Developed Temperature Profile as a Function of Kn Number, Microchannel (κ =1.667)

For κ =1.667, temperature jump exists at the wall, and increases as rarefaction increases. Dimensionless fully developed temperature is 0 at the wall for Kn =0, for both cases; and increases to 0.422 for constant wall temperature case, and 0.440 for constant wall heat flux case for Kn =0.1 Unlike κ =0 case, as rarefaction increases, the gradient at the wall decreases, and the maximum dimensionless temperature decreases for both cases. Larger values of κ will lead to more increase in temperature jump, and more decrease in maximum dimensionles temperature.

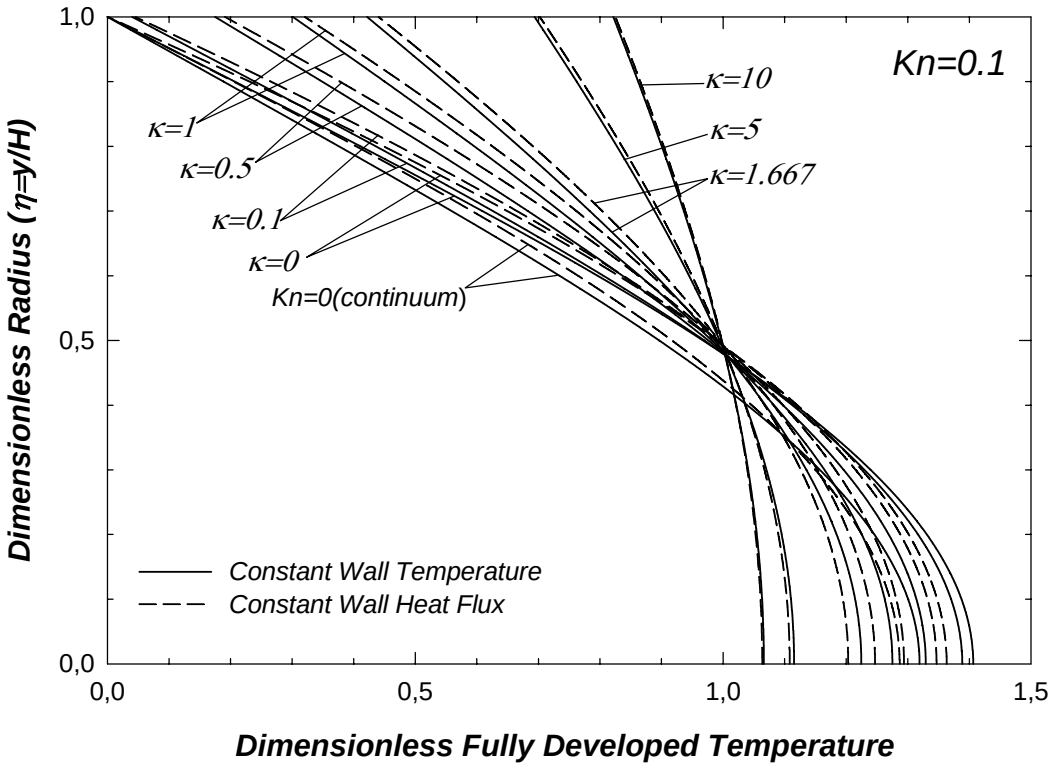

Figure 4.6. Dimensionless Fully Developed Temperature Profile as a Function of κ Parameter, Microchannel (Kn=0.1)

Figure 4.6 shows the dimensionless fully developed temperature profile as a function of κ parameter for Kn =0.1 for both constant wall temperature and constant wall heat flux cases. As κ increasing, the temperature jump increases; the amount of temperature jump at the wall approaches to each other for both boundary conditions, and the dimensionless fully developed temperature profile approaching to a uniform distribution for both boundary conditions. The maximum dimensionless temperature also decreases as κ increasing. The decrease is 61% for constant wall temperature, and 58% for constant wall heat flux.

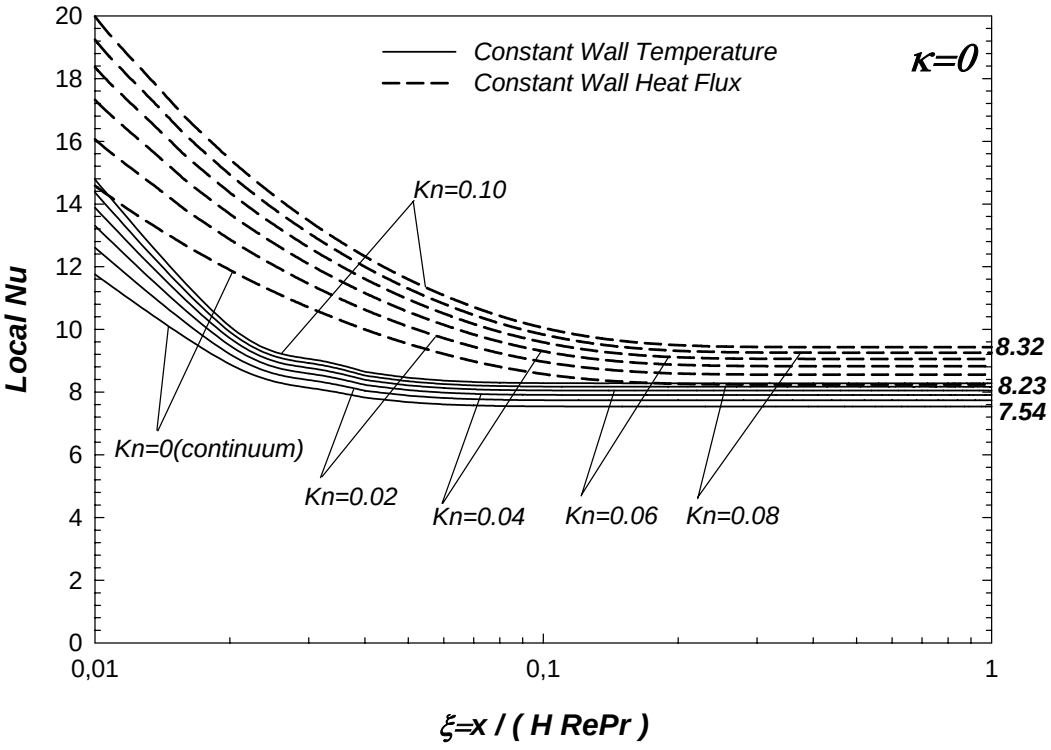

Figure 4.7. Variation of Local Nu as a Function of Dimensionless Axial Coordinate for Different Kn Numbers, Microchannel (κ =0)

Figure 4.7 shows variation of local Nu number with the dimensionless axial coordinate for different Kn numbers for $\kappa = 0$. Nu number gradually increases from 7.54 to 4.38 for constant wall temperature, and from 8.24 to 5.63 for constant wall heat flux, as the Kn increases due to the neglection of the temperature jump at the wall, for both cases. Local Nu numbers reach their fully developed value around ξ=0.1 for constant wall temperature, and ξ =0.2 for constant wall heat flux case.

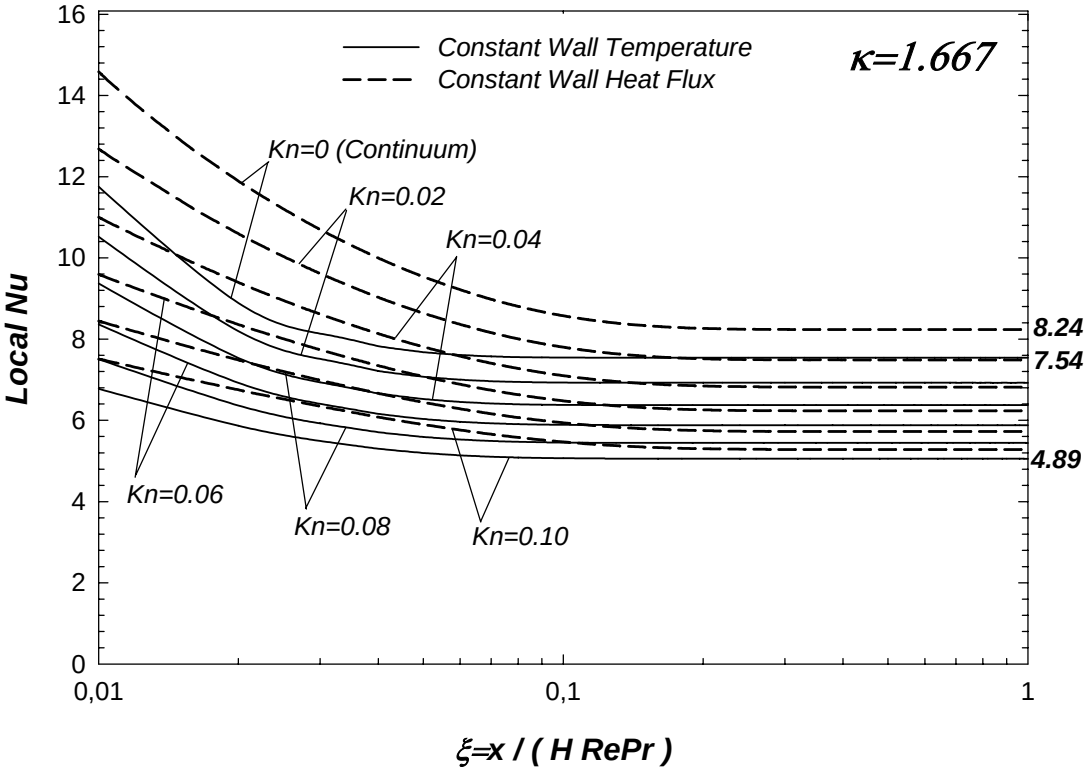

Figure 4.8. Variation of Local Nu as a Function of Dimensionless Axial Coordinate for Different Kn Numbers, Microchannel (κ =1.667)

Figure 4.8 shows the behavior of the air, as rarefaction increases for both cases. As Kn increases, local Nu decreases from 7.54 to 5.06 for constant wall temperature, and from 8.24 to 5.28 for constant wall heat flux. As the temperature jump at the wall increases, the gradient at the wall decreases; therefore fully develored Nu decreases for both cases.

.

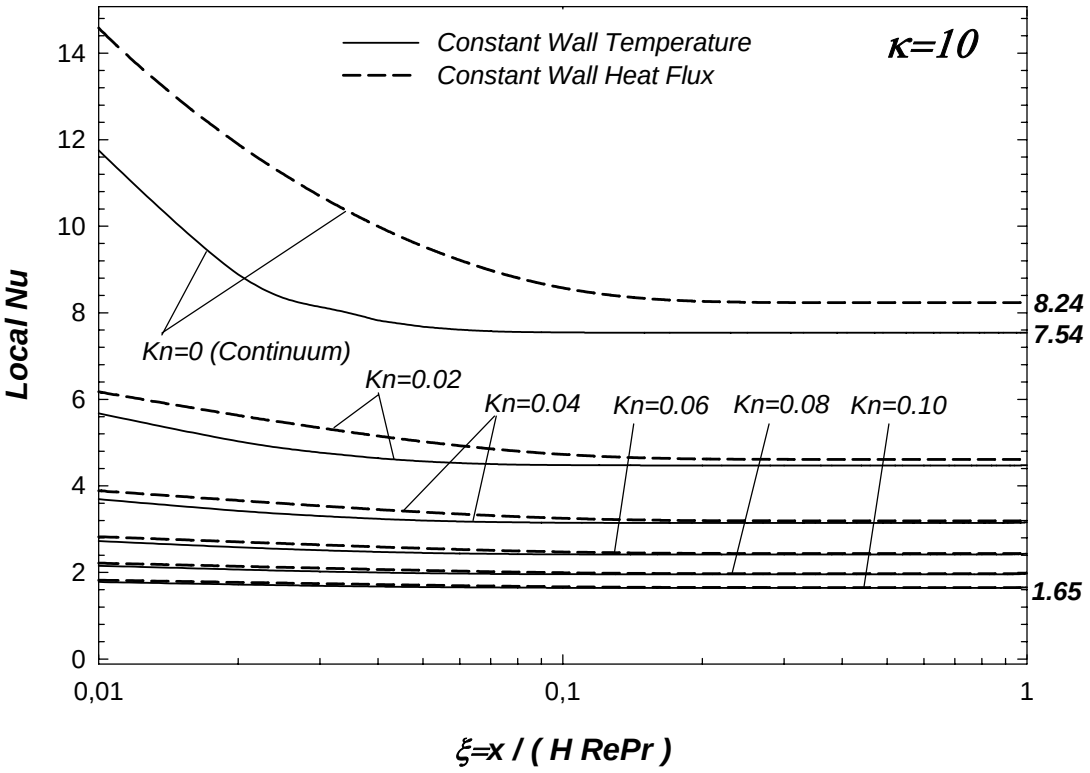

Figure 4.9. Variation of Local Nu as a Function of Dimensionless Axial Coordinate for Different Kn Numbers, Microchannel (κ =10)

Figure 4.9 shows the behavior of a gas with a large temperature jump. For large Kn number values, the local Nu curves coincide for both cases. Again, local Nu decreases from 7.54 to 1.64 for constant wall temperature, and from 8.24 to 1.65 for constant wall heat flux with increasing Kn number. The effect of rarefaction is very dominant; even for Kn=0.02, the deviation from continuum is significant for both cases, and the deviations are more significant than the microtube case.

The results of the Figures 4.7, 4.8 and 4.9 are tabulated in Tables 4.1 and 4.2

Table 4.1. Variation of Local Nu as a Function of Dimensionless Axial Coordinate for Different Kn Numbers and κ Values for Constant Wall Temperature, Microchannel

ξ	Kn=0	Kn=0.02	Kn=0.04	Kn=0.06	Kn=0.08	Kn=0.10	
0.01	11.755	12.608	13.303	13.880	14.367	14.782	
0.05	7.679	7.887	8.063	8.214	8.344	8.458	
0.10	7,545	7.743	7.910	8.053	8.177	8.285	*K=0*
0.50	7.541	7.738	7.905	8.048	8.172	8.283	
1.00	7.541	7.738	7.905	8.048	8.172	8.283	
0.01	11.755	10.523	9.371	8.364	7.506	6.779	
0.05	7.679	7.073	6.525	6.033	5.592	5.197	
0.10	7.545	6.931	6.380	5.889	5.454	5.067	*K=1.667*
0.50	7.541	6.926	6.374	5.882	5.445	5.053	
1.00	7.541	6.926	6.374	5.882	5.445	5.053	
0.01	11.755	5.675	3.692	2.724	2.154	1.779	
0.05	7.679	4.567	3.200	2.451	1.982	1.662	
0.10	7.545	4.480	3.149	2.418	1.959	1.645	*K=10*
0.50	7.541	4.474	3.145	2.415	1.957	1.655	
1.00	7.541	4.474	3.145	2.415	1.957	1.655	

Table 4.2. Variation of Local Nu as a Function of Dimensionless Axial Coordinate for Different Kn Numbers and κ Values for Constant Wall Heat Flux, Microchannel

ξ	Kn=0	Kn=0.02	Kn=0.04	Kn=0.06	Kn=0.08	Kn=0.10	
0.004	19.273	23.108	25.521	27.463	29.056	30.386	
0.02	11.889	12.863	13.674	14.354	14.931	15.250	
0.04	9.996	10.627	11.158	11.608	11.994	12.327	
0.10	8.575	8.968	9.302	9.588	9.835	10.050	K=0
0.50	8.235	8.555	8.825	9.057	9.257	9.432	
1.00	8.235	8.555	8.825	9.057	9.257	9.432	
0.004	19.273	16.682	13.789	11.571	9.892	8.601	
0.02	11.889	10.592	9.392	8.356	7.482	6.748	
0.04	9.996	9.027	8.133	7.345	6.664	6.080	
0.10	8.575	7.802	7.100	6.480	5.940	5.469	K=1.667
0.50	8.235	7.487	6.819	6.233	5.724	5.281	
1.00	8.235	7.487	6.819	6.233	5.724	5.281	
0.004	19.273	6.980	4.181	2.973	2.302	1.876	
0.02	11.889	5.626	3.661	2.705	2.141	1.770	
0.04	9.996	5.152	3.453	2.590	2.069	1.721	
0.10	8.575	4.728	3.252	2.473	1.993	1.668	K=10
0.50	8.235	4.611	3.192	2.437	1.968	1.650	
1.00	8.235	4.611	3.192	2.437	1.968	1.650	

Figure 4.10 illustrates the effect of κ on local Nu for a fixed value of Kn=0.1. For large κ values, local Nu curves coincide for both cases, since the fully developed temperature profiles for these cases are very similar as seen from the Figure 4.6. Besides the large deviation from continuum for large κ values, local Nu curves also become flat for large κ values. Fully developed Nu values change between 8.28 and 1.64 for constant wall temperature and between 9.43 and 1.65 for constant wall heat flux. The results of the Figure 4.10 are tabulated in Tables 4.3 and 4.4.

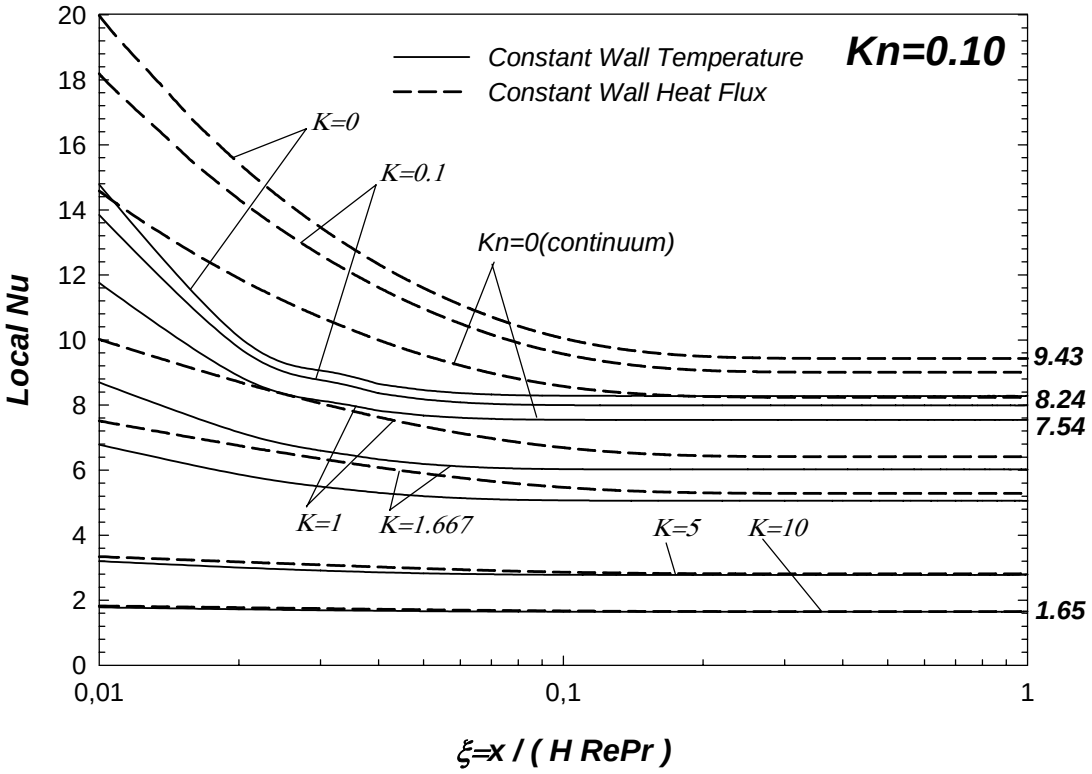

Figure 4.10. Variation of Local Nu as a Function of Dimensionless Axial Coordinate for Different κ Values, Microchannel (Kn=0.10)

Table 4.3. Variation of Local Nu as a Function of Dimensionless Axial Coordinate for Different κ Values for Constant Wall Temperature, Microchannel (Kn=0.10)

ξ	κ=0	κ=0.1	κ=0.5	κ=1	κ=1.667	κ=5	κ=10
0.01	14.782	13.845	10.993	8.698	6.779	3.198	1.779
0.05	8.458	8.173	7.175	6.188	5.197	2.826	1.662
0.10	8.285	7.996	6.997	6.027	5.067	2.780	1.645
0.50	8.279	7.990	6.989	6.019	5.058	2.775	1.643
1.00	8.279	7.990	6.989	6.019	5.058	2.775	1.643

Table 4.4. Variation of Local Nu as a Function of Dimensionless Axial Coordinate for Different κ Values for Constant Wall Heat Flux, Microchannel (Kn=0.10)

ξ	κ=0	κ=0.1	κ=0.5	κ=1	κ=1.667	κ=5	κ=10
0.004	30.386	26.378	17.268	12.061	8.601	3.535	1.876
0.02	15.250	14.320	11.132	8.708	6.748	3.176	1.770
0.04	12.327	11.612	9.423	7.627	6.080	3.020	1.721
0.10	10.050	9.570	8.032	6.689	5.469	2.861	1.668
0.50	9.432	9.007	7.632	6.409	5.281	2.809	1.650
1.00	9.432	9.007	7.632	6.409	5.281	2.809	1.650

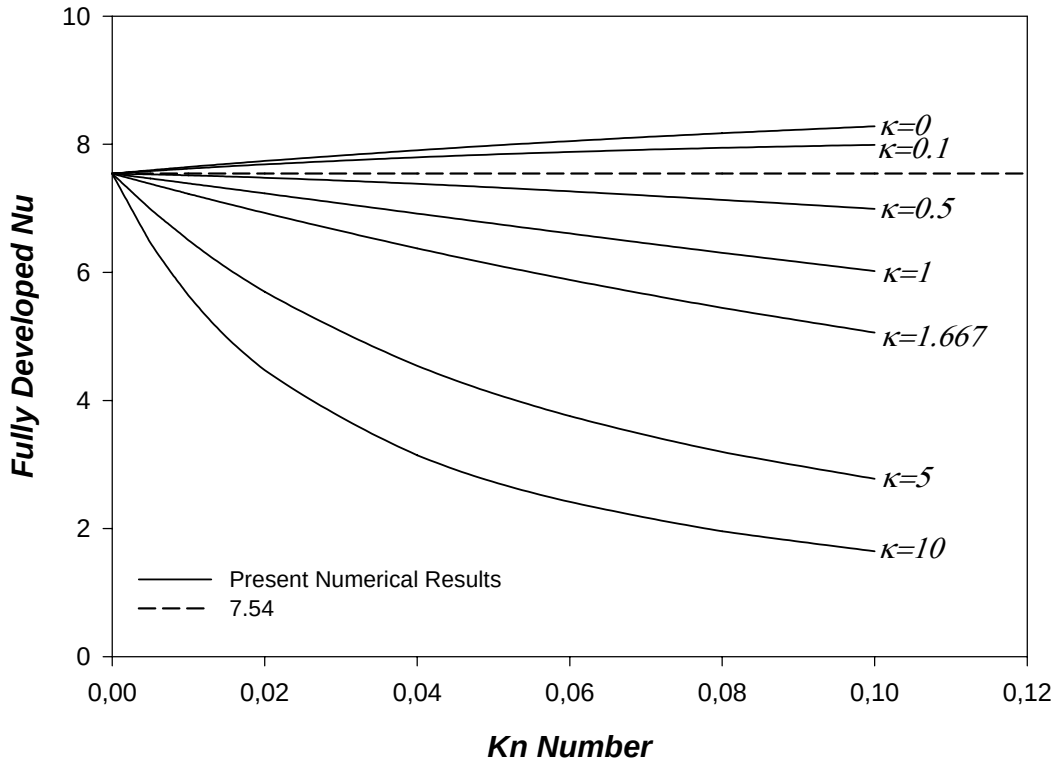

Figure 4.11. Fully Developed Nu as a Function of Kn Number and κ for Constant Wall Temperature, Microchannel

Figures 4.11 and 4.12 illustrate the fully developed Nu as a function of Kn for different κ values for both constant wall temperature and constant wall heat flux cases. As κ increases, fully developed Nu number decreases. But; depending on κ value, fully developed Nu number can be higher or lower than the continuum case. This effect is due to the small temperature gradient in radial direction at the wall. The results of the Figures 4.11 and 4.12 are tabulated in Tables 4.5 and 4.6.

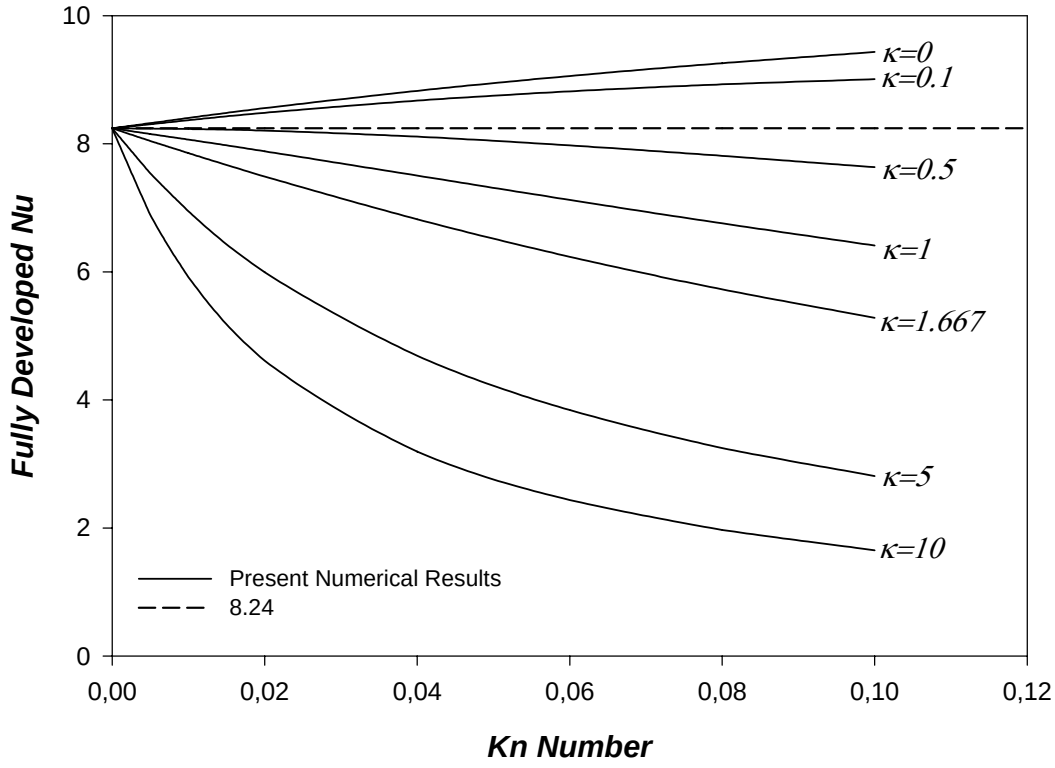

Figure 4.12. Fully Developed Nu as a Function of Kn Number and κ for Constant Wall Heat Flux, Microchannel

Generally, the behavior of the flow in microchannels between parallel plates is similar to the flow in microtube. Therefore; author has came up with the similar conclusions for the this two flow configurations.

Table 4.5. Fully Developed Nu as a Function of Kn Number and κ for Constant Wall Temperature, Microchannel

Kn	κ=0	κ=0.1	κ=0.5	κ=1	κ=1.667	κ=5	κ=10
0.00	7.541	7.541	7.541	7.541	7.541	7.541	7.541
0.005	7.594	7.581	7.529	7.465	7.381	6.987	6.209
0.01	7.644	7.618	7.514	7.388	7.226	6.502	5.639
0.02	7.739	7.686	7.478	7.232	6.925	5.696	4.476
0.04	7.905	7.795	7.382	6.917	6.374	4.539	3.145
0.06	8.048	7.880	7.264	6.606	5.882	3.756	2.415
0.08	8.172	7.943	7.131	6.305	5.445	3.195	1.957
0.10	8.279	7.990	6.989	6.019	5.058	2.775	1.643

Table 4.6. Fully Developed Nu as a Function of Kn Number and κ for Constant Wall Temperature, Microchannel

Kn	κ=0	κ=0.1	κ=0.5	κ=1	κ=1.667	κ=5	κ=10
0.00	8.235	8.235	8.235	8.235	8.235	8.235	8.235
0.005	8.321	8.303	8.235	8.151	8.042	7.537	6.888
0.01	8.402	8.367	8.229	8.063	7.852	6.944	5.917
0.02	8.555	8.483	8.204	7.881	7.487	5.992	4.611
0.04	8.825	8.672	8.110	7.501	6.819	4.688	3.192
0.06	9.057	8.817	7.973	7.122	6.233	3.840	2.437
0.08	9.257	8.926	7.811	6.755	5.724	3.246	1.968
0.10	9.432	9.007	7.632	6.409	5.281	2.809	1.650

CHAPTER 5

SINGLE PHASE HEAT TRANSFER IN MICROTUBES WITH VISCOUS DISSIPATION

5.1. Introduction

Brinkman number, the dimensionless viscous dissipation parameter, is usually neglected in low viscosity and low speed flows through macrochannels with short lengths. But, Brinkman number is significant for long pipelines. Since length over diameter ratio (L/D~100) is large in microchannels, Brinkman number may become important for flows in microchannels like in long pipelines; and may be the answer of the unusual behavior of microscale heat transfer together with the rarefaction effect.

In this section, effect of Brinkman number on single phase heat transfer analysis of hydrodynamically developed and thermally developing single phase laminar flow of a viscous fluid in microchannels between parallel plates is analyzed. The thermo-physical properties are assumed to be constant. Viscous dissipation term is included in the energy equation. The energy equation is solved numerically for constant wall temperature and constant wall heat flux thermal boundary conditions for slip-flow regime.

5.2. Heat Transfer Analysis

5.2.1. Formulation

The geometry of the problem is given in Figure 3.1, and the fully developed velocity profile in terms of mean velocity and dimensionless radius is given in Eq. (3.15). Two dimensional energy equation in cylindrical coordinates with viscous dissipation, constant properties, and negligible axial conduction can be written as [57];

$$u\frac{\partial T}{\partial x}=\frac{\alpha}{r}\frac{\partial}{\partial r}\left(r\frac{\partial T}{\partial r}\right)+\frac{\nu}{c_p}\left(\frac{\partial u}{\partial r}\right)^2 \tag{5.1}$$

The boundary conditions for constant wall temperature boundary condition are,

$$\text{at } r=R \qquad T=T_s \tag{5.2-a}$$

$$\text{at } \ r=0 \qquad \frac{\partial T}{\partial r}=0 \tag{5.2-b}$$

$$\text{at } \ x=0 \qquad T=T_i \tag{5.2-c}$$

where T_i and T_s are the temperature of the gas at the inlet and at the surface, respectively.

The boundary conditions for constant wall heat flux boundary condition are,

$$\text{at } r=R \qquad \frac{\partial T}{\partial r}=\frac{q''}{k} \tag{5.3-a}$$

$$\text{at } \ r=0 \qquad \frac{\partial T}{\partial r}=0 \tag{5.3-b}$$

$$\text{at } \ x=0 \qquad T=T_i \tag{5.3-c}$$

Introducing the dimensionless quantities given in Eq. (3.20) and the first derivative of the fully developed velocity profile, the energy equation becomes,

$$\bar{u}\frac{\partial\theta}{\partial\xi}=\frac{\partial^2\theta}{\partial\eta^2}+\frac{1}{\eta}\frac{\partial\theta}{\partial\eta}+\frac{\beta Br}{(1+8Kn)^2}\eta^2 \tag{5.4}$$

where, Br is the Brinkman number and defined as,

$$Br=\frac{\mu {u_m}^2}{k(T_i-T_w)} \tag{5.5}$$

for constant wall temperature, and

$$Br=\frac{\mu {u_m}^2}{q''D} \tag{5.6}$$

for constant wall heat flux case. β in Eq. (5.4) is a constant coming from the non-dimensionaliztion, and is equal to 16 for constant wall temperature, and is equal to 32 for constant wall heat flux case.

Using the dimensionless quantities, Eq. (3.20) and the temperature jump boundary condition, Eq. (1.5), the boundary conditions for constant wall temperature become,

$$\text{at } \eta=1 \qquad \theta=-2\kappa Kn\left(\frac{\partial\theta}{\partial\eta}\right)_{\eta=1} \tag{5.7-a}$$

$$\text{at } \eta=0 \qquad \frac{\partial\theta}{\partial\eta}=0 \tag{5.7-b}$$

$$\text{at } \xi=0 \qquad \theta=1 \tag{5.7-c}$$

where κ is defined in Eq. (3.23).

The boundary conditions for constant wall heat flux become,

$$\text{at } \eta = 1 \qquad \frac{\partial \theta}{\partial \eta} = 1 \tag{5.8-a}$$

$$\text{at } \eta = 0 \qquad \frac{\partial \theta}{\partial \eta} = 0 \tag{5.8-b}$$

$$\text{at } \xi = 0 \qquad \theta = 0 \tag{5.8-c}$$

Once the temperature distribution is determined, local Nu numbers are determined by using Eqs. (3.26), (3.27) and (3.28).

5.2.2. Numerical Solution

Like the problem in microtubes without viscous dissipation, the energy equation is transformed into a transient problem for the simplicity of the numerical solution.

$$\frac{\partial \theta}{\partial \tau} + \frac{\overline{u}}{2}\frac{\partial \theta}{\partial \xi} = \frac{\partial^2 \theta}{\partial \eta^2} + \frac{1}{\eta}\frac{\partial \theta}{\partial \eta} + \frac{\beta Br}{(1+8Kn)^2}\eta^2 \tag{5.9}$$

By defining the dimensionless time as,

$$\tau = \frac{\alpha t}{R^2} \tag{5.10}$$

Introducing the dimensionless time also, the initial condition and the boundary conditions of the transient energy equation, Eq. (3.29) become,

$$\text{at } \tau = 0 \qquad \theta = 1 \tag{5.11-a}$$

$$\text{at } \eta = 0 \qquad \frac{\partial \theta}{\partial \eta} = 0 \tag{5.11-b}$$

$$\text{at } \xi = 0 \qquad \theta = 1 \tag{5.11-c}$$

$$\text{at } \eta = 1 \qquad \theta = -2\kappa Kn\left(\frac{\partial \theta}{\partial \eta}\right)_{\eta=1} \tag{5.11-d}$$

for constant wall temperature; and,

$$\text{at } \tau = 0 \;\; \theta = 0 \tag{5.12-a}$$

$$\text{at } \eta = 0 \;\; \frac{\partial \theta}{\partial \eta} = 0 \tag{5.12-b}$$

$$\text{at } \xi = 0 \;\; \theta = 0 \tag{5.12-c}$$

$$\text{at } \eta = 1 \;\; \frac{\partial \theta}{\partial \eta} = 1 \tag{5.12-d}$$

for constant wall heat flux boundary condition.

The derivative at the wall during the calculation of local Nu number, is computed by using same finite difference approximation that used in the discretization of the Eq. (5.9); and Simpson' s 1/3 rule is used in the calculation of dimensionless mean temperature.

5.2.2.1. Domain Discretization

The same solution domain used in Chapter 3 is used for this problem. For constant wall temperature case, 100x500 grids; and for constant wall heat flux case, 250x250 grids which are distributed uniformly in the radial and longitudinal directions are used for the computation. For constant wall temperature case, the length of the tube is assigned as the dimensionless longitudinal coordinate, ξ=5 to see the effect of Brinkman number. For constant wall heat flux case, the length of the tube is assigned

as the dimensionless longitudinal coordinate, ξ=1 like in the flow without viscous dissipation.

5.2.2.2. Equation Discretization

Discretization of the Eq. (5.9) and the related boundary conditions requires second and first derivatives in space and first derivative in time. Substuting the appropriate finite-divided differences defined in Eqs. (3.33-a) through (3.33-j), the algebraic forms of the energy equation for the related nodes are determined for constant wall temperature and constant wall heat flux cases, and are listed below..

- **Nodes at the Interior Region**

For an interior node, central differences for space; Eqs (3.33-c), (3.33-f), (3.33-i) and forward difference for time, Eq. (3.33-j) are substituted into the energy equation, Eq. (5.9). The algebraic form of the energy equation becomes;

$$\theta_{i,j}^{k+1} = \theta_{i,j}^{k} + C_1(\theta_{i+1,j}^{k} - 2\theta_{i,j}^{k} + \theta_{i-1,j}^{k}) + C_2 \frac{1}{\eta_i}(\theta_{i+1,j}^{k} - \theta_{i-1,j}^{k}) - C_3 \overline{u}(\eta_i)(\theta_{i,j+1}^{k} - \theta_{i,j-1}^{k}) + C_4 \eta^2 \quad (5.13)$$

- **Nodes at the Inlet**

$$\theta_{0,j}^{k+1} = 1 \text{ for constant wall temperature} \quad (5.14)$$

$$\theta_{0,j}^{k+1} = 0 \text{ for constant wall heat flux} \quad (5.15)$$

- **Nodes at the Exit**

For an exit node, central differences in radial direction, Eqs. (3.33-c), (3.33-f), backward difference in longitudinal direction, Eq. (3.33-h) and forward difference in time, Eq. (3.33-j) are substituted into the energy equation, Eq. (5.9). The algebraic form of the energy equation becomes;

$$\theta_{i,j}^{k+1} = \theta_{i,j}^{k} + C_1(\theta_{i+1,j}^{k} - 2\theta_{i,j}^{k} + \theta_{i-1,j}^{k}) + C_2 \frac{1}{\eta_i}(\theta_{i+1,j}^{k} - \theta_{i-1,j}^{k})$$
$$-C_3 u^*(\eta_i)(3\theta_{i,j}^{k} - 4\theta_{i,j-1}^{k} + \theta_{i,j-2}^{k}) + C_4\eta^2 \qquad (5.16)$$

- **Nodes at the Centerline**

For a centerline node Eqs. (3.33-i), (3.33-j), (3.41), (3.42) are substituted into energy equation, Eq. (5.9). The algebraic form of the energy equation becomes;

$$\theta_{i,j}^{k+1} = \theta_{i,j}^{k} + 4C_1(\theta_{1,j}^{k} - \theta_{0,j}^{k}) - C_3 u^*(\eta_0)(\theta_{0,j+1}^{k} - \theta_{0,j-1}^{k}) \qquad (5.17)$$

- **Nodes at the Boundary**

For constant wall temperature, Eq. (3.44) is substituted into the Eq. (5.13). The algebraic form of the energy equation for a boundary node becomes,

$$\theta_{n-1,j}^{k+1} = \theta_{n-1,j}^{k} + C_1\left(\kappa \frac{4\theta_{n-1,j}^{k} - \theta_{n-2,j}^{k}}{2\Delta\eta(1+\frac{3\kappa}{2\Delta\eta})} - 2\theta_{n-1,j}^{k} + \theta_{n-2,j}^{k}\right)$$
$$+C_2 \frac{1}{\eta_i}\left(\kappa \frac{4\theta_{n-1,j}^{k} - \theta_{n-2,j}^{k}}{2\Delta\eta(1+\frac{3\kappa}{2\Delta\eta})} - \theta_{n-2,j}^{k}\right) - C_3 u^*(\eta_i)(\theta_{i,j+1}^{k} - \theta_{i,j-1}^{k}) + C_4\eta^2 \qquad (5.18)$$

For constant wall heat flux, Eq. (3.46) is substituted into the Eq. (5.13). The algebraic form of the energy equation for a boundary node becomes,

$$\theta_{n-1,j}^{k+1} = \theta_{n-1,j}^{k} + C_1\left(\frac{2\Delta\eta + 4\theta_{n-1,j} - \theta_{n-2,j}}{3} - 2\theta_{n-1,j}^{k} + \theta_{n-2,j}^{k}\right)$$
$$+C_2\frac{1}{\eta_i}\left(\frac{2\Delta\eta + 4\theta_{n-1,j} - \theta_{n-2,j}}{3} - \theta_{n-2,j}^{k}\right) - C_3 u^*(\eta_i)(\theta_{i,j+1}^{k} - \theta_{i,j-1}^{k}) + C_4\eta^2 \qquad (5.19)$$

where C_1, C_2, C_3, C_4 are the coefficients and defined as,

$$C_1 = \frac{\Delta\tau}{(\Delta\eta)^2} \qquad (5.20)$$

$$C_2 = \frac{\Delta\tau}{2\Delta\eta} \qquad (5.21)$$

$$C_3 = \frac{\Delta\tau}{4\Delta\xi} \qquad (5.22)$$

$$C_4 = \Delta\tau\frac{\alpha Br}{(1+8Kn)^2} \qquad (5.23)$$

and $\bar{u}(\eta)$ is the dimensionless fully developedvelocity profile, given by Eq. (3.15).

5.2.2.3. Stability and Convergence

Again, the step size in time should satisfy the stability criteria for stable solution [58]. It can be written as,

$$C_1 < \frac{1}{2} \qquad (5.24)$$

where C_1 is the coefficient that is given in Eq. (5.20). By trial and error, it is seen that

$$\Delta\tau = 0.4\Delta\eta^2 \tag{4.30}$$

is again a safe choice for this problem to get a stable solution.

For this study, the convergence criterian is that the difference between fully developed Nu values of two successive time step is less than 10^{-3}. To satisfy this criterian dimensionless time is chosen as $\tau = 10$ for constant wall temperature and $\tau = 3$ for constant wall heat flux cases, respectively.

5.3. Results and Discussion

To show the effect of Brinkman number, the energy equation is solved numerically including the viscous dissipation term. The dimensionless temperature distribution and the local Nu number are determined as a function of dimensionless axial coordinate for different Kn number values, ranging between 0 and 0.1; for different κ values, ranging between 0 and 10; and for different Brinkman number values, ranging between 0 and 0.1(0, 0.001, 0.01, 0.1). Br =0 is the case without viscous dissipation which is discussed in Chapter 3.

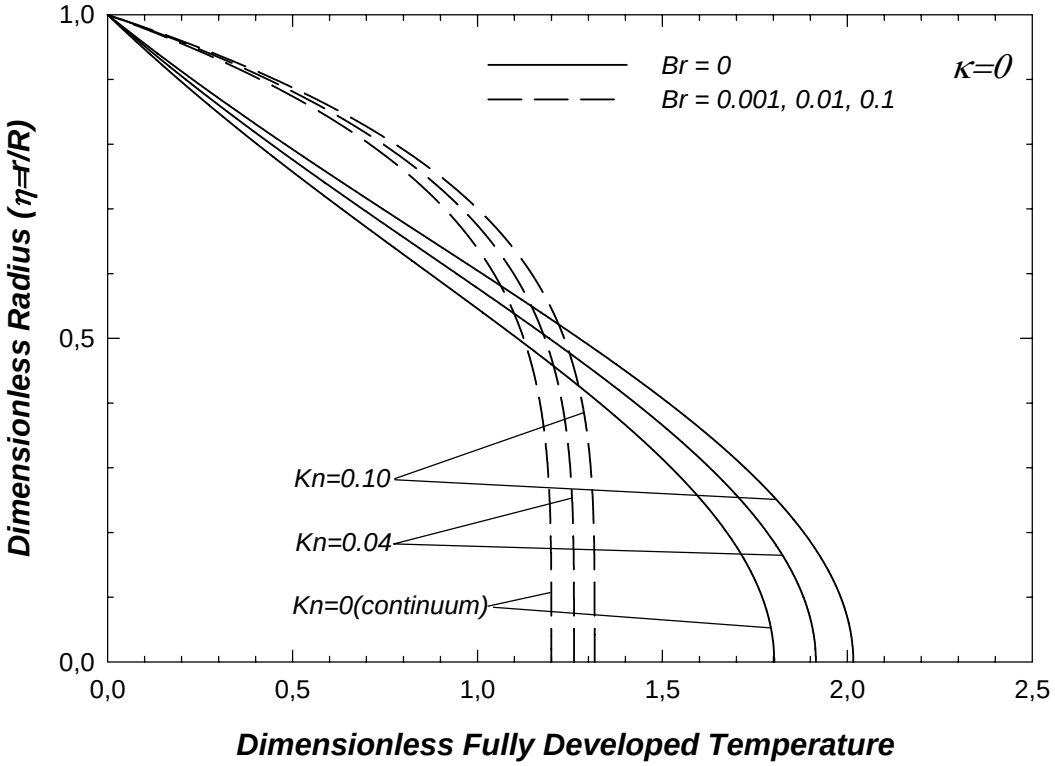

Figure 5.1. Dimensionless Fully Developed Temperature Profile as a Function of Kn Number for Constant Wall Temperature, Microtube (κ =0)

Figures 5.1 and 5.2 show the dimensionless fully developed temperature profile as a function of Kn number and Br number, for κ =0 and κ =1.667 for constant wall tempearture case. Independent of Br number, the dimensionless fully developed temperature profiles are same for same Kn number and κ values. For κ =0, the gradient at the wall increases with increasing rarefaction and increasing Br number, which will lead to an increase in Nu number. As Br number increases, the maximum dimensionless temperature decreases from 1.803 to 1.200 for Kn =0, and from 2.017 to 1.317 for Kn =0.1.

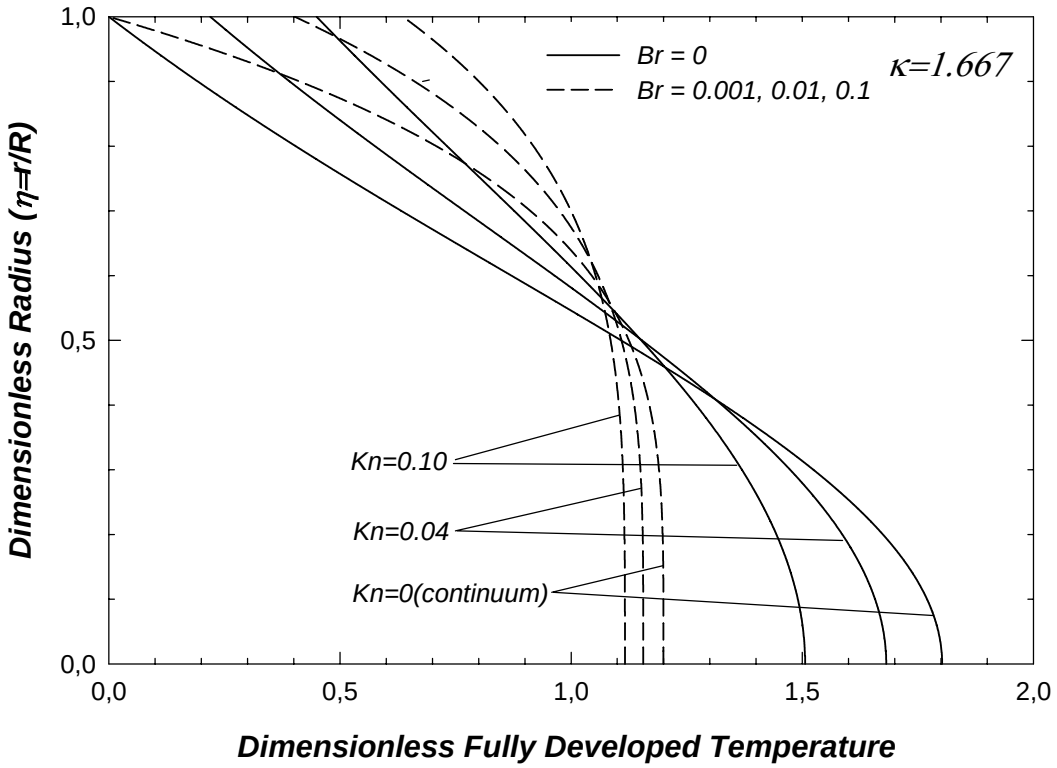

Figure 5.2. Dimensionless Fully Developed Temperature Profile as a Function of Kn Number for Constant Wall Temperature, Microtube (κ =1.667)

For κ =1.667, the gradient at the wall increases with increasing Br number, which will lead to an increase in Nu number for fixed rarefaction. For fixed Br number, the gradient at the wall decreases with increasing rarefaction like in Br =0.As Br number increases, the maximum dimensionless temperature decreases from 1.351 to 1.172 for Kn =0, and from 1.281 to 1.105 for Kn =0.1.

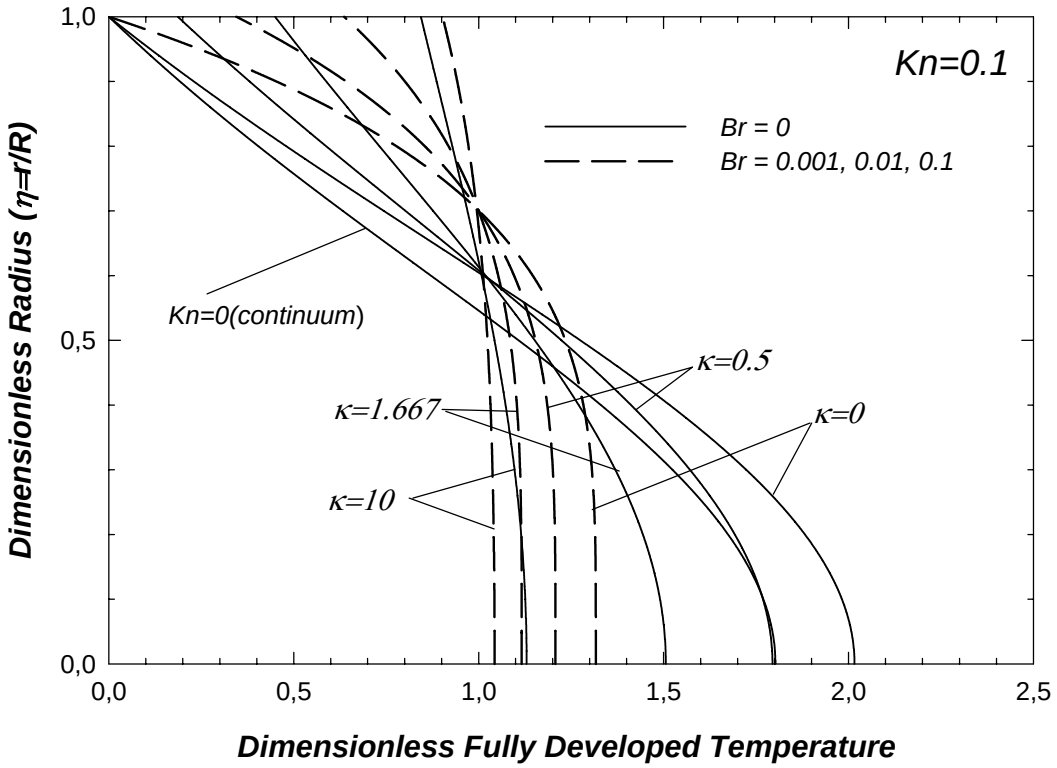

Figure 5.3. Dimensionless Fully Developed Temperature Profile as a Function of κ Parameter for Constant Wall Temperature, Microtube (Kn=0.1)

Figure 5.3 shows the dimensionless fully developed temperature profile as a function of κ parameter for Kn =0.1 for constant wall temperature case. As κ increases, the temperature jump also increases; the amount of change is increasng with Br number. The deviation of the dimensionless temperature profile from Br =0 case is decreasing with increasing κ. For large κ and viscous dissipation, the temperature profile approaches to uniform temperature distribution which diminishes the heat transfer. The maximum dimensionless temperature also decreases with increasing κ and Br number. The percentage decrease is 89 % for Br =0, and 20 % for Br different than 0.

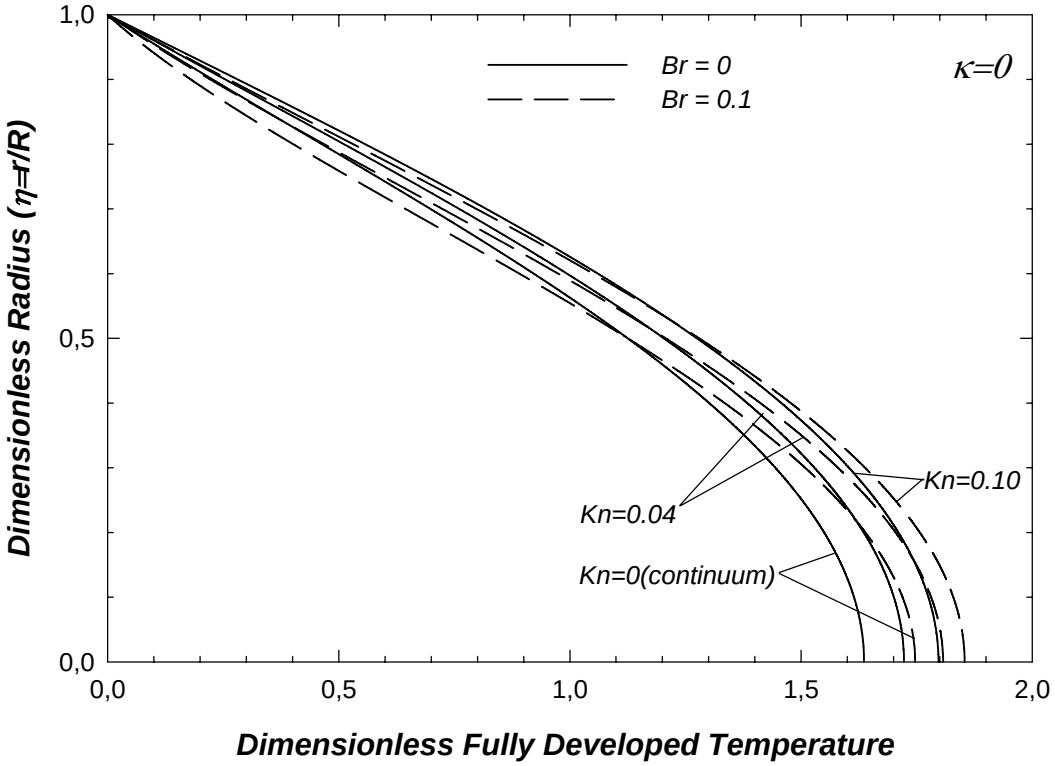

Figure 5.4. Dimensionless Fully Developed Temperature Profile as a Function of Kn Number for Constant Wall Heat Flux, Microtube (κ =0)

Figures 5.4 and 5.5 show the dimensionless fully developed temperature profile as a function of Kn number and Br number, for κ =0 and κ =1.667 for constant wall heat flux case. Unlike the constant wall temperature case, the dimensionless fully developed temperature profiles are deviates from the Br =0 case of the same Kn number and κ values. This deviation is strongly depends on the magnitude of Br number. Since the deviation is negligible for Br =0.001, 0.01 cases, the dimensionless fully developed temperature profiles corresponding to the Br =0.1 is shown on the Figures 5.4 and 5.5. For κ =0, the gradient at the wall decreases with increasing rarefaction and increasing Br number, which results in an decrease in Nu

number. As Br number increases, the maximum dimensionless temperature increases from 1.636 to 1.747 for Kn =0, and from 1.797 to 1.854 for Kn =0.1.

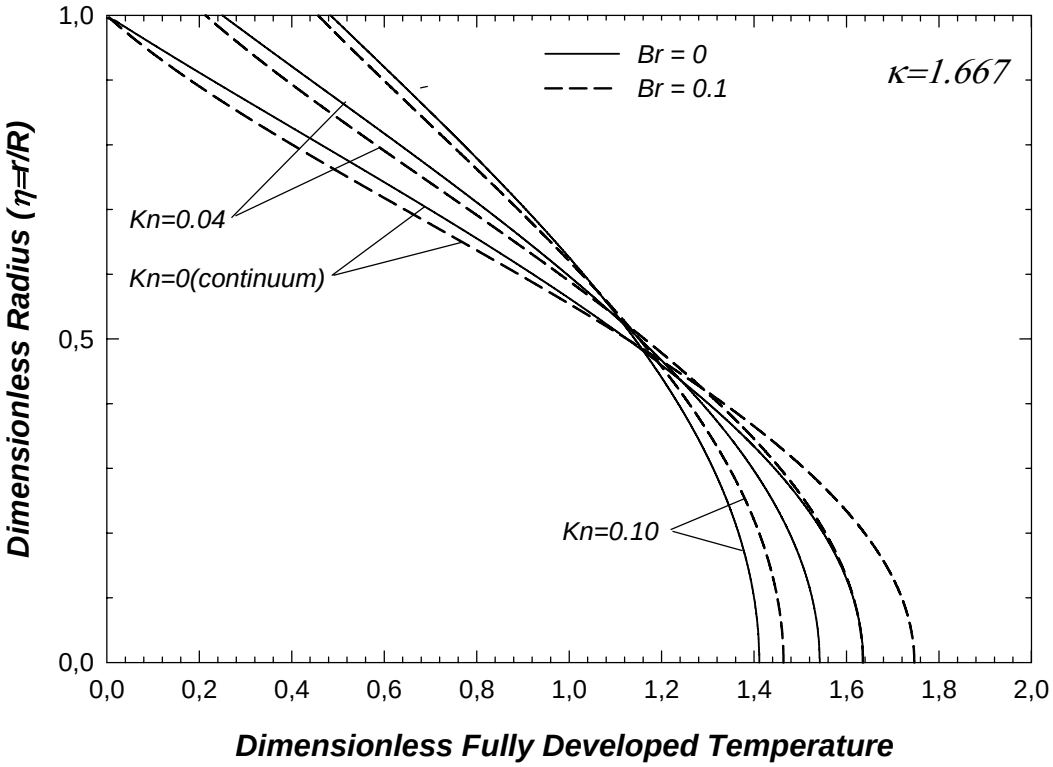

Figure 5.5. Dimensionless Fully Developed Temperature Profile as a Function of Kn Number for Constant Wall Heat Flux, Microtube (κ =1.667)

For κ =1.667, the gradient at the wall decreases with increasing Br number, which results in an decrease in Nu number for fixed rarefaction, unlike the constant wall temperature case. As Br number increases, the maximum dimensionless temperature increases from 1.636 to 1.747 for Kn =0, and from 1.412 to 1.464 for Kn =0.1.

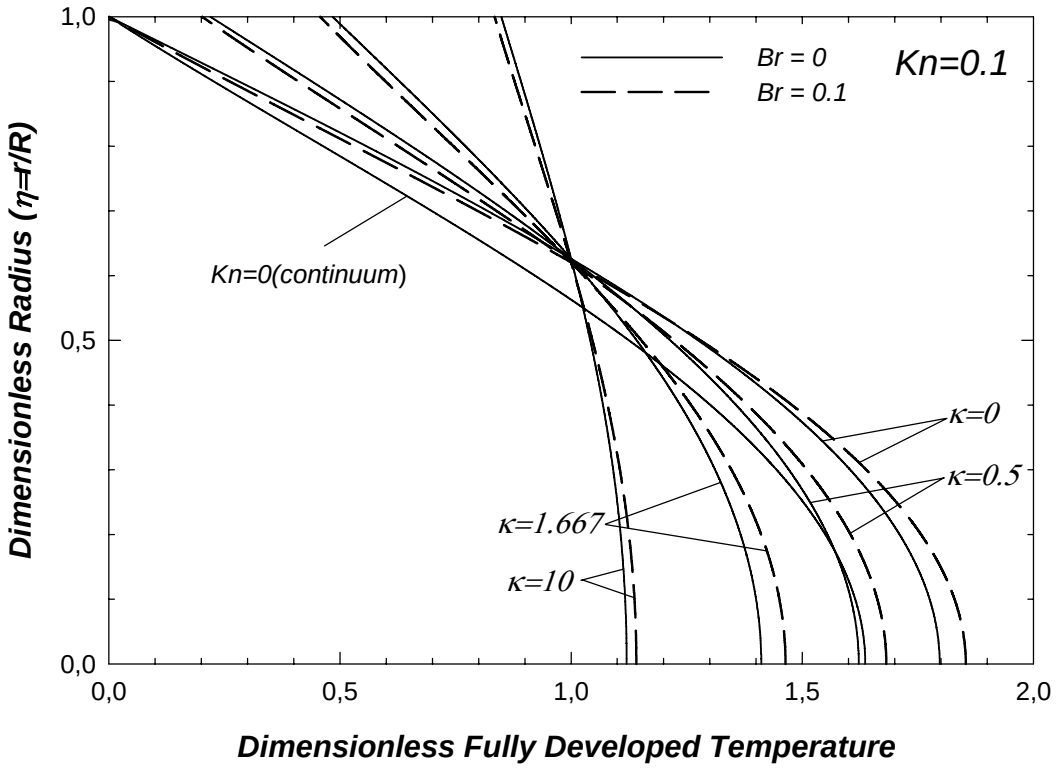

Figure 5.6. Dimensionless Fully Developed Temperature Profile as a Function of κ Parameter for Constant Wall Heat Flux, Microtube (Kn=0.1)

Figure 5.6 shows the dimensionless fully developed temperature profile as a function of κ parameter for Kn =0.1 for constant wall heat flux case. As κ increases, temperature profile approaches to uniform temperature distribution. Again, the deviation of the dimensionless temperature profile from Br =0 case is decreasing with increasing κ.. The maximum dimensionless temperature also decreases with increasing κ and Br number.

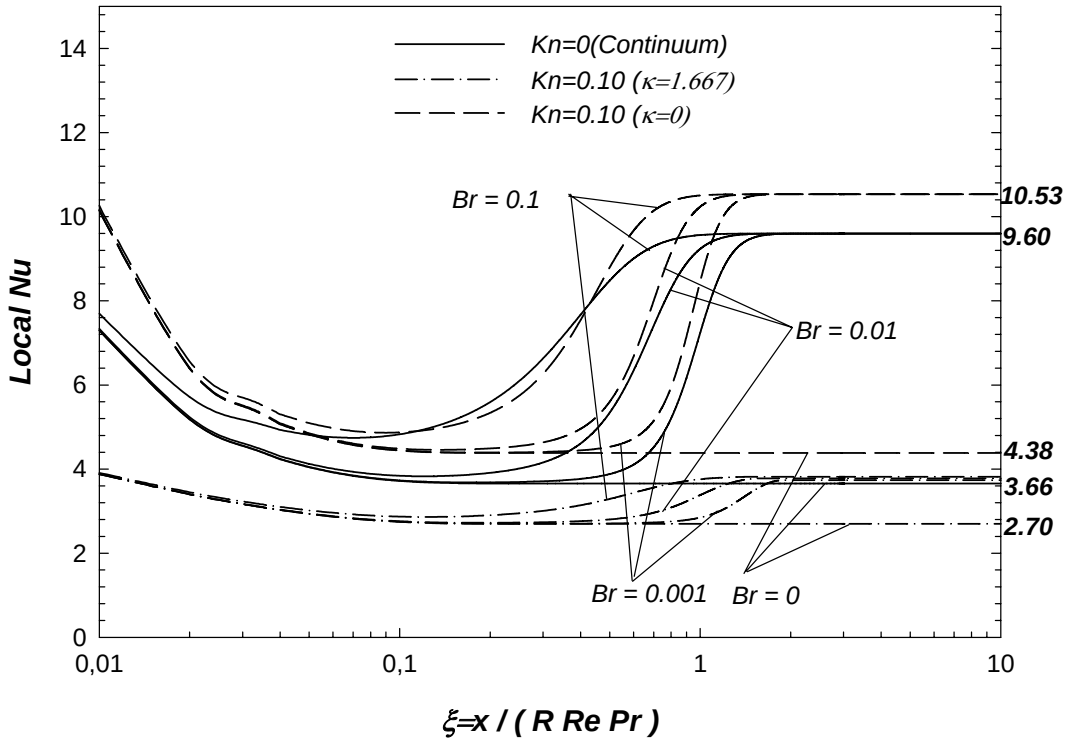

Figure 5.7. Variation of Local Nu as a Function of Dimensionless Axial Coordinate for Different κ and Br Numbers for Constant Wall Temperature, Microtube (Kn=0.10)

Figure 5.7 shows variation of local Nu number with the dimensionless axial coordinate for different κ values and Br numbers for constant wall temperature for Kn=0.1. The continuum case is also shown in the figure. By the effect of increasing Br number, local Nu value experiences a jump from 3.66 to 9.60 for Kn =0. Independent of Br number, all curves converge to a same number for fixed Kn and κ combination. Br number only affects the location of the jump. The jump point is getting closer to the entrance as Br number increases. This conclusion points out that for short channels, the effect of Br number can be neglected. However, for long channels, the effect of Br number should be considered, even for small Br numbers.

For κ =0, local Nu jumps from 4.38 to 10.53, indicating 140 % increase; and for κ =1.667, locak Nu jumps from 2.70 to 3.80, indicating 40 % increase. Therefore, with increasing κ, the significance of the jump decreases. Another conclusion is that, with increasing κ, the axial location of the jump moves far away from the entrance.

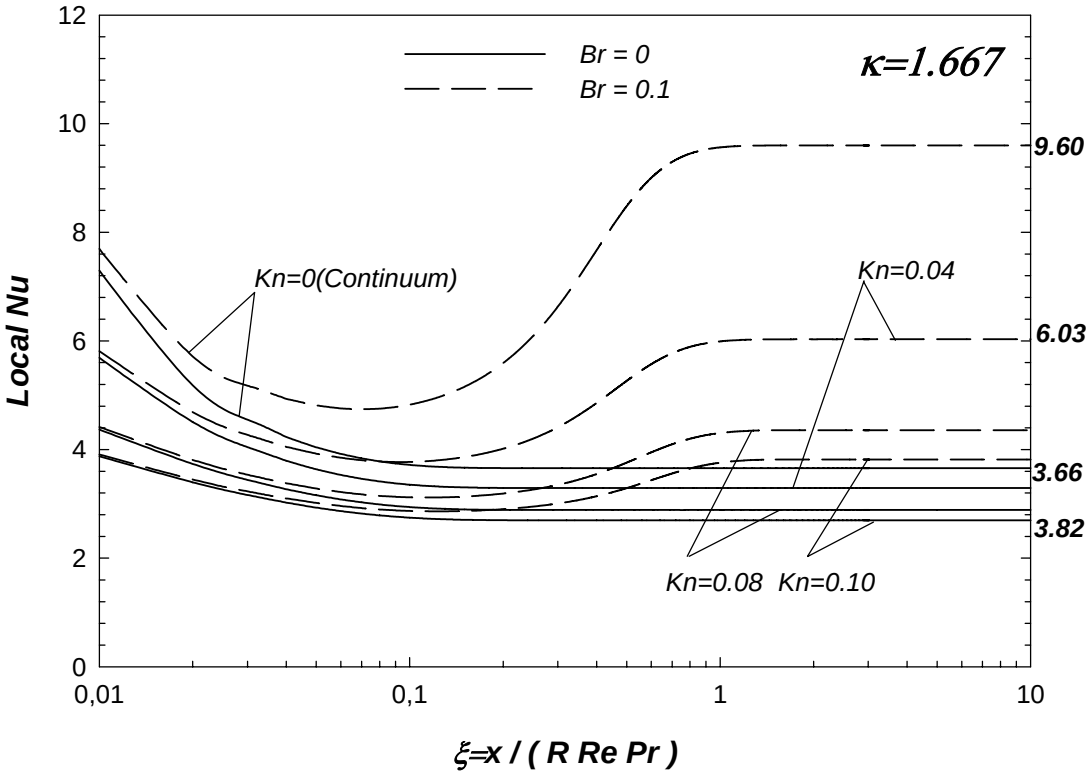

Figure 5.8. Variation of Local Nu as a Function of Dimensionless Axial Coordinate for Different Kn and Br Numbers for Constant Wall Temperature, Microtube (κ=1.667)

Figure 5.8 shows variation of local Nu number with the dimensionless axial coordinate for different κ values and Kn numbers for constant wall temperature for Br =0 and Br =0.1. As rarefaction increases, the magnitude of the jump decreases. For Kn =0, local Nu number jump from 3.66 to 9.60, which indicates 162 % increase. For Kn =0.1, local Nu number jump from 2.70 to 3.82, which indicates 41 % increase. As Kn increases, the axial location of the jump point moves far away from the entrance.

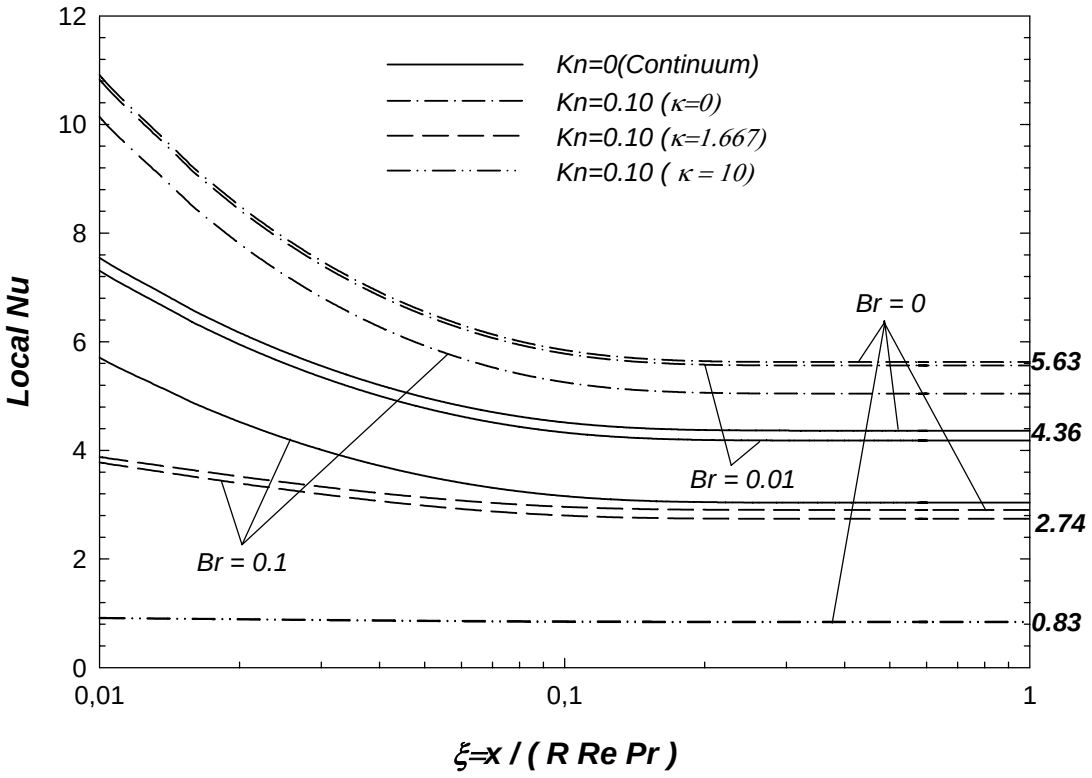

Figure 5.9. Variation of Local Nu as a Function of Dimensionless Axial Coordinate for Different κ and Br Numbers for Constant Wall Heat Flux, Microtube (Kn=0.10)

Figure 5.9 shows variation of local Nu number with the dimensionless axial coordinate for diffrent Kn numbers, κ values and Br numbers for constant wall heat flux. The effect of Br number is different than the constant wall temperature case. By the effect of Br number, local Nu value decreases for fixed Kn and κ combination. The decrease is very small for small Br numbers, and become significant with increasing Br number. The significance of this increase diminishes with increasing κ value. The effect of Br =0.001 on local Nu number is calculated, but not shown in the figure due to its negligible effect. For κ =1.667, only the effect of Br =0.1 is shown, and for κ =10, even the effect of Br =0.1 is very slight, which can not be distinguished from the figure. For different Kn and κ values, the curves would converge to different numbers ranging between the values on this figure.

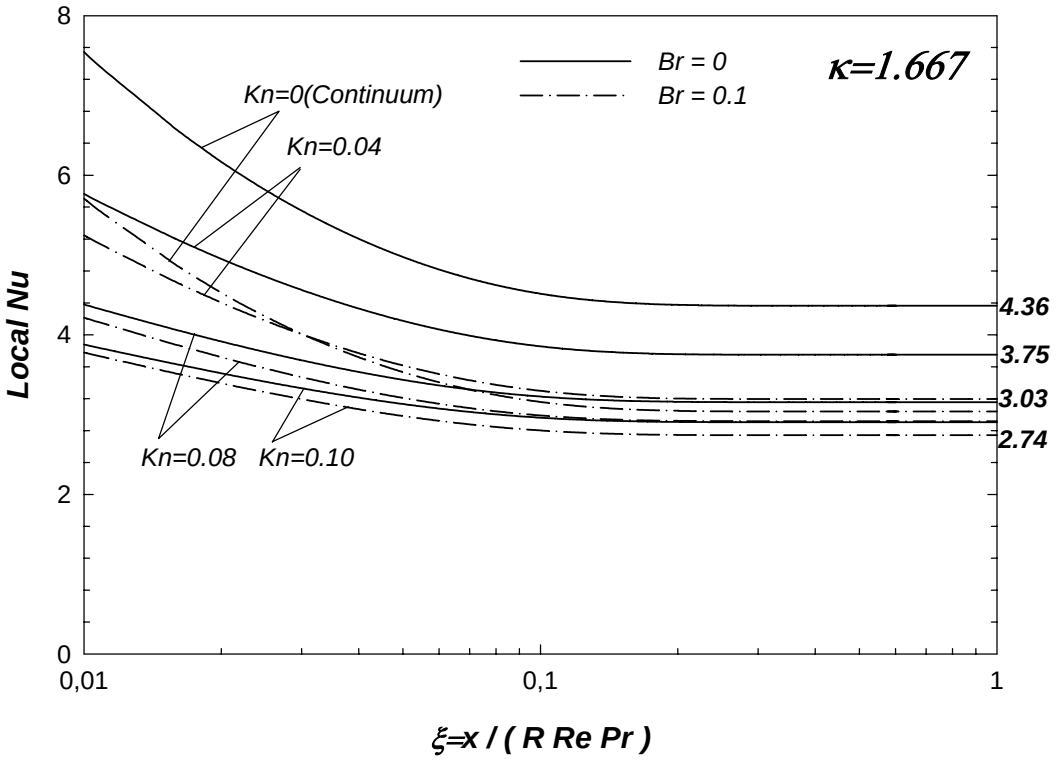

Figure 5.10. Variation of Local Nu as a Function of Dimensionless Axial Coordinate for Different Kn and Br Numbers for Constant Wall Heat Flux, Microtube (κ=1.667)

Figure 5.10 shows variation of local Nu number with the dimensionless axial coordinate for different κ values and Kn numbers for constant wall heat flux for Br =0 and Br =0.1. As rarefaction increases, the fully developed Nu number decreases. For Kn =0, local Nu number decreases from 4.36 to 3.04, which indicates 30 % decrease. For Kn =0.1, local Nu number decreases from 2.90 to 2.74, which indicates 6 % decrease. As Kn increases; unlike the constant wall temperature, the the length of the thermal entrance region does not change.

Table 5.1. Fully Developed Nu as a Function of Kn Number, κ and Br Number for Constant Wall Temperature

Kn	κ=0	κ=0.1	κ=0.5	κ=1	κ=1.667	κ=5	κ=10	
0.00	3.656	3.656	3.656	3.656	3.656	3.656	3.656	Br = 0
0.005	3.710	3.704	3.682	3.655	3.618	3.445	3.209	
0.01	3.761	3.749	3.704	3.649	3.577	3.250	2.843	
0.02	3.855	3.832	3.739	3.628	3.488	2.902	2.291	
0.04	4.020	3.970	3.778	3.557	3.292	2.356	1.624	
0.06	4.160	4.081	3.785	3.458	3.087	1.961	1.247	
0.08	4.279	4.136	3.767	3.342	2.887	1.670	1.008	
0.10	4.382	4.240	3.732	3.218	2.697	1.448	0.844	
0.00	9.598	9.598	9.598	9.598	9.598	9.598	9.598	Br = 0.1
0.02	9.871	9.679	8.984	8.243	7.426	4.967	3.319	
0.04	10.087	9.696	8.393	7.186	6.031	3.340	2.003	
0.06	10.264	9.668	7.846	6.352	5.064	2.508	1.434	
0.08	10.411	9.610	7.347	5.679	4.359	2.003	1.116	
0.10	10.534	9.530	6.900	5.129	3.818	1.681	0.913	

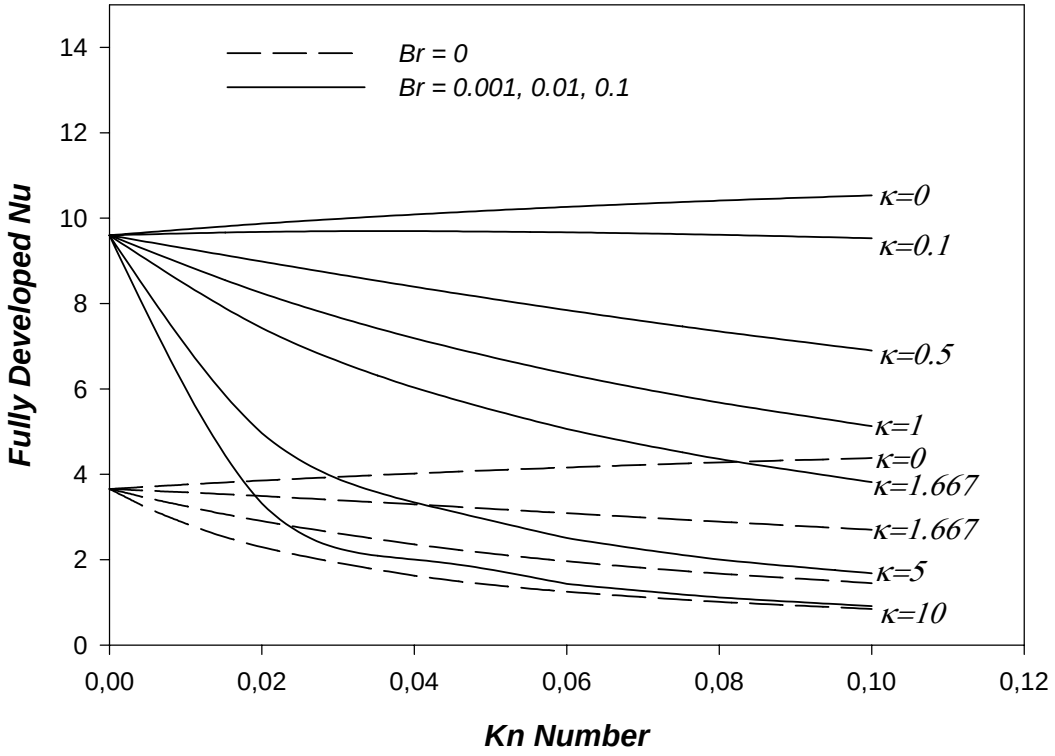

Figure 5.11. Fully Developed Nu as a Function of Kn Number, κ and Br Number for Constant Wall Temperature, Microtube

Figures 5.11 and Table 5.1 show the fully developed Nu as a function of Kn for different κ and Br number values for constant wall temperature case. The deviation of the local Nu from the continuum case Br =0.1 is more significant than the Br =0 case. The general trend of the curves are very similar to the curves corresponding to the Br =0 case.

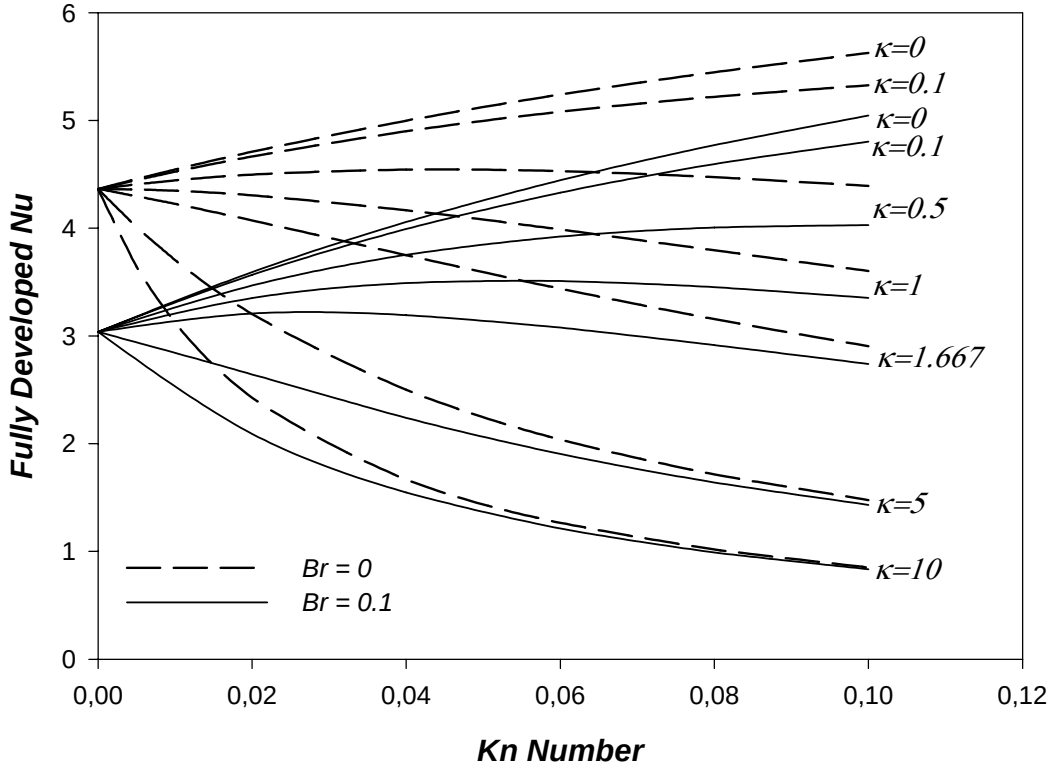

Figure 5.12. Fully Developed Nu as a Function of Kn Number, κ and Br Number for Constant Wall Heat Flux, Microtube

Figures 5.12 and Table 5.2 show the fully developed Nu as a function of Kn for different κ and Br number values for constant wall heat flux case. The value of the fully developed Nu numbers are depend on the value of Br number. Only the values corresponding to the Br =0.1 are shown on the Figure 5.10 since the effect of Br =0.001, 0.01 are negligible; but the results corresponds to Br =0.001, 0.01 are tabulated in Table 5.2.. The values corresponding to Br =0.001, 0.01 are tabulated below. Again, the deviation of the local Nu from the continuum case for Br =0.1 is more significant than the Br =0 case. The general trend of the curves are again very similar to the curves corresponding to the Br =0 case.

Table 5.2. Fully Developed Nu as a Function of Kn Number, κ and Br Number for Constant Wall Heat Flux, Microtube

Kn	κ=0	κ=0.1	κ=0.5	κ=1	κ=1.667	κ=5	κ=10	
0.00	4.364	4.364	4.364	4.364	4.364	4.364	4.364	Br = 0
0.005	4.457	4.447	4.408	4.360	4.297	4.010	3.645	
0.01	4.545	4.525	4.444	4.348	4.225	3.704	3.125	
0.02	4.710	4.666	4.498	4.304	4.071	3.202	2.425	
0.04	4.998	4.900	4.544	4.165	3.749	2.499	1.666	
0.06	5.241	5.081	4.529	3.987	3.438	2.037	1.265	
0.08	5.448	5.220	4.473	3.794	3.155	1.714	1.017	
0.10	5.627	5.327	4.391	3.601	2.903	1.476	0.849	
0.00	4.345	4.345	4.345	4.345	4.345	4.345	4.345	Br = 0.001
0.02	4.695	4.652	4.485	4.292	4.060	3.195	2.421	
0.04	4.986	4.889	4.534	4.157	3.742	2.497	1.665	
0.06	5.231	5.072	4.522	3.982	3.434	2.036	1.264	
0.08	5.440	5.213	4.468	3.791	3.153	1.713	1.016	
0.10	5.620	5.321	4.387	3.598	2.902	1.475	0.849	
0.00	4.181	4.181	4.181	4.181	4.181	4.181	4.181	Br = 0.01
0.02	4.568	4.527	4.368	4.186	3.964	3.136	2.387	
0.04	4.885	4.791	4.450	4.086	3.685	2.471	1.654	
0.06	5.149	4.994	4.460	3.934	3.399	2.023	1.259	
0.08	5.372	5.150	4.422	3.757	3.130	1.706	1.014	
0.10	5.563	5.270	4.352	3.574	2.886	1.471	0.848	
0.00	3.038	3.038	3.038	3.038	3.038	3.038	3.038	Br = 0.1
0.02	3.593	3.567	3.468	3.352	3.209	2.643	2.091	
0.04	4.058	3.993	3.753	3.491	3.194	2.240	1.547	
0.06	4.446	4.330	3.923	3.510	3.077	1.905	1.212	
0.08	4.771	4.596	4.007	3.453	2.916	1.640	0.991	
0.10	5.046	4.804	4.029	3.354	2.741	1.432	0.835	

CHAPTER 6

DISCUSSION AND CONCLUSION

Heat transfer analysis of two-dimensional, incompressible, constant property, hydrodynamically developed, thermally developing, single phase laminar flow in microtubes and microchannels between parallel plates with negligible axial conduction is performed for constant wall temperature and constant wall heat flux thermal boundary conditions for slip flow regime. Fully developed velocity profile is determined analytically, and energy equation is solved by using finite difference method for both geometries. The rarefaction effect is imposed to the boundary conditions of the momentum and energy equations. The viscous dissipation term is included in the energy equation. The effects of rarefaction and viscous heating on temperature profile and local Nusselt number are discussed. The results of the numerical method are verified with the well-known analytical results of the flow in macrochannels (i.e. Kn =0, Br =0) and with the available analytical results of flow in microchannels for simplified cases.

The effects of three parameters; Kn number, κ parameter and Br number, on the flow are discussed. Kn number ranges from Kn =0, which is the continuum case(i.e. flow in macrochannels), to Kn =0.1, which is the upper limit of the slip flow regime. κ parameter ranges from κ =0, which is a fictious case introducing the effect of rarefaction only on the velocity, to κ =10, which stands for the large temperature jump at the wall. κ =1.667 is discussed frequently, since it is the typical value for air, the working fluid for most of the engineering applications. Brinkman number is

ranging from Br =0, which stands for the without viscous dissipation case, to Br =0.1.

For Br =0 case; for both geometies, the Kn number and the κ parameter have the similar effects on the flow. For practical purposes, to calculate the fully developed Nu number, a simplified expression for both geometries and for both thermal boundary conditions is found as,

$$\frac{Nu(Kn,\kappa=0)}{Nu(\kappa,Kn)}-1=a_1(\kappa Kn)^2+a_2(\kappa Kn) \tag{6.1}$$

where Nu(κ,Kn) is the desired fully developed Nu number and the Nu(κ=0) is the value of the fully developed Nu number corresponds to same Kn number when κ =0. a_1, a_2 are the constants depends on the geometry and the boundary condition of the problem. Nu(κ =0) can be calculated with the following expression,

$$Nu(Kn,\kappa=0)=b_1Kn^2+b_2Kn+Nu(Kn=0) \tag{6.2}$$

where Nu(Kn=0) is the continuum fully developed Nu number for the given configuration and the boundary condition. b_1, b_2 are the constants depends on the geometry and the bounary condition of the problem. a_1, a_2, b_1, b_2 constant and are tabulated in Table 6.1.

From this study, the following general conclusions can be obtained;

(1) Velocity gradient at the wall decreases with increasing rarefaction which leads to a reduction in the friction factor for flows in microchannels.

Table 6.1. Constants in Eqs. (6.1) and (6.2)

Geometry	Boundary Condition	Nu(Kn=0)	a_1	a_2	b_1	b_2
Microtube	Const. Wall Temp.	3.66	0.69	3.51	-29.56	10.15
Microtube	Const. Wall Heat Flux.	4.36	0.56	5.04	-55.25	18.12
Microchannel	Const. Wall Temp.	7.54	0.35	3.70	-29.26	10.28
Microchannel	Const. Wall Heat Flux.	8.24	0.27	4.43	-44.95	16.37

(2) For fixed κ parameter, the deviation from the continuum increases with increasing rarefaction for both constant wall temperature and constant wall heat flux cases without viscous heating.

(3) For fixed Kn number , the deviation from the continuum increases, and dimensionless fully developed temperature approaches to uniform distribution with increasing κ parameter without viscous heating.

(4) The fully developed Nu number decrease or increase compared to the continuum fully developed Nu number values depending on the Kn number and κ values, without viscousing heating.

(5) For viscous heating case; even for small Br numbers, there is a deviation from the Br =0 case for constant wall temperature case. Fully developed Nu number value experiences a jump in magnitude. The magnitude of the Br number affects the axial location of the jump. Therefore, the effect of viscous heating should be considered even for small Br numbers with large length over diameter (L/D) ratios, which is the case for flows in microchannels.

(6) For constant wall heat flux case with viscous heating, the deviation is proportional to the magnitude of the Br number. For small Br numbers, the effect can be neglected.

To optimize design parameters in microchannel heat sinks, the dynamic behavior of the fluid motion should be understood. This study considers rarefaction and viscous heating effects in microtubes and in microchannels between parallel plates. To understand the flow in microchannels better, some further extensions in addition to the rarefaction and viscous heating such as; axial conduction in the fluid, axial conduction at the channel wall, variation of thermophysical properties, compressibility effect, different geometrical configurations, different thermal boundary conditions, should be included in the analysis.

REFERENCES

[1] Yener, Y., Kakac, S. and Avelino, M., Single Phase Forced Convection in Microchannels- State-of Art-Review, *Microscale Heat Transfer- Fundamentals and Applications in Biological Systems and MEMS,* (edits) Kakac, S., Vasiliev, L., Bayazitoglu, Y., Yener, Y., Kluwer Academic Publisher, The Netherlands, 2005.

[2] Eckert, E. G. R., Drake, R.M. Jr., Analysis of Heat and Mass Transfer, McGraw-Hill, New York, (1972) 467-486.

[3] Larrode, F. E., Housiadas, C., and Drossinos, Y., Slip-flow heat transfer in circular tubes, *Int. J. Heat and Mass Transfer,* 43(2000) 2669-2680.

[4] Tuckerman, D. B. and Pease, R. F., Optimized convective cooling using micromachined structure, *J. Electrochem. Soc.*, 1982, 129 (3) P. C 98.

[6] Peng, X. F. and Peterson, G. P., The effect of thermofluid and geometrical parameters on convection of liquids through rectangular microchannels, *Int. J. Heat and Mass Transfer,* 1995b, 38 (4), 755-758.

[7] Peng X F and Peterson G P, Convective heat transfer and flow friction for water flow in microchannels, *Int. J. Heat and Mass Transfer*, 1996, 39, No.12, 2599-2608.

[8] Mala Mohiuddin G; Li Dongqing, Dale J., Flow characteristics of water in microtubes, *Int. J. Heat Fluid Flow,* 1999, 20, 142-148

[9] Rahman, M. M., Measurements of heat transfer in microchannel heat sinks, *Int. Comm. Heat Mass Transfer*, Vol 27, No 4, 495-506, 2000.

[10] Harms, T.M., Kazmierczak, M.J., Gerner, F.M., Developing convective heat transfer in deep rectangular microchannels, , *Int. J. Heat Fluid Flow,* 1999, 20, 149-157.

[11] Wu, H.Y. and Cheng, P., An experimental study of convective heat transfer in silicon microchannels with different surface conditions, *Int. J. Heat Mass Transfer*, 2003, 46, 2547-2556.

[12] Tso, C. P. and Mahulikar, S. P., The use of the Brinkman number for single phase forced convective heat transfer in microchannels, *Int. J. Heat Mass Transfer*, 1998a, 41 (12), 1759-1769.

[13] Tso, C. P. and Mahulikar, S. P., The role of the Brinkman number in analyzing flow transitions in microchannels, *Int. J. Heat Mass Transfer*, 1998b, 42, 1813-1833.

[14] Tso, C. P. and Mahulikar, S. P., Experimental verification of the role of Brinkman number in microchannels using local parameters, *Int. J. Heat Mass Transfer*, 2000, 43, 1837-1849.

[15] Wang, B. X. and Peng, X. F., Experimental investigation of heat transfer in flat plates with rectangular microchannels, *Int. J. Heat Mass Transfer*, 1995, 38(1), 127-137.

[16] Chen, Y.T., Kang, S.W., Tuh, W.C., Hsiao, T.H., Experimental investigation of fluid flow and heat transfer in microchannels, *Tamkang J. Science and Engineering*, 7 (1), 11-16, 2004.

[17] Pfahler, J., Harley, J., Bau, H. H., and Zemel, J., Liquid and gas transport in small channels, *Proceedings of ASME WAM Micro Structures*, *Sensors, and Actuators*, DSC 19, 1990a, 149-157.

[18] Pfahler, J., Harley, J., Bau, H. H., and Zemel, J., Liquid transport in micron and submicron channels, *Sensors and Actuators*, A21-A23, 1990b, 431-434.

[19] Pfahler, J., Harley, J., Bau, H. H., and Zemel, J., Gas and liquid flow in small channels, *Micromechanical Sensors, Actuators, and Systems,* ASME DSC 32, 1991, 49-60.

[20] Wu, P. Y. and Little, W. A., Measurement of friction factor for the flow of gases in very fine channels used for microminiature Joule-Thompson Refrigerators, *Cryogenics*, 1983, 23 (5), 273-277.

[21] Wu, P. Y. and Little, W. A., Measurement of heat transfer characteristics of gas flow in fine channels heat exchangers used for microminiature refrigerators, *Cryogenics*, 1984, 24 (5), 415-420.

[22] Choi, S. B., Barron R. F. and Warrington R. O., Fluid flow and heat transfer in microtubes, *Micromechanical Sensors, Actuators, And Systems*, ASME DSC 32, 1991, 123-134.

[23] Arkilic, E. B., Breuer, K. S., and Schmidt, M. A., Gaseous slip flow in long microchannels. Ieee *J. Microelectromech. Systems*, 6 (2), 167-178, 1997..

[24] Xin, M.D., Zhang, P.J., Influence of the hydraulic diameter on flow characteristics in microchannels, *ICHMT Int. Symp. Molecular and Microscale Heat*

Transfer in Materials Processing and Other Applications, March 1997, Tokyo, Japan.

[25] Telles, A.S., Queiroz, E.M., and Filho, E., Solution of extended Graetz problem, , *Int. J. Heat Mass Transfer*, 2001, 44, 471-483.

[26] Beskok, A., Karniadakis, G. E., Simulation of heat and momentum transfer in complex micro geometries, *AIAA J. Thermophysics and Heat Transfer*, 1994, 8 (4), 647-655.

[27] Beskok, A., Karniadakis, G. E., and Trimmer, W., Rarefaction, compressibility effects in gas microflows, *J. Fluids Eng.*, September 1996, 118, 448-456.

[28] Beskok, A., Karniadakis, G. E., A model for flows in channels, pipes, and ducts at micro and nano scales, *Microscale Thermophysical Eng.*, 1999, 3, 43-77.

[29] Mikhailov, M.D., Cotta R.M., and Kakac, S., Steady state and periodic heat tansfer in micro conduits, *Microscale Heat Transfer- Fundamentals and Applications in Biological Systems and MEMS,* (edits) Kakac, S., Vasiliev, L., Batazitoglu, Y., Yener, Y., Kluwer Academic Publisher, The Netherlands, 2005.

[30] Barron, R. F., Wang, X. M., Warrington,R. O., and Ameel, T. A., The Graetz problem extended to slip flow, , *Int. J. Heat Mass Transfer,* 1997, 40 (8), 1817-1823.

[31] Barron, R. F., Wang, X. M., Warrington,R. O., and Ameel, T. A., Evaluation of the eigenvalues for the Graetz problem in slip-flow, *Int. Comm. Heat Mass Transfer*, 1996, 23 (4), 563-574.

[32] Mikhailov, M.D., Cotta R.M., Eigenvalues for the Graetz problem in slip-flow, *Int. Comm. Heat Mass Transfer*, 1997, 24 (3), 449-451.

[33] Ameel, T. A., Barron, R. F., Wang, X. M., and Warrington,R. O., Laminar forced convection in a circular tube with constant heat flux and slip flow, *Microscale Thermophysical Eng.,* 1997, 1, 303-320.

[34] Housiadas, C., Larrode, F. E., and Drossinos, Y., Technical note numerical evaluation of the Graetz series, *Int. J. Heat and Mass Transfer,* 1999, 43, 2669-2680.

[35] Bayazitoglu, Y., Kakac, S., Flow regimes in microchannel single phase gaseous fluid flow*, Microscale Heat Transfer- Fundamentals and Applications in Biological Systems and MEMS*, (edits) Kakac, S., Vasiliev, L., Bayazitoglu, Y., Yener, Y., Kluwer Academic Publisher, The Netherlands, 2005.

[36] Tunc, G., Bayazitoglu, Y., Heat transfer in microtubes with viscous dissipation, *Int. J. Heat Mass Transfer*, 2001a, 44 (13), 2395-2403

[37] Tunc, G., Bayazitoglu, Y., Convection at the entrance of micropipes with sudden wall temperature change , *Proceedings of IMECE 2002*, November 17-22, New Orleans, Lousiana.

[38] Li, J.M., Wang, B.X., and Peng, X.F., The wall effect for laminar flow through microtube, *ICHMT Int. Symp. Molecular and Microscale Heat Transfer in Materials Processing and Other Applications*, March 1997, Tokyo, Japan..

[39] Guo, Z.Y., Wu, X.B., Further study on compressibility effects on the gas flow and heat transfer in a microtube, *Microscale Thermophysical Eng.*, 1998, 2, 111-120

[40] XU, B., Ooi, K.T., Mavriplis, C., and Zaghloul, M.E., Evaluation of viscous dissipation in liquid flow in microchannels, *J. Micromech. Microeng.*, 2003, 13, 53-57.

[41] Barber, R.W., Emerson, D.R., The influence of Knudsen number on the hydrodynamic development length within parallel plate microchannels, *Advances in Fluid Mechanics IV*, 2002, 207-216.

[42] Kavehpour,H. P., Faghri, M., and Asako,Y., Effects of compressibility and rarefaction in gaseous flows in microchannels, *Numerical Heat Transfer*, 1997, Part A, 32, 677-696.

[43] Hadjiconstantinou, N.G., Simek, O., Nusselt number in micro and nano channels under conditions of constant wall temperature*, Proceedings of IMECE 2001*, November 11-16, New York, NY.

[44] Zhu, X., Xin, M.D., and Liao, Q., Analysis of heat transfer between two unsymmetrically heated parallel plates with microspacing in the slip-flow regime, *Microscale Thermophysical Eng.*, 2002, 6, 287-301.

[45] Maynes and Webb, Fully developed electro-osmotic heat transfer in microchannels, *Int. J. Heat Mass Transfer*, 2003, 46, 1359-1369.

[46] Yu, S. and Ameel, T.A., Slip-flow heat transfer in rectangular microchannels, *Int. J. Heat Mass Transfer*, 2001, 44, 4225-4235.

[47] Yu, S. and Ameel, T.A, A universal Entrance number for internal slip flow, *Int. Comm. Heat Mass Transfer*, 2001, 28 (7), 905-910.

[48] Tunc, G., Bayazitoglu, Y., Heat transfer in rectangular microchannels, *Int. J. Heat Mass Transfer*, 2002, 45, 765-773.

[49] Papautsky, I., Brazzle, J., Ameel, T., and Frazier, A.B., Laminar fluid behavior in microchannels using micropolar fluid theory, *Sensors and Actuators*, 1999, 73, 101-108.

[50] Ryu, J.H., Choi, D.H., abd Kim, S.J., Three-dimensional numerical optimization of a manifold microchannel heat sink, *Int. J. Heat Mass Transfer*, 2003, 46, 1553-1562.

[51] Qu, W., Mudawar, I., Analysis of three-dimensional heat transfer in microchannel heat sinks, *Int. J. Heat Mass Transfer*, 2002, 45, 3973-3985.

[52] Fan, Q., Xue, H. and Shu, C., DSMC simulation of gaseous flows in microchannels, *5th ASME/JSME Thermal Engineering Joint Conference,* San Diego, U.S.A, AJTE99-6519, 1999.

[53] Toh, K.C., Chen, X.Y. and Chai, J.C., Numerical computation of fluid flow and heat transfer in microchannels, *Int. J. Heat Mass Transfer*, 2002, 45, 5133-5141.

[54] Guo, Z.Y., Li, Z.X., Size effect on single-phase channel flow and heat transfer at microscale, *Int. J. Heat Mass Transfer*, 2003, 24, 284-298.

[55] Papautsky, I., Ameel, T., and Frazier, A.B., A review of laminar single-phase flow in microchannels, *Proceedings of IMECE 2001*, November 11-16, New York, NY.

[56] Kakac, S., Vasiliev, L., Bayazitoglu, Y., Yener, Y., Microscale Heat Transfer-Fundamentals and Applications in Biological Systems and MEMS, Kluwer Academic Publisher, The Netherlands, 2005.

[57] Kakac, S. and Yener, Y., Convective Heat Tranfer, Pub. No: 65, METU, Ankara, 1980.

[58] Chapra, S. C., Canale, R. P., Numerical Methods for Engineers, 3rd Edition, McGraw-Hill, 1998.